

TECHNISCHE UNIVERSITÄT MÜNCHEN

Lehrstuhl für Technische Chemie II

Elementary Reactions of 1-Propanol on HZSM-5

Yuchun Zhi

Vollständiger Abdruck der von der Fakultät für Chemie der Technischen Universität München zur Erlangung des akademischen Grades eines

Doktors der Naturwissenschaften (Dr. rer. nat.)

genehmigten Dissertation.

Vorsitzender: Univ. -Prof. Dr. K.-O. Hinrichsen

Prüfer der Dissertation: 1. Univ. -Prof. J. A. Lercher

2. Univ. -Prof. H. A. Gasteiger

Die Dissertation wurde am 10.02. 2015 bei der Technischen Universität München eingereicht und durch die Fakultät für Chemie am 02.03.2015 angenommen.

"Wherever you go, go with your heart."

Confucius (551BC-479BC)

Acknowledgements

It would not have been possible to complete this thesis without the assistance, support and encouragement from all the following individuals and organization. I would like to express my sincere thanks to all of them who have contributed to my work during my PhD study at Technische Universität München.

First and foremost, I want to give my deepest gratitude to Prof. Dr. Johannes A. Lercher for offering me the opportunity to work and complete my doctoral thesis in his excellent group. I am grateful for his inspiration and thoughtful guidance throughout my PhD work, for the each enlightening discussion with him, and also for his invaluable advice and warm encouragement when I met difficulty. I also greatly appreciate the scholarship he granted me after my financial support from China Scholarship Council (CSC) was ended.

I am deeply indebted to my supervisor Prof. Dr. Chen Zhao, for her consistent support, especially for her kind discussions and suggestions on the experiments in the early stage of my PhD study. Without her important advice and constant encouragement, I would never have finished my thesis.

I would like to acknowledge Prof. Dr. Andreas Jentys for sharing his expert knowledge in calorimetric and infrared spectroscopy measurement with me and Dr. Eszter Baráth for the encouragement and support in the laboratory and daily life.

Many thanks to Xaver Hecht for the BET measurements and especially for his great help for solving any technical problem for my setup; to Martin Neukamm for AAS measurement; to Andreas Marx for tackling lots of computer problems and to Steffi Maier, Ulrike Sanwald, Bettina Federmann, Karen Schulz for their kind help in administrative matters.

I want to express my special gratitude to Dr. Baoxiang Peng for his introduction of the continuous flow and batch setup and supervision of the experiments at the beginning stage of my PhD study. I also want to thank Dr. Hui Shi and Dr. Yue Liu for

the fruitful scientific discussion and sharing valuable experiences in laboratory work; Stanislav Kasakov and Peter Hintermeier for the translation; Dr. Oliver Gutiérrez, Dr. Erika Ember, Dr. Maricruz Sanchez-Sanchez, Dr. Xianyong Sun, Dr. Yanzhe Yu, Dr. Lin Lin, Dr. Jiayue He, Dr. Wenhao Luo, Dr. Lei Zhong, Dr. John Ahn, Dr. Robin Kolvenbach, Moritz Schreiber, Navneet Gupta, Bo Peng, Wenji Song, Kai Sanwald, Yuanshuai Liu, Yu Lou, Guoju Yang, Yang Song, Yang Zhang, Wanqiu Luo, Sebastian Eckstein, Jennifer Hein, Andreas Ehrmaier, Sebastian Grundner, Claudia Himmelsbach, Sebastian Müller, Eva Schachtl, Maximilian Hahn, Daniel Melzer and all other members of Technische Chemie II group who I did not mention for all kinds of help.

Furthermore, China Scholarship Council (CSC) was sincerely thanked for providing me the financial support.

Last but not least, I want to thank my family, relatives and friends for their unconditional love and support.

Yuchun Zhi

February 2015

Abstract

The mechanism as well as thermodynamic and kinetic parameters of 1-propanol dehydration on HZSM-5 zeolite were elucidated. Water and 1-propanol in excess to one molecule per Brønsted acid site inhibit the reaction similarly. The decrease in rate by water is not caused by competitive adsorption, but by the more effective stabilization of adsorbed 1-propanol. Ether is formed exclusively via the associative pathway, allowing to exclude the participation of propyl carbenium ion.

Der Mechanismus und die thermodynamischen und kinetischen Parameter der Dehydratisierung von 1-Propanol am Zeolith HZSM-5 wurden untersucht. Wasser und zusätzliches 1-Propanol behindern die Reaktion gleichermaßen. Das Absinken der Reaktionsrate durch Wasser wird nicht durch kompetitive Adsorption von Wasser und 1-Propanol, sondern durch die bessere Stabilisierung von adsorbiertem 1-Propanol hervorgerufen. Ether wird ausschließlich über den assoziativen Reaktionspfad gebildet, der Propylcarbeniumion als Zwischenprodukt ausschließt.

Table of contents

Acknowledgements	i
Abstract.....	iii
Table of contents.....	vi

Chapter 1

1. Introduction.....	1
1.1 General background	2
1.2 Utilization and conversion of bioalcohols	4
1.3 Lower alcohols dehydration reaction	5
1.3.1 Zeolites.....	6
1.3.2 Methanol dehydration	8
1.3.3 Ethanol dehydration	9
1.3.4 Propanol dehydration	10
1.3.5 Butanol dehydration.....	12
1.4 Water effect on alcohol dehydration.....	14
1.4.1 Water adsorption on zeolite.....	14
1.4.2 Water effect on dehydration reaction	18
1.5 Scope of the thesis	19
1.6 References	21

Chapter 2

2. Water impact on 1-propanol dehydration: a mechanistic and kinetic study.....	25
2.1 Introduction	27
2.2 Experimental methods	28
2.2.1 Zeolite sample and AHFS treatment	28
2.2.2 Characterization methods.....	29

2.2.3 Catalytic measurements of 1-propanol dehydration	30
2.2.4 Computational methods	31
2.3. Results and discussion.....	34
2.3.1 Catalyst characterization.....	34
2.3.2 Mechanism and kinetics of 1-propanol elimination to propene.....	37
2.3.3 Mechanism and kinetics of 1-propanol dehydration to dipropyl ether	51
2.3.4 Mechanistic understanding of the kinetic attenuation effect of water	57
2.4 Conclusions	63
2.5 Appendix	65
2.6 References	69

Chapter 3

3. Ethanol conversion to propylene with enhanced stability on P and

Zr modified HZSM-5.....73

3.1 Introduction	75
3.2 Experimental section	76
3.2.1 Chemicals.....	76
3.2.2 Catalyst preparation	77
3.2.3 Catalyst characterization.....	77
3.2.4 Catalytic measurements	78
3.3 Results and discussion.....	79
3.3.1 The influence of pore confinement on products distribution.....	79
3.3.2 Reaction conditions optimizations on ethanol conversion.....	80
3.3.3 Influence of P and Zr modifications on HZSM-5 90.....	84
3.3.4 Characterization of changes of HZSM-5 after P and Zr modifications	88
3.4 Conclusions	95
3.5 Appendix	97
3.6 References	102

Chapter 4

4. Summary and conclusions104

Curriculum vitae.....107

List of publications.....108

Chapter 1

Introduction

1.1 General background

Alternative and sustainable renewable energy supply is fundamental to human development and industrial progress. Nowadays, petroleum and natural gas still remain the world's leading fuels. As the reserve of fossil fuels such as petroleum is limited and diminishing, the blooming social development and the oil consumption will prompt the price of fossil-based fuels continually rising. On the other hand, the pollution from the consumption of fossil-based fuels is leading to severely environmental problems or even undesirable effects on the world's climate [1]. In addition, there is a strong political focus on renewable biofuel alternatives. The United Nation is aiming for a reduction in greenhouse gas emissions of up to 8% by 2010 and 50-80% by 2050 [2]. All these aspects make it an urgent task to develop clean and efficient renewable energy and fuels.

One of the logical solutions to meet the growing demand for energy and chemicals is utilization of the biomass resources, since biomass is abundant, renewable and carbon-neutral in life cycle. Moreover, the combustion of biomass does not lead to the increase of CO₂ in the atmosphere, because the biomass can be photo-synthesized from CO₂ in atmosphere. Therefore, a recent emerging strategy is to develop biorefinery and biotransformation technologies to convert biomass feedstock into clean energy fuels [3]. Inter-conversion of various biomass and energy forms in the carbon cycle is illustrated in **Fig. 1.1** [3].

A major challenge in biorefinery operations is to convert a variety of biomass-derived feedstocks (such as bio-oils, aqueous sugar streams, vegetable oils, alcohols, glycerol and lignin) into fuels and chemicals in a petroleum refinery [2, 4, 5]. This process involves the *co*-feeding of biomass-derived feedstocks with petroleum feedstocks as shown in **Fig. 1.2** [5]. Zeolite-based catalysts are commonly used for fluid catalytic cracking (FCC), hydrocracking and hydrotreating process, which demonstrates the potential possibility of zeolites in sustainable production of energy and fuels from renewable biomass sources [2, 5].

Since most of the biomass-derived feedstocks are composed of carbohydrates and

the derived intermediates typically containing hydroxyl groups, hence, the selective removal of these hydroxyl groups via dehydration is one of the major challenges for production of fuels and chemicals from biomass [6-8].

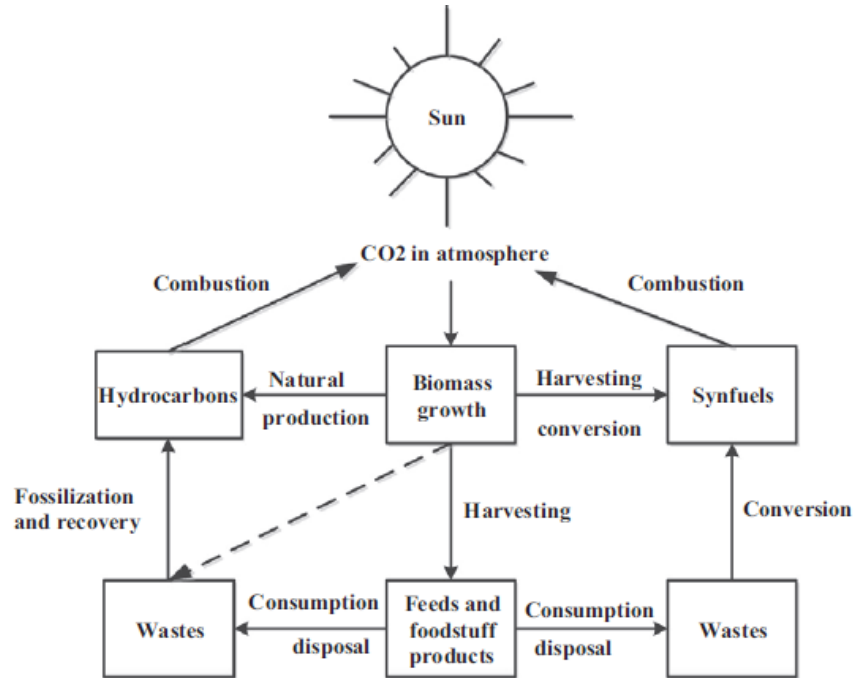


Fig. 1.1 Main features of the biomass energy technology [3].

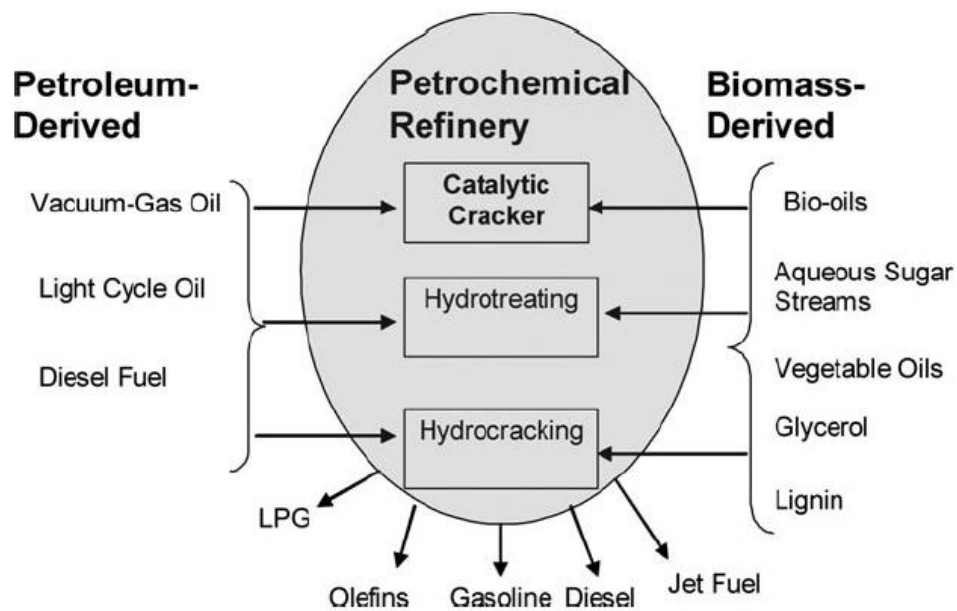


Fig. 1.2 Conversion of petrochemical- and biomass-derived feedstocks in a petroleum refinery [5].

1.2 Utilization and conversion of bioalcohols

Recently, more attention has been given to the conversion or direct utilization of bioalcohols, since these substances are not only industrially but also fundamentally important. These biomass-derived alcohols can be directly used as fuels, but also can be further transformed into high value fuels and chemicals [9, 10].

Bioalcohols, or biological produced alcohols, mainly refer to biomethanol, -ethanol, and -butanol [11]. Bioethanol is currently the most commonly used bioalcohol, especially in the USA and Brazil [10, 11]. Its main application is served as an additive in the gasoline to increase the octane number and improve the vehicle emission. In addition, bioethanol can also be transformed into many other important raw materials, such as ethylene [12, 13], propylene [14-16], acetic acid [17] et al. A series of industrially important hydrocarbons that can be produced from bioethanol are illustrated in **Fig. 1.3** [18].

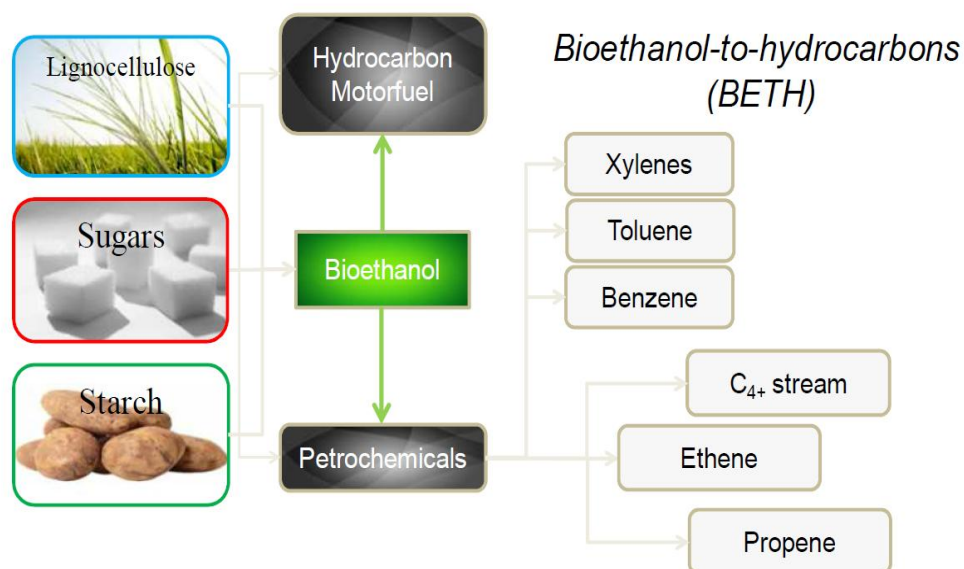


Fig. 1.3 Conversion of bioethanol to hydrocarbons [18].

As bioethanol has already been widely used as additive in the gasoline, more and more attention is being given to long-chain alcohols, which also has the potential to be used as liquid fuels, such as butanol [11]. Biobutanol can be used as the feedstock for a new route to green jet fuel [19]. As a liquid fuel, it should have a low flash point

and higher energy content. Butanol tends to have higher energy content and lower NO_x emission, but the high flash point and low production are the main disadvantages of butanol [11].

Besides fuel application, bioalcohols also show great potential as a feedstock for catalytic conversion into valuable chemicals, in the same way as conversion of fossil oil products. But challenges are still existing. Bioalcohols are mostly fermentation product from agricultural commodities and accompanied by a significant amount of water. In general, fermentation to ethanol results in mixtures containing about 95% water [20]. It can be concentrated by distillation, resulting in 4% water content. However, it is an energy-consuming and high-cost process to remove the higher than 90% percentage of water in the product mixture by distillation, and to remove the remaining 4% water requires special treatment. So it would be much more economically beneficial to convert the bioalcohols directly with large amounts of water.

1.3 Lower alcohols dehydration reaction

Among various biomass conversion processes, dehydration of alcohols represents a crucial step in the conversion of biomass to fuels and chemicals. Alcohols dehydration can be taken as a probe reaction to probe the acidity of catalysts and provide insight into mechanism of alcohols conversion. Lower alcohols are also ideal molecules to develop a basic understanding on oxygen removal since they are the least complex group of biomass-derived oxygenates.

The alcohols dehydration reaction can be accelerated by heterogeneous acidic catalysts [21]. The dehydration of lower alcohols gives alkene and ether at relatively lower temperature. The reaction occurs in the presence of Brønsted acid sites, such as perfluorinated sulfonated cation exchangers, heteropoly acids, microporous SAPO zeolites, and polyphosphoric acid [21]. Due to the well-defined microporous structure, acidity and shape selectivity, zeolites are considered to be one of the best choices as catalyst for alcohol dehydration [22].

1.3.1 Zeolites

Zeolites are crystalline aluminosilicates with well-defined three-dimensional porous structures. They are mainly composed of SiO_4 and $[\text{AlO}_4]^-$ tetrahedral units. Because the $[\text{AlO}_4]^-$ units are negative-charged, additional cations (inorganic and organic cations, such as metal ions and protons) are needed to compensate or balance the charge. If the cations are protons, the Brønsted acid sites are generated. In addition, different types of extra-framework aluminum (EFAL) species, neutral (AlOOH and $\text{Al}(\text{OH})_3$) or cationic (AlO^+ , $\text{Al}(\text{OH})^{2+}$, and AlOH^{2+}), can be formed depending on synthesis procedures and on the conditions of dehydroxylation, dealumination of zeolites by post-synthesis treatment [23-26]. EFAL species are commonly regarded as the origin for the appearance of Lewis acidity of the zeolites and also for the presence of IR hydroxyl vibrational bands at 3780 and 3656 cm^{-1} [23, 27].

The coexistence of Brønsted and Lewis acid sites is common in a large amount of zeolites. Three models have been proposed to describe the role of EFAL: (1) some EFAL species themselves can serve as catalytic sites (Lewis acid sites) [26, 28]; (2) the EFAL species can stabilize the negative charges on the lattice in the absence of acidic proton [26, 29]; (3) the synergistic effect between EFAL species and nearby Brønsted acid sites can increase acidity strength [23, 26, 30]. Recently, the combination of IR spectra of adsorbed pyridine and NH_3 and ^{27}Al MAS NMR, together with the catalytic activity of n-pentane on HZSM-5 demonstrated that the overall enhanced n-pentane cracking activity is a result of the higher constraint around the Brønsted acid site induced by the EFAL [27]. The presence of EFAL enhances the interaction of the alkane with the Brønsted acid site via dispersion forces (“solvation”), which causes the higher increase of catalytic activity [27].

Another important feature of zeolites is the porosity, which is formed by the connection of tetrahedral units [31]. The diameter of these pores (also called channels, or cavities) is about 0.1-2 nm, which is quite similar to the dimensions of organic molecules. Therefore, the unique pore structure of zeolites merely allows the certain molecules to diffuse into or out of them. On one hand, the pore allows the access of

the molecules with suitable size to the internal acid sites. On the other hand, the pore structure can select the products with particular geometry and dimension. The selectivity of the zeolite increases with decreasing pore diameter. This character is the so-called shape selectivity [32].

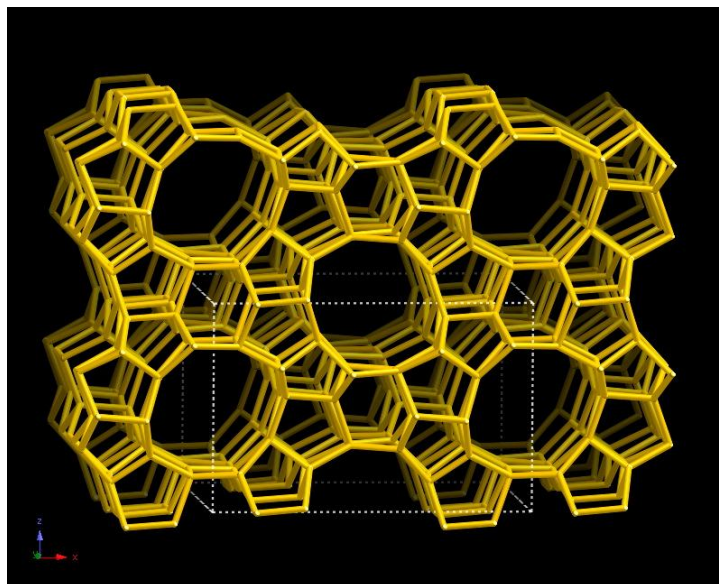


Fig. 1.4 Framework topology of HZSM-5(MFI) catalyst, showing the three dimensional channel system with 10-membered rings. The image is from the IZA website.

As a member of synthesized zeolites, ZSM-5 is characterized by an MFI structure [22]. It can be represented as $\text{Na}_n\text{Al}_n\text{Si}_{96-n}\text{O}_{192}\cdot\text{H}_2\text{O}$. Via ion exchange, Na^+ cation can be replaced by H^+ to obtain the protonic form, HZSM-5 [22]. HZSM-5 has a three-dimensional 10-member ring channel network shown in **Fig. 1.4**. Due to its well-defined topology, acidity and shape selectivity based on spatial constraints, HZSM-5 has been widely applied in the petrochemical industry, particular in a number of commercially important hydrocarbon reactions such as FCC, alkylation of aromatics, production of ethyl-benzene and xylene isomerization [31]. Recently, the zeolite catalyzed alcohols conversion is attracting more and more attention [7, 13, 14]. HZSM-5 was selected as an effective catalyst for the conversion of oxygen containing compounds, especially for dehydration reaction [6, 31].

1.3.2 Methanol dehydration

Dimethyl ether (DME) can be formed via methanol bimolecular dehydration reaction. DME has recently attracted a worldwide attention not only as an alternative clean diesel fuel due to its high thermal efficiencies and low nitrogen oxides emissions [33], but also as a very useful chemical intermediate for the preparation of many important chemicals [34, 35].

The simple pathway for methanol dehydration to form DME can be described as follows:



The mechanism of methanol dehydration on solid acids is still on dispute; and different mechanisms have been proposed for DME synthesis in the literatures. Bandiera and Naccache have suggested that methanol dehydration occurs at the BAS and its adjacent LAS via formation of the two surface species $[\text{CH}_3\cdot\text{OH}_2]^+$ and $[\text{CH}_3\text{O}]^-$ [36]; Kubelková has illustrated that methanol is initially adsorbed at the acid site, then the methoxonium ion (CH_3OH_2^+) is formed via protonation etc. [37]. Recently, Iglesia confirmed that the associative route, that is protonated methanol dimer ($\text{CH}_3\text{OH}\cdot\text{H}^+\cdot\text{CH}_3\text{OH}$) forms DME directly in one step, prevails on zeolites [38] and polyoxometalates [39] on the basis of kinetic analysis.

Another important route for the methanol conversion is the methanol-to-hydrocarbons (MTH) process. MTH is the key step of methanol conversion into other important chemicals. Based on the main products, MTH can be classified into production of gasoline-rich products (MTG) process and production of olefin-rich products (MTO) process.

MTG process mainly consists of two steps: firstly, the crude methanol is dehydrated in an adiabatic reactor over acidic catalyst into DME and water. Then, DME will be further converted into $\text{C}_1\text{-C}_{11}$ hydrocarbons in the adiabatic reactor. The MTG process is typically catalyzed by HZSM-5 at 300-400°C under the pressure around 20 bar. Since the reaction is strongly exothermic, the byproducts are recycled

to dilute the feed to control the temperature [35].

MTO process is another effective zeolite catalyzed reaction of methanol conversion that has come into industrial use [40]. Typically MTO process is catalyzed by HSAPO-34 with selectivity to light olefins (ethene and propene) over 80%. Compared to HZSM-5, coking on HSAPO-34 is faster, so the process requires the frequent catalyst regeneration. Furthermore, in order to enhance the selectivity of light olefins, the MTO process is usually combined with an olefin cracking process (OCP) [40].

In parallel to the MTO process, HZSM-5 catalyzed methanol-to-propene (MTP) process focuses on improving the yield of propene. The process is designed to consist of a parallel fixed bed quench reactor to recycle ethylene and C₄₊ products. The reaction condition is typically set at 460-480°C under atmospheric pressure [35].

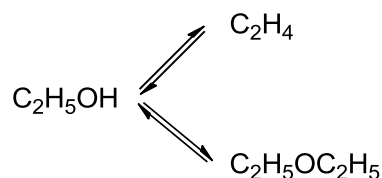
1.3.3 Ethanol dehydration

As the most commonly used bioalcohol [10, 11], ethanol can not only be used as additive in the gasoline, but also be used to produce more valuable hydrocarbon compounds, especially the dehydration product, ethylene. Ethylene is one of the most important raw materials in the petrochemical industry that can be used to synthesize a wide range of organic compounds, including acetaldehyde, acetic acid, ethylene oxide, ethylene glycol, etc [13].

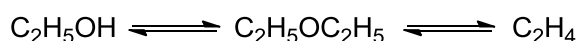
At present, about 99% of the global ethylene is produced by hydrocarbon cracking [12]. Because of the demand of fuels increased year by year, the research of alternative renewable energy source has attracted more and more attention. Additionally, to make ethanol dehydration more industry-friendly, many researchers have investigated different catalysts to increase ethylene yield and to lower the reaction temperature [12].

Catalytic dehydration of ethanol to ethylene over zeolites is the earliest used process in the industry. It is generally agreed that the conversion of ethanol to ethylene can take place via three kinds of routes: parallel reactions, a series of reactions and a parallel series reactions [13] (**Fig. 1.5**).

1. Parallel reactions



2. A series of reactions



3. A parallel series reactions

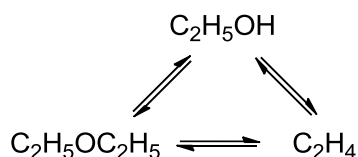


Fig. 1.5 Reaction routes of ethanol dehydration [13].

Ethanol dehydration is often chosen as probe reaction to develop the basic understanding of the dehydration mechanism [41]. Some studies [42, 43] showed that the dehydration is started with the direct interaction of the hydroxyl group of ethanol with the BAS of zeolite, then the adsorbed ethanol can dehydrate to a surface-bonded ethoxide species, and finally the ethoxide intermediate will be converted to ethylene via deprotonation.

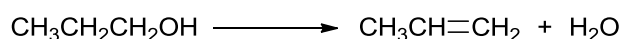
1.3.4 Propanol dehydration

1-propanol and 2-propanol can be obtained via fermentation pathway from agricultural commodities. They can be used to produce propene, which is fundamental to chemical industry. A variety of catalysts have been investigated to forward the dehydration of propanol. Bond et al. and Dias et al. studied the kinetic of heteropoly acid H₃PW₁₂O₄₀ (HPW) catalyzed 1-propanol and 2-propanol dehydration respectively [44, 45]. The results indicate that on the bulk catalysts, 2-propanol

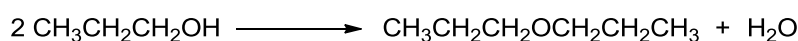
dehydration is suggested to occur via E1 elimination pathway, whereas on the supported catalysts it might also involve the contribution of E2 elimination pathway [45]. Mourgues et al. performed the dehydration of 2-propanol over alumina, and modified silica-alumina catalysts, which showed that silica-alumina catalysts have a higher activity than alumina, silica or sodium silica-alumina [46].

Like ethanol, the dehydration of 1-propanol can also take place by intra-molecular reaction to propene and inter-molecular reaction to dipropyl ether.

Intra-molecular dehydration:



Inter-molecular dehydration:



According to previous studies [42, 43, 47], the reaction is initiated by the direct interaction of the hydroxyl group of 1-propanol with the BAS to form alcohol-zeolite adsorption complex [48, 49]. 1-propanol can be absorbed via physisorption or protonated chemisorption over BAS and both structures are stabilized by hydrogen bonding shown in **Fig. 1.6** [50].

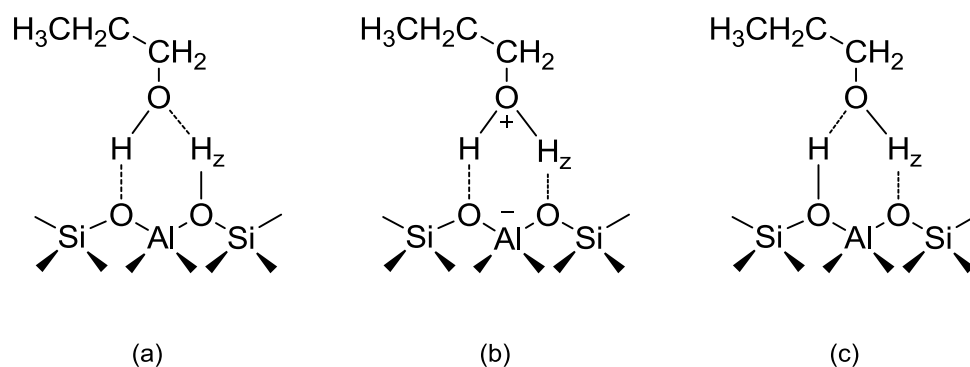


Fig. 1.6 1-propanol-zeolite adsorption complex via physisorption (a, c) and protonated chemisorption (b). H_z: proton of zeolite [50].

The intra-molecular dehydration of 1-propanol proceeds via E1 or E2 mechanisms. E1 mechanism refers to a unimolecular elimination reaction, which can be divided into two steps: the hydroxyl group leaves first to form a propoxide as the reaction intermediate via the carbocation transition state, then the β-hydrogen is lost quickly to

generate propene. The first step is the rate-limiting step for the overall reaction. E2 mechanism refers to a concerted reaction pathway for unimolecular elimination reaction. The reaction is finished only in one step, which means the loss of β -hydrogen and hydroxyl group happens at the same time.

The inter-molecular dehydration has been supposed under the S_N1 or S_N2 mechanisms. The S_N1 mechanism refers to nucleophilic substitution reaction, which can also be divided into two steps: loss of the leaving group to generate a propoxide intermediate and nucleophile attack on the propoxide to form the ether. S_N2 mechanism refers to a bimolecular nucleophilic substitution reaction. In the S_N2 mechanism, the nucleophile attack and the loss of the leaving group proceed concomitantly, and there's no propoxide intermediate generated in the reaction.

The overall mechanism for 1-propanol dehydration is suggested in **Fig. 1.7** on basis of the proposed ethanol dehydration pathway [39].

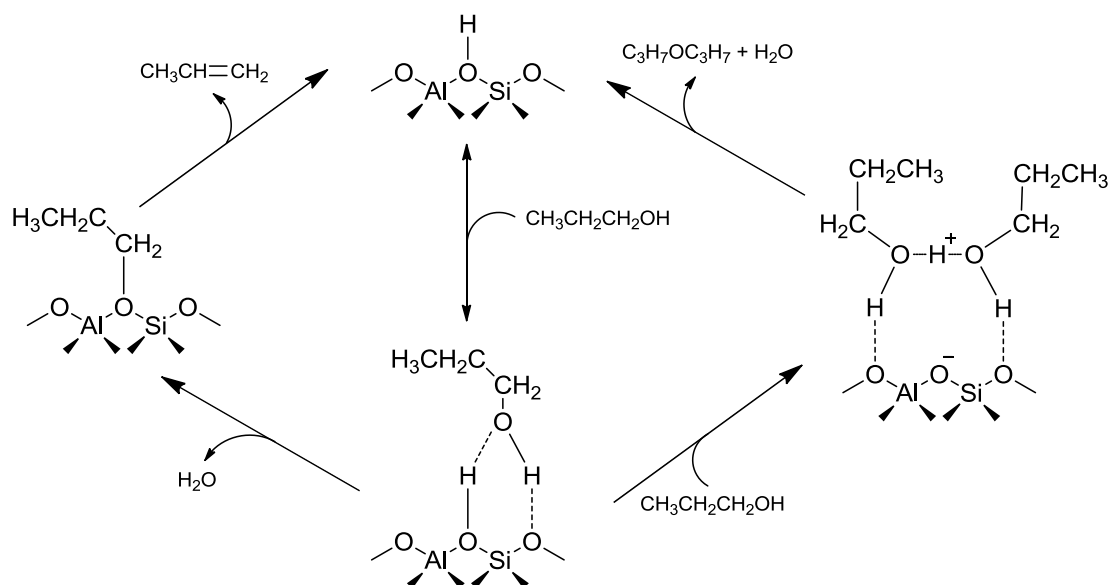


Fig. 1.7 Favored reaction pathways for 1-propanol intra- and inter-molecular dehydration.

1.3.5 Butanol dehydration

Beside ethanol, butanol is another potential product produced by fermentation of the biomass feedstocks. As biofuel, butanol can be used to blend with gasoline as well, with higher energy density and higher octane number [11]. Furthermore, 1-butanol can

be upgraded to high-octane gasoline by catalytic conversion over HZSM-5. The recent interest on 1-butanol is focused on the conversion of 1-butanol to green jet fuel (**Fig. 1.8**) [19].

The dehydration of all various butanol is of great academic interest, besides industrial importance. Due to the comparable molecular dimension of butanol with the diameter of zeolite pores, the study of butanol dehydration can help to understand the adsorption and dehydration reaction mechanism on zeolite as well as the influence of shape selectivity and pore confinement of zeolite on the reaction pathways and the intermediates [51, 52].

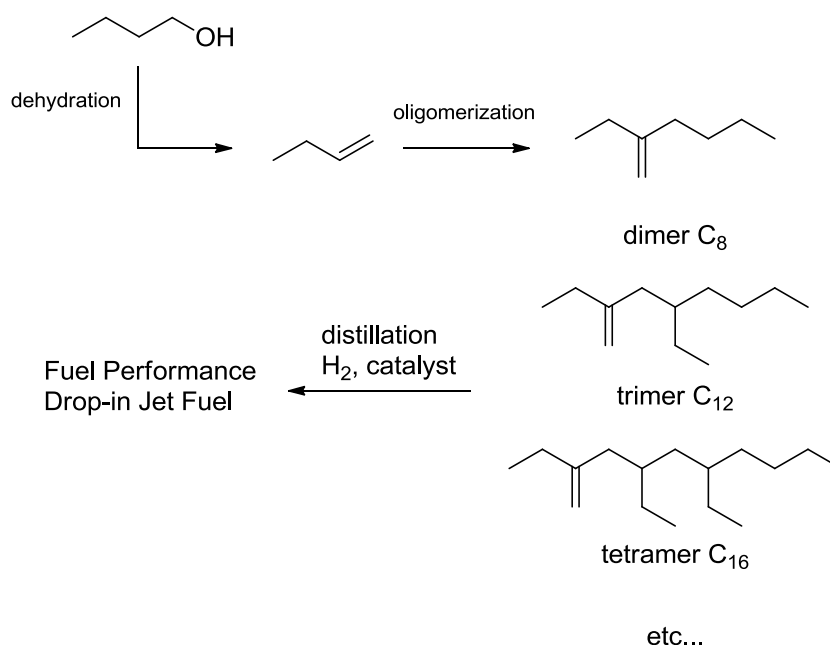


Fig. 1.8 A new route to produce jet fuel from 1-butanol [19].

By means of kinetic studies, Makarova et al.[53] found that the activation energy of butene formation direct from *n*-butanol and from *n*-dibutyl ether is identical. The pore confinement can influence the reaction pathways by changing the diffusion of the product. The diffusion rate of the product may result in shifting the reaction equilibrium to alter the product selectivity or even the blocking the active sites resulting from the lower mobility of product. The previous studies have investigated the influence of different crystallite size on the dehydration rates of butanol (*n*-butanol

and *iso*-butanol) [54]. The results indicate that the dehydration rate is independent on the crystallite size, but the oligomerization rate is reduced significantly with decreasing crystallite size, owing to the oligomerization of butene proceeds inside the pore and diffusion path is shortened apparently with the decreasing of crystallite size.

1.4 Water effect on alcohol dehydration

As mentioned above, bioalcohols are mostly obtained from biomass fermentation; they are produced usually accompanying by a significant amount of water. Furthermore, water is also the byproduct of the bioalcohols dehydration. Therefore the effect of water on the alcohol dehydration should be studied intensively.

1.4.1 Water adsorption on zeolite

Water can be adsorbed on the acid sites of zeolite via forming hydrogen bonding. Experimental evidence shows that the water adsorption on the zeolite decreases with decreasing aluminum content [55]. According to previous studies, there are several possibilities existing for the water interaction with BAS of the zeolite. Jentys et al. [55] has suggested that water may adsorb as protonated form (H_3O^+) or as cluster of more water molecules on HZSM-5. Furthermore, at higher water equilibrium pressure, it tends to form larger cluster of water molecules, the number of water molecules in the cluster is dependent on the water equilibrium pressure (**Fig. 1.9**).

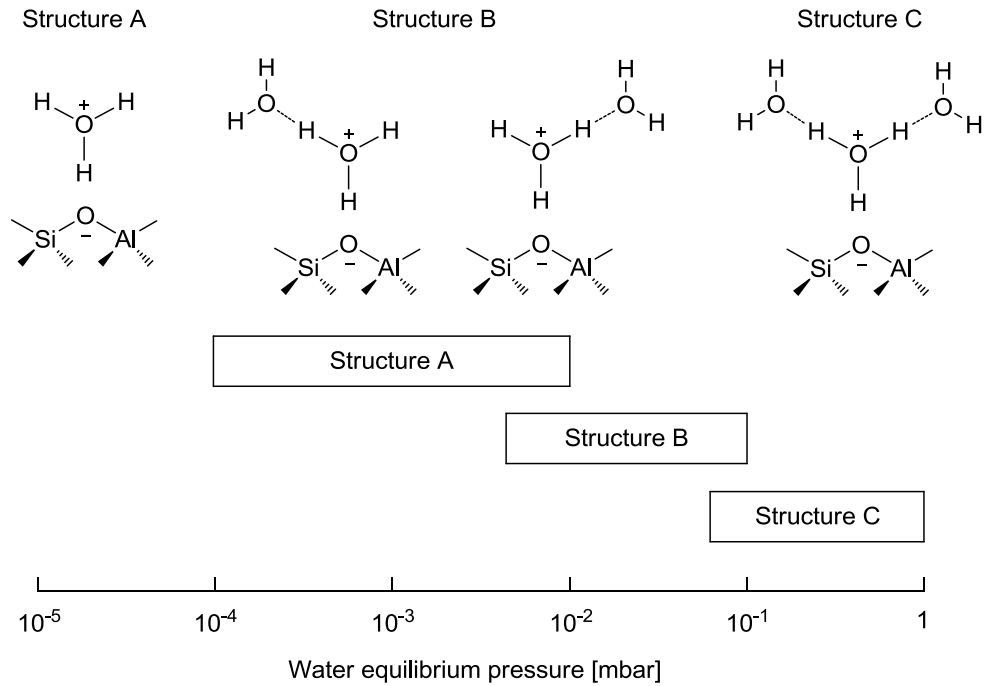


Fig. 1.9 Adsorbate structures of water on HZSM-5 with increasing water equilibrium pressure [55].

Besides, Smith et al. [56] and Sauer et al. [57] have also suggested another bridging water adsorption model on zeolite and silicoaluminophosphate (SAPO) catalysts through ab initio simulation. In this model, the hydrogen of water can be bond to the zeolitic OH group to form a neutral complex or the hydroxonium ion that attaches to the negatively charged zeolite surface to form an ion pair structure. The adsorption structures are shown in **Fig. 1.10**.

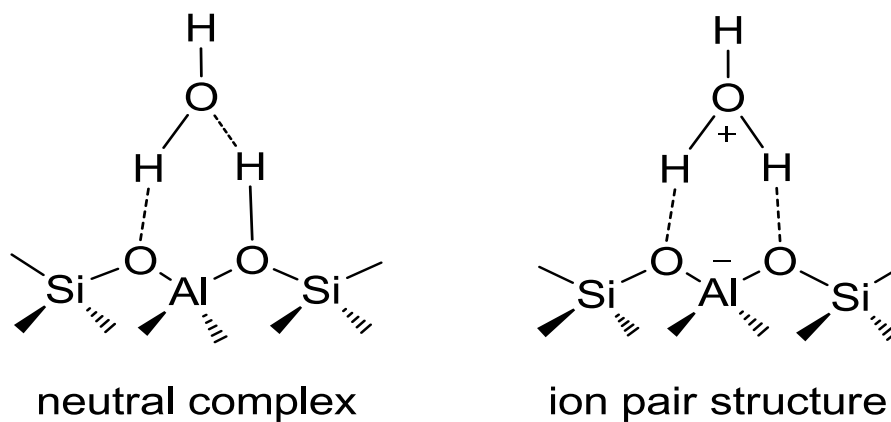


Fig. 1.10 Interaction structures of water adsorption on zeolite [56, 57].

According to *ab initio* studies, the hydrogen bonded complex is the only stable structure, while the hydroxonium ion pair is only a transition structure, but the potential energy difference between them is only 10 kJ mol⁻¹ [57]. This small energy difference can be easily achieved by adsorbing more water molecules per BAS. Furthermore, the results of quantum mechanics have confirmed that water can be adsorbed as cluster of four water molecules on each BAS [58].

Although both adsorbed water structures can be proven by powder neutron diffraction [56], it is still not accessible by diffraction experiments averaging over all sites, because the calculations neglect the possibility of multiple hydrogen bonds and long-range interaction with the lattice. To simulate the water adsorption in a narrow microporous structure, Termath et al. [59] used an eight-membered ring channel of HSAPO-34 for the study. **Fig. 1.11** represents the eight-membered ring channel filled by one, two and three water molecules. With respect to the adsorption with less than three water molecules, the protonated water cluster is unstable, resulting in a spontaneous dissociation of hydronium ions. The protonated cluster as well as the ion pair structure can be stabilized by formation of H₃O⁺(H₂O)_n cluster, among them H₃O⁺(H₂O)₂ is the first stable protonated cluster [59].

For one water molecule adsorption, two hydrogen bonds are formed for the interaction of water with the BAS (**Fig. 1.11a**) [59]. Note that this structure is always a “disorder” pair, and the H-O distances of hydrogen bonds are different. For the adsorption of two water molecules, a very short-lived H₅O₂⁺ type complex appears. This H₅O₂⁺ type complex is just a transition structure with 18 kJ mol⁻¹ higher energy than the neutral stable complex [59]. In the stable structure (**Fig. 1.11b**), the dimer of water molecules is stabilized by two short and two long hydrogen bonds with oxygen of catalyst, while the two water molecules are also bonded by hydrogen bond. So there are a total of five hydrogen bonds stabilizing the two water molecules in the eight-membered ring. For the adsorption of three water molecules (**Fig. 1.11c**), the trimer of water molecules is stabilized by three hydrogen bonds, and the first stable protonated cluster (H₃O⁺(H₂O)₂) is formed [59]. The protonation equilibrium of the cluster is determined by acidic strength of the solid acid, proton affinity and relative

stabilization of the water cluster [59].

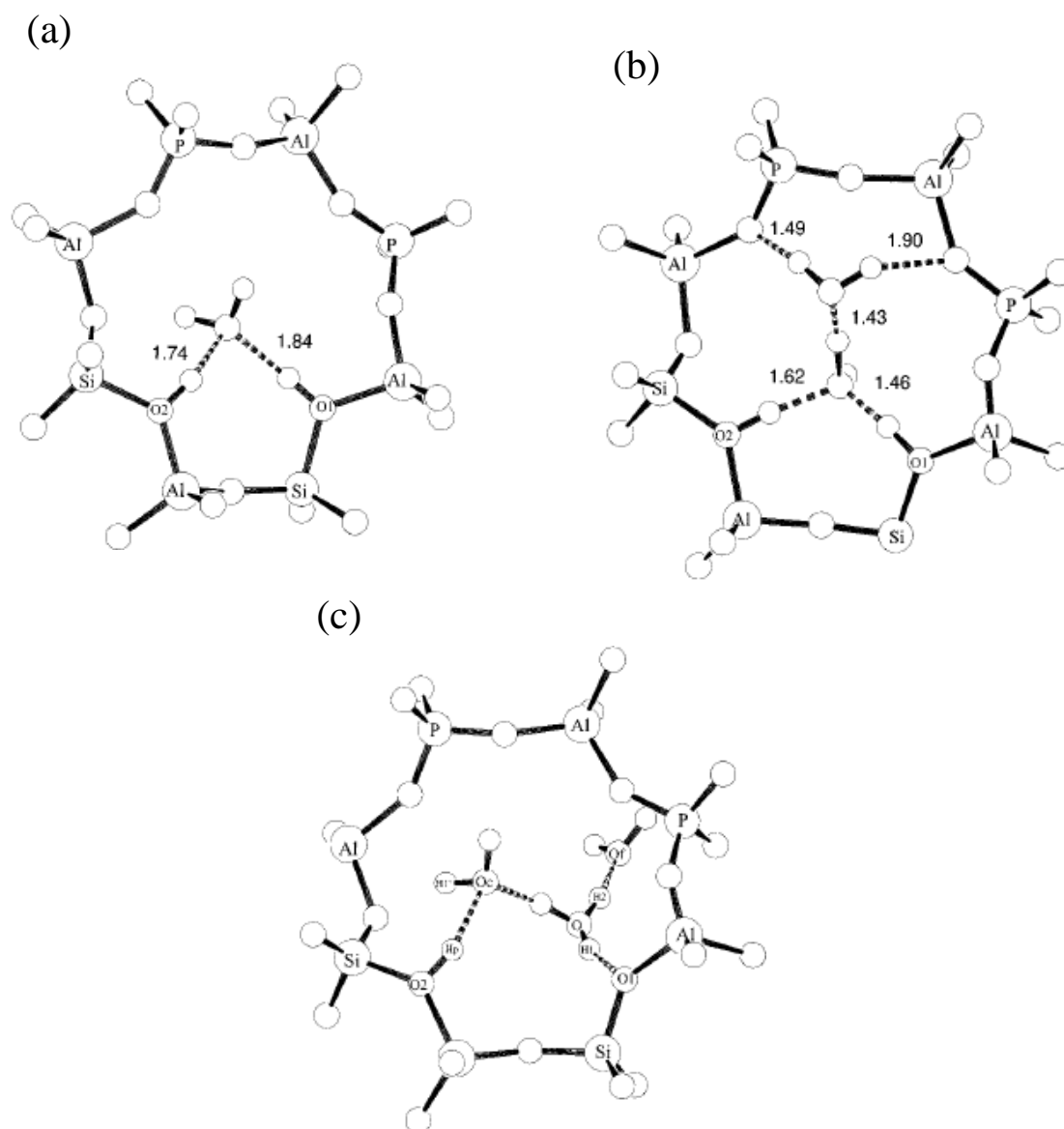


Fig. 1.11 An eight-ring channel of HSAPO-34 filled by one (a), two (b) and three (c) water molecules [59].

1.4.2 Water effect on dehydration reaction

The water in the bioalcohols dehydration is mainly derived from two sources: produced during fermentation in significant amounts and generated during the dehydration in stoichiometric amounts. For the kinetic study, the reaction conversion is usually lower than 10%. As a result, the effect of water as a byproduct is often ignored.

Water has been observed to exert inhibition effect on the process of methanol and ethanol transformation to hydrocarbons over zeolite catalysts [60, 61]. It was found that the kinetic of methanol dehydration is attenuated by the presence of water. Bilbao and coworkers used a kinetic model to quantify the inhibition effect of water content on the conversion kinetics of ethanol to ethylene over HZSM-5 zeolites [61]. Moreover, high water content can also significantly suppress the ethanol dehydration. It was found that in the $\text{TiO}_2/\text{Al}_2\text{O}_3$ catalyzed ethanol dehydration, if water content increases from 5 to 90 wt%, the ethanol conversion will decrease from 86 to 65 wt% [62]. This retard effect of water can be weakened by raise the reaction temperature. However, in the case of zeolite, high temperature favors secondary reactions, such as oligomerization and cracking [62]. Therefore, development of the catalysts with good resistance to water is necessary and crucial for the biomass conversion in the presence of water. Resasco and co-workers have showed a viable route that zeolite catalysts after hydrophobic modifications can prevent the structure degradation in an aqueous solvent environment [63, 64].

Besides, water can influence the methanol and ethanol dehydration not only on reaction rate, but also on the product distribution. It was observed that with increasing water content the yield of olefin increases, but the yield of other byproducts like aromatics and coke decreases [65].

So far, most of the observed effect is that water acts as an inhibitor in the dehydration reaction. But recently, Chen et al. [66] reported that water may also enhance the reaction rate in the zeolite-based reactions. In the reactions involving hydrophobic reactants, like isobutane, water may act as an active participant in

stoichiometric amounts by stabilizing the transition state.

1.5 Scope of the thesis

As the less complex group of biomass-derived oxygenates, 1-propanol dehydration was chosen as a probe reaction to develop the basic understanding on the mechanism and kinetics of oxygen removal via dehydration reaction, especially on the kinetic attenuation effect of water. In this doctoral thesis, the reaction mechanism and kinetics of 1-propanol dehydration to form propene and dipropyl ether was systematically investigated. In terms of the kinetics data and DFT calculation results, water inhibiting effect on dehydration reaction was clarified.

Prior to carrying out the dehydration reaction, the ZSM-5 catalyst was first carefully treated by AHFS to remove the extra-framework aluminum, which allows to specifically assess the mechanism and kinetics of alcohol dehydration reaction taking place on bare BAS in the absence of synergistic effect exerted by the LAS.

The substantial efforts has been devoted to investigate the mechanism of alcohols dehydration via theory or experiment, however, the theory only focuses on microscopic aspects and most of the experiments were performed under relatively low pressure range. Hence, the first part of this work is aiming to address the reaction rate dependence on reactant pressure with largely extended reactant pressure range. Based on the kinetic results, the mechanism for 1-propanol dehydration to propene has been newly developed and was further confirmed by accurate kinetic analysis. In light of the new reaction mechanism for propene formation, the rate equation was also derived on basis of elementary steps. Additionally, associative route prevails for 1-propanol dimolecular dehydration to form dipropyl ether, a conclusion achieved by the accurate analysis of the turnover rate dependence on reactant pressure.

The competitive adsorption between alcohol and water was one of the common reasons to explain the inhibiting effect of water. Herein, calorimetry and infrared spectroscopy, taken together with the DFT calculation, were used to unravel the interactions between 1-propanol, water and acid sites of zeolite. The results

demonstrate that the competitive adsorption between 1-propanol and water does not exist. Consequently, the attenuating effect of water on the dehydration reaction lies in the kinetic process. The kinetic and thermodynamic parameters at different reaction temperatures were estimated in terms of the mechanism-derived rate equation to evaluate the kinetic influence of introduced water. In addition to the detailed kinetic analysis, the microscopic DFT calculation was also used to provide insights into the dehydration mechanism and water impact on dehydration diagram. The combination of the kinetic assessment and DFT calculation suggests that thermodynamics of adsorption governs the inhibition of water more than the kinetics of dehydration.

1.6 References

- [1] A.J. Ragauskas, C.K. Williams, B.H. Davison, G. Britovsek, J. Cairney, C.A. Eckert, W.J. Frederick, J.P. Hallett, D.J. Leak, C.L. Liotta, J.R. Mielenz, R. Murphy, R. Templer, T. Tschaplinski, *Science*, 311 (2006) 484-489.
- [2] M. Stocker, *Angew. Chem. Int. Edit.*, 47 (2008) 9200-9211.
- [3] O. Ellabban, H. Abu-Rub, F. Blaabjerg, *Renew. Sust. Energ. Rev.*, 39 (2014) 748-764.
- [4] L. Petrus, M.A. Noordermeer, *Green Chem.*, 8 (2006) 861-867.
- [5] G.W. Huber, A. Corma, *Angew. Chem. Int. Edit.*, 46 (2007) 7184-7201.
- [6] H. Chiang, A. Bhan, *J. Catal.*, 271 (2010) 251-261.
- [7] M. Bjorgen, S. Svelle, F. Joensen, J. Nerlov, S. Kolboe, F. Bonino, L. Palumbo, S. Bordiga, U. Olsbye, *J. Catal.*, 249 (2007) 195-207.
- [8] C. Zhao, S. Kasakov, J.Y. He, J.A. Lercher, *J. Catal.*, 296 (2012) 12-23.
- [9] M.X. Wang, Y.H. Chen, X.F. Xia, J. Li, J.G. Liu, *Bioresour. Technol.*, 163 (2014) 74-81.
- [10] L. Luo, E. van der Voet, G. Huppes, *Renew. Sust. Energ. Rev.*, 13 (2009) 1613-1619.
- [11] C. Jin, M.F. Yao, H.F. Liu, C.F.F. Lee, J. Ji, *Renew. Sust. Energ. Rev.*, 15 (2011) 4080-4106.
- [12] D. Fan, D.J. Dai, H.S. Wu, *Materials*, 6 (2013) 101-115.
- [13] M.H. Zhang, Y.Z. Yu, *Ind. Eng. Chem. Res.*, 52 (2013) 9505-9514.
- [14] W. Xia, A. Takahashi, I. Nakamura, H. Shimada, T. Fujitani, *J. Mol. Catal. A: Chem.*, 328 (2010) 114-118.
- [15] Z.X. Song, A. Takahashi, N. Mimura, T. Fujitani, *Catal. Lett.*, 131 (2009) 364-369.
- [16] Z.X. Song, A. Takahashi, I. Nakamura, T. Fujitani, *Appl. Catal. A: Gen.*, 384 (2010) 201-205.
- [17] V.V. Brei, M.E. Sharanda, S.V. Prudius, E.A. Bondarenko, *Appl. Catal. A: Gen.*, 458 (2013) 196-200.

- [18] V.G. K. van der Borgh, G. B. Marin, i-SUP, Bruges, Belgium, (2012).
- [19] M.E. Wright, B.G. Harvey, R.L. Quintana, *Energ. Fuel*, 22 (2008) 3299-3302.
- [20] J.C. Oudejans, P.F. Vandenoosterkamp, H. Vanbekkum, *Appl. Catal.*, 3 (1982) 109-115.
- [21] R.V. Ermakov, V.A. Plakhotnik, *Petrol. Chem.*, 48 (2008) 1-5.
- [22] G. Busca, *Chem. Rev.*, 107 (2007) 5366-5410.
- [23] Q.L. Wang, G. Giannetto, M. Guisnet, *J. Catal.*, 130 (1991) 471-482.
- [24] D. Coster, A.L. Blumenfeld, J.J. Fripiat, *J. Phys. Chem.*, 98 (1994) 6201-6211.
- [25] R.J. Pellet, C.S. Blackwell, J.A. Rabo, *J. Catal.*, 114 (1988) 71-89.
- [26] S.H. Li, A.M. Zheng, Y.C. Su, H.L. Zhang, L. Chen, J. Yang, C.H. Ye, F. Deng, *J. Am. Chem. Soc.*, 129 (2007) 11161-11171.
- [27] S. Schallmoser, T. Ikuno, M.F. Wagenhofer, R. Kolvenbach, G.L. Haller, M. Sanchez-Sanchez, J.A. Lercher, *J. Catal.*, 316 (2014) 93-102.
- [28] R. Carvajal, P.J. Chu, J.H. Lunsford, *J. Catal.*, 125 (1990) 123-131.
- [29] J.H. Lunsford, *J. Phys. Chem.*, 72 (1968) 4163-&.
- [30] P.O. Fritz, J.H. Lunsford, *J. Catal.*, 118 (1989) 85-98.
- [31] E. Taarning, C.M. Osmundsen, X.B. Yang, B. Voss, S.I. Andersen, C.H. Christensen, *Energ. Environ. Sci.*, 4 (2011) 793-804.
- [32] C. Fernandez, I. Stan, J.P. Gilson, K. Thomas, A. Vicente, A. Bonilla, J. Perez-Ramirez, *Chem. Eur. J.*, 16 (2010) 6224-6233.
- [33] K.W. Jun, H.S. Lee, H.S. Roh, S.E. Park, *B Korean. Chem. Soc.*, 24 (2003) 106-108.
- [34] S.R. Blazzkowski, R.A. vanSanten, *J. Am. Chem. Soc.*, 118 (1996) 5152-5153.
- [35] U. Olsbye, S. Svelle, M. Bjorgen, P. Beato, T.V.W. Janssens, F. Joensen, S. Bordiga, K.P. Lillerud, *Angew. Chem. Int. Edit.*, 51 (2012) 5810-5831.
- [36] J. Bandiera, C. Naccache, *Appl. Catal.*, 69 (1991) 139-148.
- [37] L. Kubelkova, J. Novakova, K. Nedomova, *J. Catal.*, 124 (1990) 441-450.
- [38] A.J. Jones, E. Iglesia, *Angew. Chem. Int. Edit.*, 53 (2014) 12177-12181.
- [39] R.T. Carr, M. Neurock, E. Iglesia, *J. Catal.*, 278 (2011) 78-93.
- [40] D.S. Wragg, M.G.O. Brien, F.L. Bleken, M. Di Michiel, U. Olsbye, H. Fjellvag,

- Angew. Chem. Int. Edit., 51 (2012) 7956-7959.
- [41] J. Macht, M.J. Janik, M. Neurock, E. Iglesia, Angew. Chem. Int. Edit., 46 (2007) 7864-7868.
- [42] J.N. Kondo, D. Nishioka, H. Yamazaki, J. Kubota, K. Domen, T. Tatsumi, J. Phys. Chem. C, 114 (2010) 20107-20113.
- [43] W. Wang, J. Jiao, Y.J. Jiang, S.S. Ray, M. Hunger, Chem. Phys. Chem., 6 (2005) 1467-1469.
- [44] J.A. Dias, S.C.L. Dias, N.E. Kob, J. Chem. Soc. Dalton, (2001) 228-231.
- [45] G.C. Bond, S.J. Frodsham, P. Jubb, E.F. Kozhevnikova, I.V. Kozhevnikov, J. Catal., 293 (2012) 158-164.
- [46] F.P. L. de Mourgues, Y. Trambouze, M. Prettre, J. Catal., 7 (1967) 117-125.
- [47] J. Ouyang, F.X. Kong, G.D. Su, Y.C. Hu, Q.L. Song, Catal. Lett., 132 (2009) 64-74.
- [48] K.I. Zamaraev, J.M. Thomas, Adv. Catal., 41 (1996) 335-358.
- [49] J. Kotrla, D. Nachtigallova, L. Kubelkova, L. Heeribout, C. Doremieux-Morin, J. Fraissard, J. Phys. Chem. B, 102 (1998) 2454-2463.
- [50] C.M. Nguyen, M.F. Reyniers, G.B. Marin, Phys. Chem. Chem. Phys., 12 (2010) 9481-9493.
- [51] C. Williams, M.A. Makarova, L.V. Malysheva, E.A. Paukshtis, E.P. Talsi, J.M. Thomas, K.I. Zamaraev, J. Catal., 127 (1991) 377-392.
- [52] M.A. Makarova, E.A. Paukshtis, J.M. Thomas, C. Williams, K.I. Zamaraev, J. Catal., 149 (1994) 36-51.
- [53] M.A. Makarova, C. Williams, J.M. Thomas, K.I. Zamaraev, Catal. Lett., 4 (1990) 261-264.
- [54] M.A. Makarova, C. Williams, V.N. Romannikov, K.I. Zamaraev, J.M. Thomas, J. Chem. Soc. Faraday T, 86 (1990) 581-584.
- [55] G.W. A. Jentys, M. Derewinski, J. A. Lercher, J. Phys. Chem., 93 (1989) 4837-4843.
- [56] L. Smith, A.K. Cheetham, R.E. Morris, L. Marchese, J.M. Thomas, P.A. Wright, J. Chen, Science, 271 (1996) 799-802.

- [57] J. Sauer, *Science*, 271 (1996) 774-775.
- [58] D.H. Olson, S.A. Zygmunt, M.K. Erhardt, L.A. Curtiss, L.E. Iton, *Zeolites*, 18 (1997) 347-349.
- [59] V. Termath, F. Haase, J. Sauer, J. Hutter, M. Parrinello, *J. Am. Chem. Soc.*, 120 (1998) 8512-8516.
- [60] A.G. Gayubo, A. Alonso, B. Valle, A.T. Aguayo, J. Bilbao, *Ind. Eng. Chem. Res.*, 49 (2010) 10836-10844.
- [61] A.G. Gayubo, A.T. Aguayo, M. Castilla, A.L. Moran, J. Bilbao, *Chem. Eng. Commun.*, 191 (2004) 944-967.
- [62] N.K. Kochar, R. Merims, A.S. Padia, *Chem. Eng. Prog.*, 77 (1981) 66-70.
- [63] P.A. Zapata, Y. Huang, M.A. Gonzalez-Borja, D.E. Resasco, *J. Catal.*, 308 (2013) 82-97.
- [64] P.A. Zapata, J. Faria, M.P. Ruiz, R.E. Jentoft, D.E. Resasco, *J. Am. Chem. Soc.*, 134 (2012) 8570-8578.
- [65] J. Schulz, F. Bandermann, *Chem. Eng. Technol.*, 17 (1994) 179-186.
- [66] K.Z. Chen, J. Damron, C. Pearson, D. Resasco, L. Zhang, J.L. White, *Acs. Catal.*, 4 (2014) 3039-3044.

Chapter 2

Water impact on 1-propanol dehydration: a mechanistic and kinetic study

1-propanol dehydration to form propene and DPE was systematically measured at varying 1-propanol pressure (0.075-4 kPa) and temperature (413-443 K). New mechanism for propene formation, that is propene is not only originated from 1-propanol monomer but can also be derived from the 1-propanol dimer, is proposed on basis of kinetic analysis of the rate dependence on reactant pressure. The consistency of the mechanism-derived rate expression with the measured propene rates supports this proposal. The preference adsorption of 1-propanol over water based on the calorimetric and IR measurement allows us to conclude that the inhibiting effect/decreased dehydration rate is not a consequence of competitive adsorption between 1-propanol and water. The kinetic and thermodynamic parameters estimated on basis of the mechanism-derived rate equation were used to assess the kinetic attenuation effect of water. And the results reveal that the kinetic

attenuation impact of water is related to the different extent of solvation effect of water on adsorption intermediate and transition state. Water appears to significantly more stabilize the adsorbed 1-propanol than the transition state, leading to the higher activation barrier for elimination step, in a manner consistent with the inhibiting effect of additional 1-propanol in 1-propanol dimer to propene route.

2.1 Introduction

Dehydration is a highly important reaction involved in converting of biomass derived mono-alcohols, polyols, and phenols, for example, dehydration of bio-ethanol to a bulk chemical bio-ethene [1, 2], selective dehydration and hydrogenation or hydrogenolysis of glycerol to valuable fine chemicals [3-5] or hydrogenation-dehydration of phenols to cycloalkanes [6]. As a model compound, the catalytic conversion of 1-propanol has been widely explored with metal or acid sites, e.g., with Pt/C and Pt/Al₂O₃ catalysts via the hydrogenation/dehydrogenation and dehydration route [7, 8] or with HZSM-5 via the dehydration and oligomerization reactions [9, 10].

Previous work [11] reported that the addition of pyridine to HZSM-5 (adsorbing onto the acid sites) poisoned the dehydration, and Brønsted acidic sites on HZSM-5 are active sites for intra- and inter- molecular dehydration producing respective alkenes and ethers. Gorte et al. [12] reported that the concentration of adsorbed alcohol molecules corresponds to the aluminum concentration in the zeolite lattice. In a previous study with C3 alcohols on Pt/Al₂O₃ catalysts [8], it was reported that Brønsted and Lewis acid sites were both active sites for dehydration at the gas solid interface, but in the aqueous phase Brønsted acid sites were more effective for dehydration due to the water caused rehydration transformation on Lewis acid sites [8].

Two models for water adsorption over H-form zeolites have been proposed: i) hydrogen-bonded, and ii) protonated complex. As one or two water molecules are adsorbed on HZSM-5, adsorption is consistently accepted to start via forming the hydrogen bond [13, 14]. But the proposed transitional structures have been controversially discussed when more water molecules are adsorbed. Dimeric H₅O₂⁺ and polymeric H₅O₂⁺ • n(H₂O) species have been proposed as adsorbed complexes [14-16]. Later studies concluded in contrast that the hydrogen-bonded structure was more stable than the protonated complex [17-19]. However, both the

hydrogen-bonded and protonated structures have been claimed to simultaneously exist having comparable adsorption energies [14, 20]. It is reported that water influences kinetics of alcohol dehydration by competing with reactants [21, 22] or reaction intermediate oxonium ions [23] for acid sites. With respect to the reaction of transformation of bioethanol into olefins [24], water was found to attenuate the rate of each step in the kinetic scheme, except the dehydration of ethanol.

In this contribution, low temperature catalyzed 1-propanol dehydration reaction on HZSM-5 was systematically explored. The mechanism for propene formation has been newly developed. The nature of the interaction of 1-propanol and water with HZSM-5 is studied via in situ IR spectroscopy as well as calorimetric measurements. The effect of water on dehydration reaction has been systematically explored by the combination of detailed kinetic analysis and the microscopic DFT calculation. The present work suggests that not only the kinetics of dehydration but also the thermodynamics of adsorption governs the inhibition of water.

2.2 Experimental methods

2.2.1 Zeolite sample and AHFS treatment

Commercial NH_4 -ZSM-5 sample was provided by *Zeolyst International* (CBV3024E, Si/Al=15). To minimize the effect of extra-framework Al on the acidity or local environment of acid sites and then the adsorption and catalytic activity of BAS [25-28], NH_4 -ZSM-5 sample was treated with $(\text{NH}_4)_2\text{SiF}_6$ (denoted as AHFS) aiming to remove the extra-framework Al according to the following procedure. 2 g NH_4 -ZSM-5 sample was added into 80 ml deionized water stirred in a 100 ml PTFE-liner, followed by the addition of 1.42 g (8.0 mmol) AHFS to the solution and then stirred vigorously at 353 K for 5 h. The resulting products were centrifuged, rinsed six times with hot deionized water (353 K) and then dried overnight at 393 K. The final calcination step was done at 823 K for 5 hours in 100 ml min^{-1} synthetic air with a heating rate of 10 K min^{-1} .

2.2.2 Characterization methods

2.2.2.1 Specific surface area and porosity

The specific surface area and porosity were analyzed by N₂ adsorption-desorption isotherms recorded on an automated BET system (PMI automated Sorptomatic 1990) at liquid nitrogen temperature (77 K). The samples were outgassed in vacuum ($p = 10^{-3}$ mbar) at 523 K for 2 h prior to adsorption.

2.2.2.2 Elemental analysis

The elemental composition of the samples was determined by atomic absorption spectroscopy in a Unicam M Series Flame-AAS equipped with an FS 95 autosampler and a GF 95 graphite furnace.

2.2.2.3 Infrared spectroscopy

The in situ infrared (IR) spectra of adsorbed 1-propanol were recorded on a Bruker Vertex 70 spectrometer (resolution 4 cm⁻¹) in the transmission absorption mode. The samples were pressed into self-supporting wafer and activated in vacuum ($p < 10^{-6}$ mbar) for 1 h at 723 K at an incremental heating rate of 10 K min⁻¹. The equilibrium of zeolite and sorbate was time-resolved monitored. All spectra after adsorption were first baseline corrected in the range of 3800-1300 cm⁻¹ and then normalized by the integral peak area of the overtones of framework vibration band between 2100 and 1735 cm⁻¹.

The concentration of acid sites were measured by IR spectroscopy of adsorbed pyridine recorded on Thermo Nicolet 5700 FTIR apparatus at a resolution of 2 cm⁻¹. The self-supporting wafer was activated in vacuum for 1 h at 723 K at a heating rate of 10 K min⁻¹. After cooling to 423 K, pyridine ($p=10^{-1}$ mbar) was fed into the wafer and then adsorbed for 1 h. Subsequently, spectra were collected after outgassing for 0.5 h at 423 K. The bands located at 1540 and 1450 cm⁻¹ are assigned to Brønsted acid sites (BAS) and Lewis acid sites (LAS), respectively. For quantification, molar

integral extinction coefficients of 0.73 and 0.96 cm μmol^{-1} were used for BAS and LAS, respectively [29].

2.2.2.4 Gravimetric and calorimetric measurement

Gravimetric and calorimetric measurements were carried out with a Setaram TG-DSC 111 thermoanalyzer with a baratron pressure transducer. The samples were pressed into thin wafers and subsequently broken into small platelets. Then 10-15 mg of the platelets were charged into a quartz sample holder of the balance, and activated at 723 K for 1 h with a heating ramp of 10 K min^{-1} under vacuum ($p < 10^{-4}$ Pa). After cooling down to 323 K, sorbent vapor was stepwise introduced into the closed system and equilibrated with the sorbate in the pressure range from 10^{-3} to 12 mbar. The weight increase and heat flux were monitored during pressure equilibration with the sorbate. The heats of adsorption were directly attained by integration of the recorded heat flux signal observed during stepwise increase of the sorbate pressure. The surface coverage is calculated via normalizing the uptake of adsorption by the concentration of BAS determined from pyridine-IR measurement.

2.2.3 Catalytic measurements of 1-propanol dehydration

The steady-state catalytic dehydration reactions of 1-propanol (Sigma-Aldrich, > 99% GC assay) were carried out in a continuous quartz tubular flow reactor with an inner diameter of 4 mm under atmospheric pressure. AHFS-treated HZSM-5 samples were pressed and sieved to retain 160-280 μm aggregates, and the mass of catalyst (2-230 mg) used for catalytic measurements was adjusted to maintain differential conversion below 5%. The catalyst was then diluted with washed SiO_2 to maintain the total sample mass no less than 0.1 g in all experiments. A K-type thermocouple was used to measure the bed temperature, which was retained at reaction temperature (413-443 K) using a resistive tube furnace. The samples were heated to 773 K with a ramp of 10 K min^{-1} in He flow (40 ml min^{-1}), kept for 1 h and then cooled to reaction temperature before catalytic measurements. All the transfer lines were held at 383 K to prevent condensation of reactants and products.

Saturated 1-propanol vapor was introduced into the reactor by He carrier gas via a saturator. When studying the effect of water, the saturated water vapor was fed into the reactor by an additional stream of He separately. The concentrations of reactions and products were analyzed by a gas chromatography (GC) Hewlett Packard 5890 (Series II) equipped with a flame ionization detector (FID) and a Supelco-Wax column. The blank tests were performed and no products were detected in empty reactors or in reactor only with SiO₂ diluent. The stability measurement was also tested at selected highest reaction temperature of 443 K; no deactivation was observed on the sample used for this study. The SigmaPlot software was used to estimate the kinetic parameters.

2.2.4 Computational methods

Periodic density functional calculations (DFT) were carried out using the CP2K code [30]. All calculations employed a mixed Gaussian and planewave basis sets. Core electrons were represented with norm-conserving Goedecker-Teter-Hutter pseudopotentials [31-33], and the valence electron wavefunction was expanded in a double-zeta basis set with polarization functions [34] along with an auxiliary plane wave basis set with an energy cutoff of 360 eV. The generalized gradient approximation exchange-correlation functional of Perdew, Burke, and Enzerhof (PBE) [35] was used. Test calculations showed that the total energy change of the reactive system was negligible (<0.01 eV) when the maximum force convergence criteria of 0.001 hartree/bohr was used. Each reaction state configuration was optimized with the Broyden-Fletcher-Goldfarb-Shanno (BGFS) algorithm with SCF convergence criteria of 1.0×10^{-8} au. Previous experimental measurements [36] and DFT calculations [37] of primary alcohols adsorption in H-ZSM-5 zeolite indicated that the dispersive van der Waals (vdW) interactions between the adsorbed alcohols and the Brønsted acid sites in the zeolite significantly stabilize the adsorbed molecule by adding adsorption enthalpy of 10-15 kJ mol⁻¹ for each carbon atom. To compensate the long-range dispersion interaction between the adsorbate and the zeolite, the DFT-D3 scheme [38]

with an empirical damped potential term was added into the energies obtained from exchange-correlation functional in all calculations. Transition states of elementary steps in the dehydration and etherification reaction routes were located using the CI-NEB method [39, 40] with seven intermediate images along the reaction pathway between initial and final states. The identified transition states were confirmed by the vibrational analysis. Only one imaginary frequency was found for each transition state.

For the zeolite acid-catalyzed reaction, the confinement and steric hindrance strongly affect the stabilities of reaction intermediates and transition states [41-45]. To account for important entropic contribution and zero-point energy (ZPE) corrections, both Gibbs free energy (ΔG) and enthalpy (ΔH) changes along reaction pathways were calculated using standard thermodynamic method [46].

$$\Delta G = \Delta H - T\Delta S$$

$$\Delta H = \Delta U_{trans} + \Delta U_{rot} + \Delta U_{vib} + \Delta(ZPE) + \Delta H_{elec}$$

$$\Delta S = \Delta S_{trans} + \Delta S_{rot} + \Delta S_{vib}$$

where the translational, rotational, and vibrational contributions to the entropy and enthalpy were given below. The electronic term (ΔH_{elec}) was directly derived from DFT calculations.

$$U_{trans} = \frac{3}{2} k_B T$$

$$U_{rot} = \frac{3}{2} k_B T$$

$$U_{vib} = \sum_i \frac{h\nu_i}{e^{h\nu_i/k_B T} - 1}$$

$$ZPE = \sum_i \frac{h\nu_i}{2}$$

$$S_{trans} = k_B \left\{ \ln \left[\left(\frac{2\pi m k_B T}{h^2} \right)^{3/2} \frac{k_B T}{P} \right] + \frac{5}{2} \right\}$$

$$S_{rot} = k_B \left\{ \ln \left[\frac{\sqrt{\pi I_A I_B I_C}}{\sigma} \left(\frac{8\pi^2 k_B T}{h^2} \right)^{3/2} + \frac{3}{2} \right] \right\}$$

$$S_{vib} = k_B \sum_i \left(\frac{h\nu_i}{k_B T} \ln \left(\frac{e^{-h\nu_i/k_B T}}{1 - e^{-h\nu_i/k_B T}} \right) \right)$$

The calculated activation barrier (ΔH^\ddagger) and activation free energy barriers (ΔG^\ddagger) then were obtained by

$$\Delta H^\ddagger = \Delta U_{trans}^\ddagger + \Delta U_{rot}^\ddagger + \Delta U_{vib}^\ddagger + \Delta(ZPE)^\ddagger + (E_{elec}^{TS} - E_{elec}^{IS})$$

$$\Delta G^\ddagger = \Delta H^\ddagger - T\Delta S^\ddagger$$

where E_{elec}^{TS} and E_{elec}^{IS} were the electronic energy difference between the transition state (TS) and initial state (IS) of each elementary reaction step.

A periodic three-dimensional HZSM-5 zeolite structure of $\text{Si}_{96}\text{O}_{192}$ with experimental lattice parameters of $20.022 \times 19.899 \times 13.383 \text{ \AA}^3$ was used in this work. The unit cell of the H-ZSM-5 with Si/Al=26 ratio then was built by simply replacing four Si atoms with four Al atoms. The resulting negative charges were compensated by adding four H atoms at the oxygen atoms which are close neighbors of Al atoms on the zeolite frame, yielding the active Brønsted acidic sites, i.e., Si-OH-Al of the HZSM-5 shown in **Fig. 2.1**.

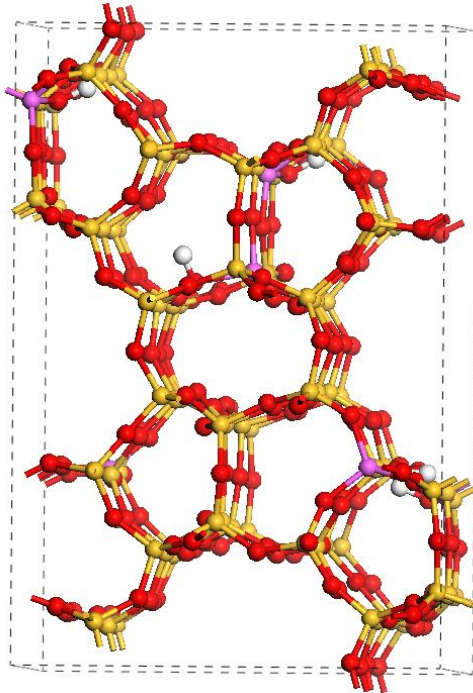


Fig. 2.1 Periodic H-ZSM-5 zeolite structure. The Si, Al, O and H atoms are represented by

yellow, magenta, red and white, respectively.

2.3. Results and discussion

2.3.1 Catalyst characterization

The results of physicochemical properties of parent and AHFS-treated MFI samples are presented in **Table 2.1**. The N₂ sorption data showed that the specific surface areas and micropore volume of MFI zeolite remains comparable value and are not altered by the AHFS treatment, confirming the microporous character of both of the samples. SEM micrographs of the parent and AHFS-treated samples indicate that the diameter of primary crystallites is smaller than 1 μm for both cases (not shown). After AHFS modification, the Si/Al of sample increased from 15 to 26, indicative of a substantial removal of Al from the zeolite structure. Concurrently the concentration of BAS decreased from 837 to 693 μmol g⁻¹, whereas the LAS density decreased largely by around 74% from 211 to 55 μmol g⁻¹, demonstrating that significant amounts of extra-framework Al was removed by AHFS treatment. The removal of extra-framework Al was confirmed by the infrared spectra of hydroxyl stretching vibration of AHFS-treated MFI-15 sample presented below.

Table 2.1 Physicochemical properties of parent MFI-15 and AHFS-treated MFI-15.

Samples	Si:Al ^a (-)	S _{BET} ^b (m ² g ⁻¹)	V _{micropore} ^b (cm ³ g ⁻¹)	BAS ^c (μmol g ⁻¹)	LAS ^c (μmol g ⁻¹)
MFI-15	15	423	0.164	837	211
MFI-15-AHFS	26	427	0.159	693	55

^a Molar ratio of Si and Al determined by AAS.

^b Determined by N₂ adsorption.

^c Acidity concentration determined by IR spectroscopy of adsorbed pyridine.

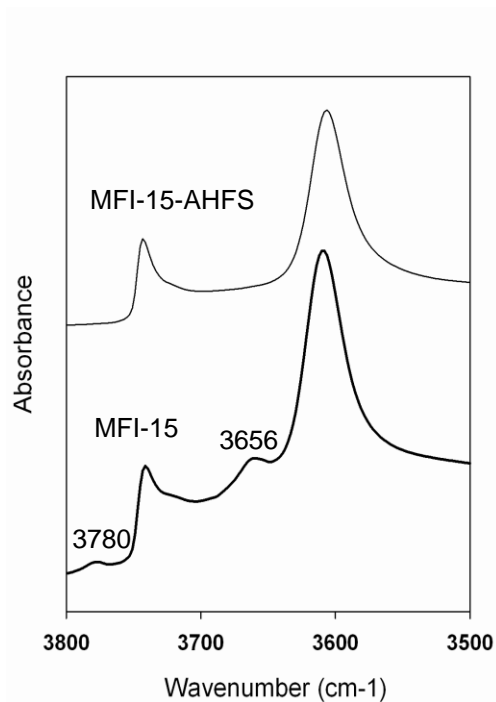


Fig. 2.2 Infrared spectra of hydroxyl stretching vibration region of activated parent and AHFS-treated MFI-15 samples.

IR spectra of MFI-15 and AHFS-treated MFI-15 in the hydroxyl stretching vibration region were shown in **Fig. 2.2**. Both samples exhibit the characteristic bands at 3610 cm^{-1} and 3745 cm^{-1} , corresponding to bridging hydroxyl group acting as Brønsted acid site and the surface terminal silanol group, respectively [27, 47]. Two additional bands centered at 3665 cm^{-1} and 3780 cm^{-1} were observed with respect to the parent zeolite. This two distinct peaks are associated with the hydroxyl bands of octahedral EFAL partially attached to the framework and free EFAL species such as charged or neutral aluminum oxides, aluminum hydroxides [27, 28], which disappeared after AHFS treatment, suggesting that the EFAL species has been removed from the zeolite channel and external surface. The significant removal of EFAL confirmed by the acidity characterization and IR spectra of hydroxyl stretching vibration allows to specifically assess the mechanism and kinetics of alcohol dehydration reaction taking place on BAS in the absence of synergistic effect exerted by LAS on the acid strength of BAS [25, 26] or on the catalytic transition state [27, 28]. All subsequent characterizations and catalytic measurements were performed on the AHFS-treated catalyst.

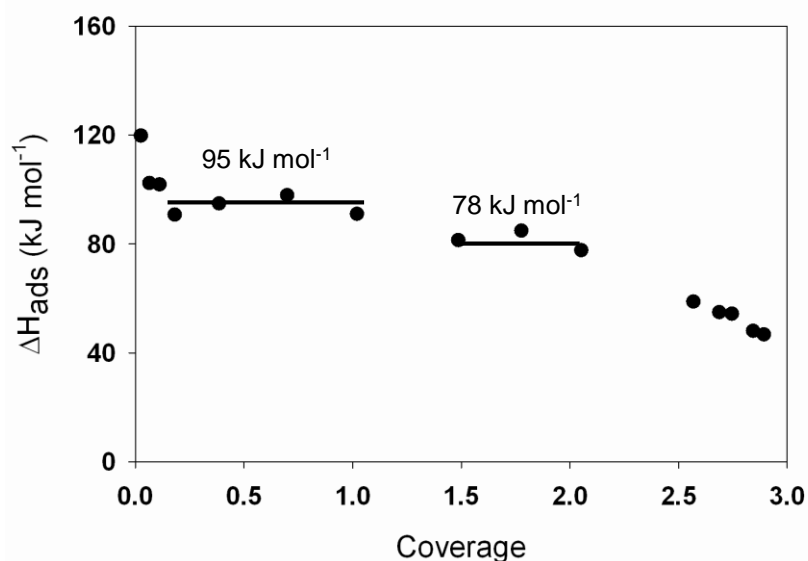


Fig. 2.3 The differential heats of adsorption as a function of 1-propanol coverage for MFI-15-AHFS sample at 323 K.

The coverage dependences for the differential heats of adsorption of 1-propanol in the pressure range from 10^{-3} to 12 mbar at 323 K were presented in **Fig. 2.3**. For the first exposure of zeolite sample to 1-propanol vapor under equilibrium pressure of 0.001 mbar, the initial heats of adsorption are around 120 kJ mol^{-1} associated with the coverage of 0.025. Thamm [48], Lee and Gorte [49] also observed the similar high heats of adsorption for C1-C4 alcohols on HZSM-5. In agreement with their work we relate the high heats of adsorption to the interaction of 1-propanol with defect sites of the sample [48, 49]. The adsorption enthalpy reached a constant value of 95 kJ mol^{-1} at coverage between 0.025 to 1, which is attributed to the local interaction of one 1-propanol molecule with one Brønsted acid sites. The differential heats did not drop largely at the coverage beyond 1 molecule/site stoichiometry, but rather were relatively high and constant (78 kJ mol^{-1}) up to the coverage of 2. This suggests that 1-propanol adsorption continues to be localized at acid sites and the appearance of adsorbate/adsorbate interactions associated with the acid sites that is 1-propanol dimer formed over one acid site, in agreement with literature results [49]. The decrease of the adsorption enthalpy above coverage of 2 is due to the contribution of adsorption at the external surface of the zeolite particles.

2.3.2 Mechanism and kinetics of 1-propanol elimination to propene

In this section, 1-propanol elimination to form propene was measured at varying 1-propanol pressure and temperature. The kinetic and thermodynamic parameters for elimination step estimated on basis of the mechanism-derived rate equation were used to assess the kinetic attenuation effect of water.

2.3.2.1 Kinetics effect of 1-propanol pressure and temperature on elimination turnover rates

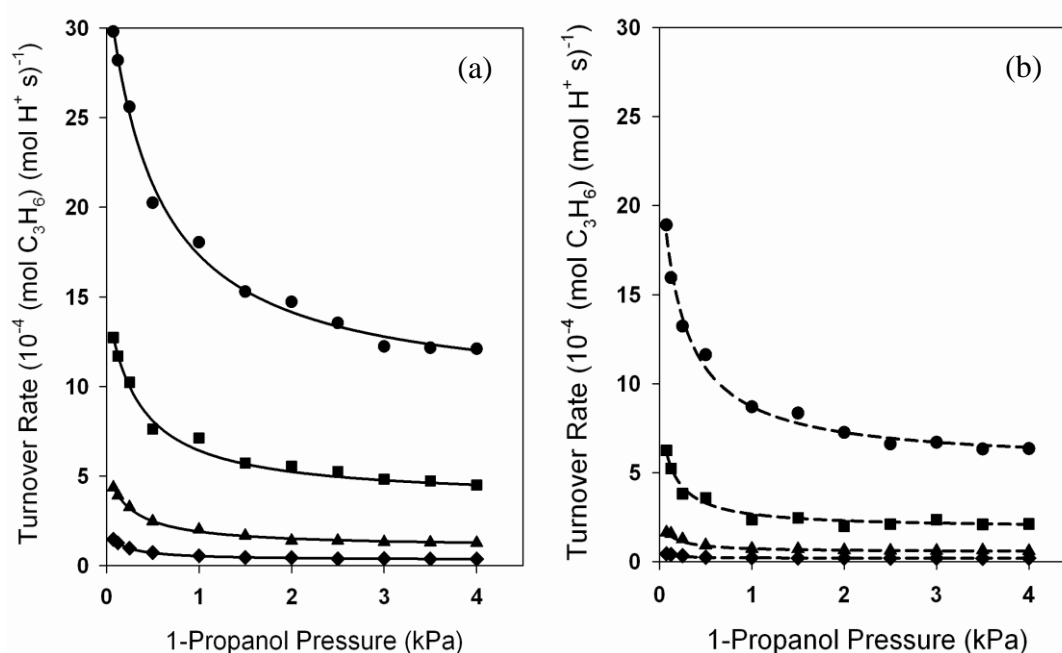


Fig. 2.4 Measured propene turnover rates (per H^+) as a function of 1-propanol pressure (0.075-4 kPa) over H-MFI (Si/Al = 26) at 413 K (\blacklozenge), 423 K (\blacktriangle), 433 K (\blacksquare), and 443 K (\bullet). The solid and dash curves represent the fitting of experimental data points to Eq. (4) in the absence of water (a) and in the presence of water (b) ($P_{\text{water}}=0.53$ kPa).

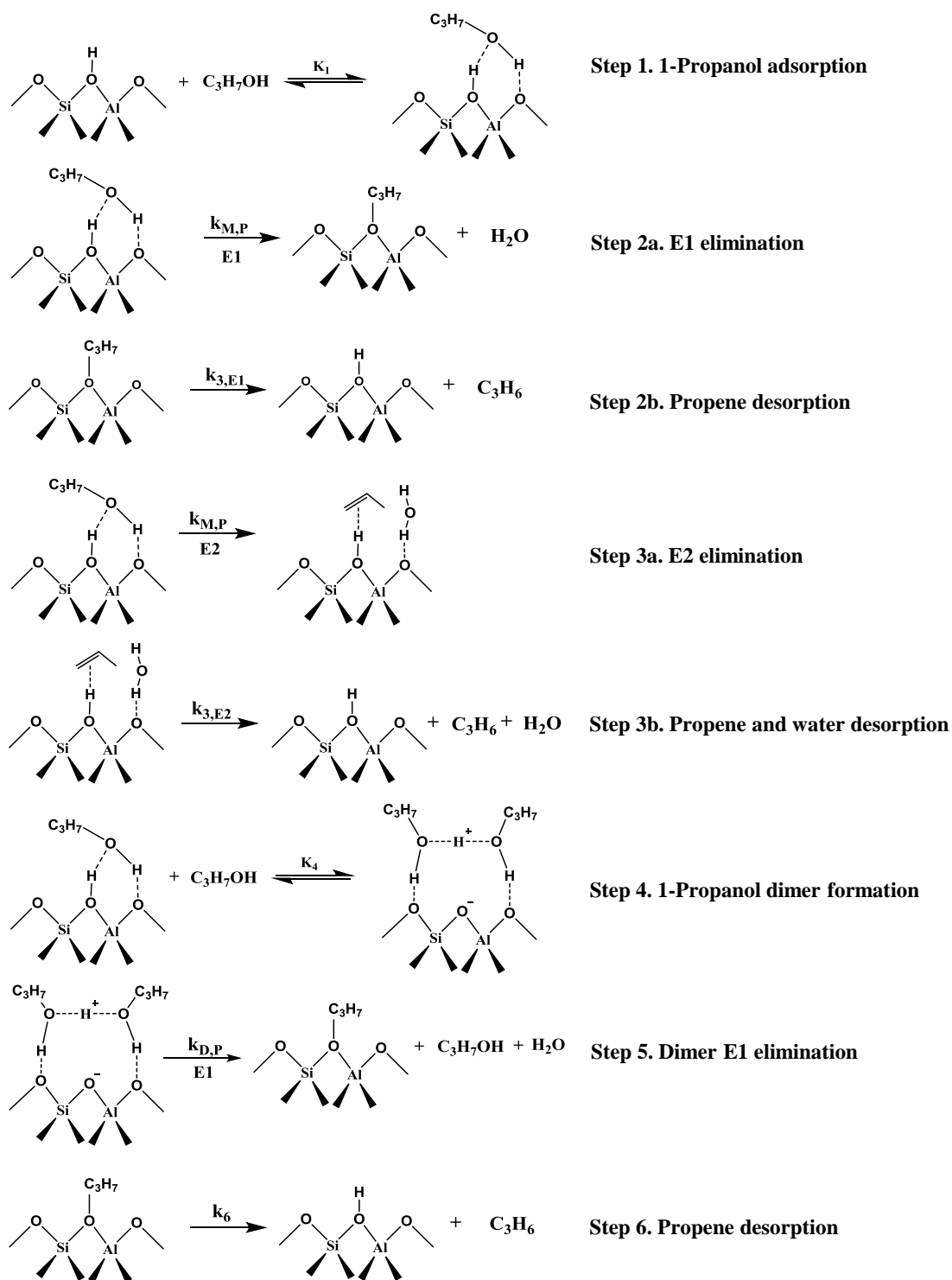
The 1-propanol dehydration reactions were carried out over H-MFI (Si/Al=26) catalyst at 413, 423, 433 and 443 K in the gas phase in the absence and presence of water. Under the reaction conditions employed, propene and dipropyl ether (DPE) as the parallel products of unimolecular and bimolecular dehydration reaction were

obtained. Turnover rates are normalized by the concentration acid protons ($693 \mu\text{mol g}^{-1}$) determined by IR spectroscopy of adsorbed pyridine shown in **Table. 2.1**.

The measured turnover rates (per H^+) for propene formation are shown in **Fig. 2.4** as a function of 1-propanol pressure (0.075-4 kPa) on H-MFI (Si/Al=26) catalyst. Propene formation rates decreased upon increasing of 1-propanol pressure and then gradually approached a lower limit both in the absence and presence of water. The observed negative kinetic effects of alcohols pressure on intramolecular dehydration rate is in agreement with previous reports for ethanol dehydration over acidic zeolites [50] and HPA catalysts ($\text{H}_3\text{PW}_{12}\text{O}_{40}$) [51], as well as 2-butanol dehydration and *sec*-butyl-methyl-ether cleavage over polyoxometalate clusters [52, 53]. The authors gave a plausible explanation that, the lowering in dehydration rate with increasing alcohols pressure is ascribed to the formation of protonated unreactive alcohol dimers that occupy acid sites and thus inhibit alcohols dehydration reaction [50-53]. Moreover, the stable and unreactive feature of 2-butanol dimers was inferred from the theoretical estimates indicating that the formed 2-butanol dimer is 84 kJ mol^{-1} enthalpically more stable than 2-butanol monomer [54]. However, our 1-propanol dehydration results demonstrate that even though 1-propanol dimers are less reactive under lower 1-propanol pressure, they can contribute for propene formation as well and account for large weight at relatively higher 1-propanol pressure.

Mechanistic and kinetics understanding of the nature and catalytic reactivity of such 1-propanol dimers along with 1-propanol and water dimers will be discussed in detail later in this section. Prior to discussing the kinetics of 1-propanol dimer to propene and the effects of introduced water on the specific activity and product selectivity of 1-propanol dehydration, it is essential to unravel reaction mechanism and elucidate kinetics and rate equation derived from the mechanism in the context of interpreting experimentally measured rate data.

2.3.2.2 Elementary steps and mechanism for 1-propanol elimination to propene



Scheme 2.1. Proposed sequence of elementary steps for 1-propanol elimination to form propene.

1-propanol elimination to form propene is initialized by the quasi-equilibrated adsorption of gas 1-propanol onto Brønsted acid sites to form H-bonded 1-propanol

monomer (Step 1, Scheme 2.1). Then, two plausible sequences for the following elementary steps can go through via E1 (stepwise) or E2 (concerted) mechanism [52, 53, 55-57]. E1 route proceeds by cleavage of C-O bond to form surface-bound propoxide intermediate and water molecule (Step 2a, Scheme 2.1), and followed by subsequent deprotonation of adsorbed propoxide to generate propene (Step 3, Scheme 1). E2 pathway involves concerted cleavage of C-O and C-H bonds in 1-propanol monomer (Step 2b, Scheme 2.1) via the acidic proton and neighboring basic oxygen of zeolite to form propene and water molecules associated with transferring the proton back to the basic oxygen of zeolite framework. 1-propanol monomer can also interact with another gas molecule to form protonated 1-propanol dimer (Step 4, Scheme 2.1). Even though the long-standing controversies are still existing on the prevalence of E1 or E2 sequence in alcohol elimination reaction [58-61], a consensus can be reached on the basis of experimental results [50, 62, 63] and theoretical calculation [53, 54, 57] that lower alcohols tend to eliminate water to form corresponding alkenes via E1 mechanism on acidic zeolite or POM clusters.

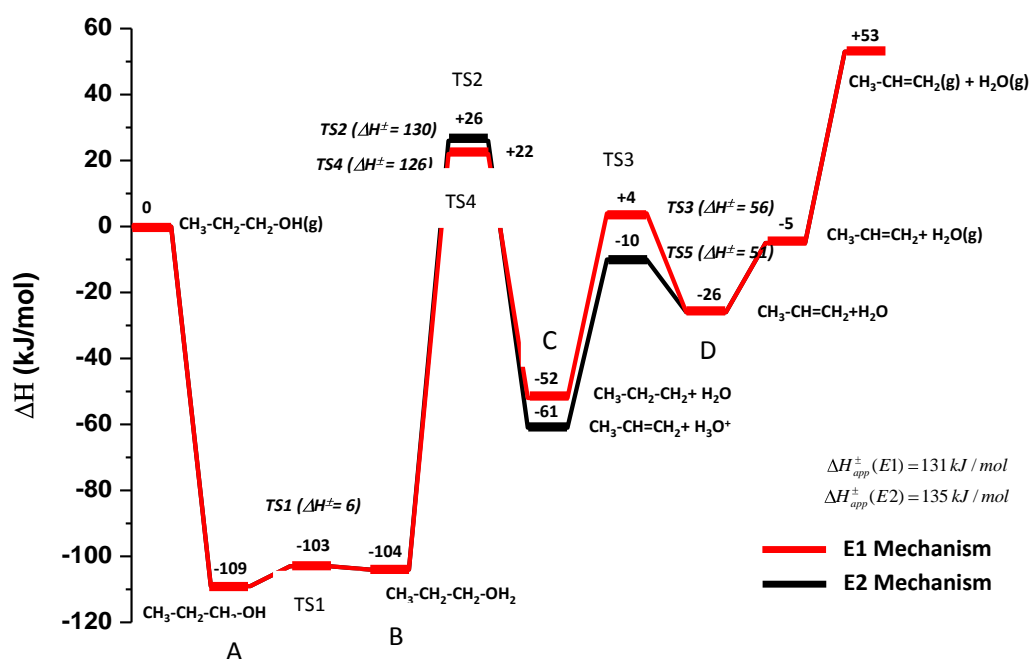


Fig. 2.5 Reaction energy diagram for 1-propanol dehydration via E1 mechanism (red line) and E2 mechanism (black line).

Herein, the relative importance of E1 and E2 pathway concerning 1-propanol elimination is estimated through DFT theoretical calculation. The optimized energies and configuration of intermediates and transition states for 1-propanol adsorption and dehydration on H-MFI zeolite for both E1 and E2 route are shown in **Fig. 2.5** and **Fig. S1**, respectively. Both pathways share the step of adsorption of 1-propanol on the Brønsted acid sites via hydrogen bonds with the O-H_z connection of 1.41 Å (A in **Fig. 2.5**). The calculated 1-propanol adsorption energy is -109 kJ mol^{-1} with vdW and ZPE corrections, which is a little higher than our measured heats of adoption of -96 kJ mol^{-1} (see **Fig. 2.3**). Upon adsorption, the protonation of 1-propanol by the zeolite proton (H_z) is facile with a low barrier of 6 kJ mol^{-1} , indicative of the quasi-equilibrium between hydrogen bonded (A in **Fig. 2.5**) and protonated 1-propanol adsorption states (B in **Fig. 2.5**). Additionally, the energy differences between these two adsorption intermediates are just 5 kJ mol^{-1} , which concurs with a similar observation for methanol interaction with the Brønsted acid sites of zeolites [64]. We performed an ab initio molecular dynamics (AIMD) simulation of the protonation of 1-propanol at 500 K and found that the quick and facile proton transfer between the zeolite and the 1-propanol was observed. Using slow annealing of the AIMD simulated configuration, as well as the frequency analysis, the formed oxonium complex of [CH₃CH₂CH₂OHH_z] (B in **Fig. 2.5**) was further verified as the reaction intermediate state, not a transition state. This is also consistent with the previous calculation of 1-propanol in H-ZSM-5 [65][66].

In the E1 mechanism, the protonated adsorbed 1-propanol (B in **Fig. 2.5**) is further dissociated into water and propoxide intermediate that the terminated C atom is bonded with the oxygen site of the zeolite (C in **Fig. 2.5**). This step was endothermic ($+52 \text{ kJ mol}^{-1}$) with an activation barrier of 126 kJ mol^{-1} . The transition state (TS2 in **Fig. 2.5**) for the E1 elimination route is characterized by the carbenium-ion feature, as indicated by sp² hybridization in which the substituents of the C_α atom are in the same

plane [54].

Additionally, the energy and configuration of TS2 resemble the following adsorbed intermediate propoxide, identifying the transition state involved in the E1 pathway as late transition state. The following deprotonation of propoxide to form adsorbed propene product (D in Fig. 2) is also endothermic (+26 kJ mol⁻¹), and the activation barrier is 56 kJ mol⁻¹, which is significantly lower compared with the barrier for water elimination step (126 kJ mol⁻¹). Consequently, the elimination step that is C-O bond cleavage in E1 pathway is involved in the kinetically relevant step, a conclusion in agreement with the solid acid-catalyzed elimination reaction for ethanol [50, 57] and 2-butanol [53, 54].

In the E2 mechanism, the protonated adsorbed 1-propanol (B in **Fig. 2.5**) decomposes concertedly to the final product propene and hydronium (H₃O⁺) with an activation barrier of 130 kJ mol⁻¹. The hydronium (H₃O⁺) then is deprotonated to water. As seen from **Fig. 2.5**, our calculation results suggest that the intrinsic activation energies, the energy difference of transition state (TS2 in **Fig. 2.5**) relative to lower adsorbed state (A in **Fig. 2.5**), for E1 and E2 mechanisms are 131 and 135 kJ mol⁻¹, comparable with our measured activation barrier of 142 kJ mol⁻¹ (details shown in Section 2.3.2.3). The similar calculated activation energies for E1 and E2 mechanism also demonstrate that relative preference of E1 or E2 mechanism cannot be enthalpically distinguished. Hence, entropies contributions to the reaction energy are considered on the basis of the dependence of rate constant on both of the activated enthalpies and entropies relative to the preceding intermediate state:

$$k = \frac{k_B T}{h} \exp\left(\frac{\Delta S^\ddagger}{R}\right) \exp\left(\frac{-\Delta H^\ddagger}{RT}\right) = A \exp\left(\frac{-\Delta H^\ddagger}{RT}\right) \quad (1)$$

The calculated activated entropies with respect to the elimination step for E1 and E2 mechanism are 40 and 17 J mol⁻¹ k⁻¹, respectively, resulting in one order of magnitude larger pre-exponential factor for E1 route (1.1×10¹⁵ s⁻¹) than E2 route (6.9×10¹³ s⁻¹). With the consideration of enthalpies term, the ratio of rate constant for

E1 path to E2 path is around 2.4, implying the relative prevalence of E1 mechanism for 1-propanol elimination. So, here we conclude that the E1 mechanism prevails for 1-propanol elimination as a consequence of a larger entropy gain in transition state relative to adsorbed intermediate and the resulting larger pre-exponential factor. Similarly, the preference of E1 mechanism for 2-butanol elimination on POM clusters was concluded on the basis of large and positive activated entropies and the concurrent large pre-exponential factor of $1.5\text{-}1.9 \times 10^{15} \text{ s}^{-1}$ (pre-exponential factor $< 10^{13} \text{ s}^{-1}$ for E2 pathway) [53]. The author accounted for the entropy gain in E1 elimination pathway in terms of the identity of late transition states in decomposition reactions that lead to the transformation of 6 vibrations (chemisorbed reactant) to 3 translational and 3 rotational degrees of freedom (transition state) [53]. In contrast, the transition state in E2 route involved the concurrent C-O bond activation and C-H interaction with basic oxygen of zeolite exhibits a highly ordered structure, resulting in the substantial loss of entropy relative to chemisorbed intermediate [53].

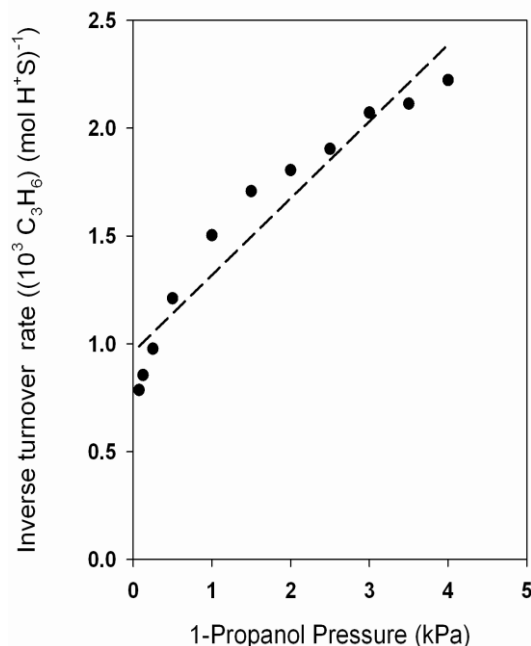


Fig. 2.6 Inverse propene formation turnover rates as a function of 1-propanol pressure over H-MFI catalyst at 433 K. The dashed line represents regression of experimental data points to Eq. (3).

In the following, the rate expression for 1-propanol elimination to propene at low conversion is derived under the assumption of quasi-equilibrated 1-propanol adsorption, irreversible water elimination and propene desorption and acid sites predominantly occupied by 1-propanol monomer and protonated dimer. The elementary steps depicted in Scheme 2.1, in addition to the previous analysis of prevailing of E1 elimination mechanism and the kinetically relevant step of C-O bond cleavage, lead to the rate equation (derivation in Appendix).

$$\frac{r_{\text{C}_3\text{H}_6}}{[\text{H}^+]_0} = \frac{k_{\text{M,P}}}{1 + K_4[\text{C}_3\text{H}_7\text{OH}]} \quad (2)$$

where $k_{\text{M,P}}$ and K_4 are the rate constant for water elimination from 1-propanol monomer (step 2, Scheme 2.1) and equilibrium constant for 1-propanol dimer formation (step 4, Scheme 2.1), respectively, while $[\text{H}^+]_0$ is the number of accessible proton sites. Eq. (2) can be written in a linear form as the following formalism.

$$\frac{[\text{H}^+]_0}{r_{\text{C}_3\text{H}_6}} = \frac{1}{k_{\text{M,P}}} + \frac{K_4[\text{C}_3\text{H}_7\text{OH}]}{k_{\text{M,P}}} \quad (3)$$

It is expected from Eq. (3) that the linear dependence of inverse propene formation rate on 1-propanol pressure would give rise to accurate estimates of $k_{\text{M,P}}$ and K_4 . However, the inverse turnover rate of propene formation increases monotonically but nonlinearly and the regression of experimental data to Eq. (3) is inconsistent with the measured effects of 1-propanol pressure (see **Fig. 2.6**). Especially when 1-propanol pressure is higher than 1.5 kPa, the inverse turnover rate tends to lower down gradually compared to rate under low reactant pressure, suggesting the much higher propene formation rate in parallel with increasing pressure. This implies, however, that 1-propanol monomers are not the only starting intermediate for propene formation, and that 1-propanol dimer can also decompose to generate propene under higher pressure conditions.

On this basis, we propose 1-propanol dimer to propene route proceeding as the

following steps. The formed 1-propanol dimer dissociates to form propoxide along with water and 1-propanol (Step 5, Scheme 2.1), and subsequently propoxide intermediate deprotonates to form propene (Step 5, Scheme 2.1). Correspondingly, the rate Eq. (2) for propene formation is developed in terms of rate contribution from both 1-propanol monomer and dimer. The revised rate equation for propene formation is shown as follows (the derivation in Appendix).

$$\frac{r_{C_3H_6}}{[H^+]_0} = \frac{k_{M,P} + k_{D,P}K_4[C_3H_7OH]}{1 + K_4[C_3H_7OH]} \quad (4)$$

where $k_{D,P}$ is the rate constant for water elimination from 1-propanol dimer (step 5, Scheme 2.1). Eq. 4 is consistent with the observation that propene formation rates do not decline largely but rather maintain in relatively high level under higher 1-propanol pressure (**Fig. 2.4**).

The revised rate equation (Eq. (4)) is consistent with the dependence of measured propene turnover rates on 1-propanol pressure at different temperatures (**Fig. 2.4**), demonstrating the proposed model based on the developed mechanism (Scheme 2.1) for propene formation is capable of describing the experimental data accurately. By deconvolution of turnover rate for propene formation, taking the rate at 433 K as an example, the respective contribution of 1-propanol monomer and dimer to form propene is markedly presented in **Fig. 2.7**. With the increasing of reactant pressure, 1-propanol to propene rate gradually decreases in parallel with the progressive increase of the weight of 1-propanol dimer to propene.

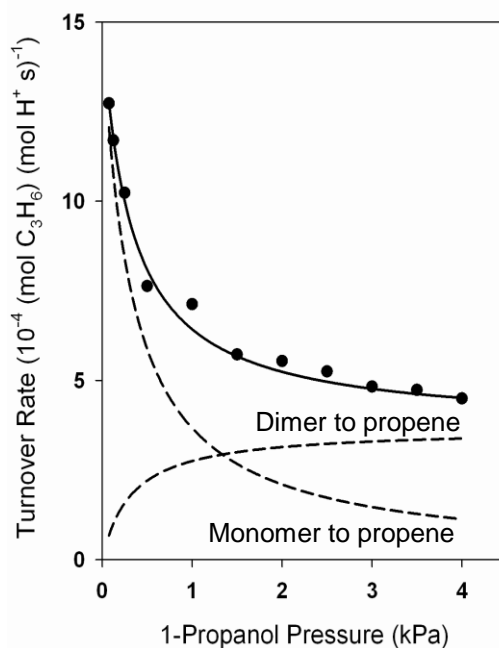


Fig. 2.7 Deconvolution of turnover rate for propene formation to the respective contribution from 1-propanol monomer and dimer at 433 K.

2.3.2.3 Kinetics understanding of 1-propanol elimination

Table 2.2. 1-propanol monomer to propene rate constant $k_{M,P}$, 1-propanol dimer to propene rate constant $k_{D,P}$ and 1-propanol dimer formation equilibrium constant K_4 for 1-propanol elimination in the absence of water. Parameters are determined by fitting Eq. (4) to experimental data (see **Fig. 2.8**).

	$k_{M,P}$ ($10^{-4} (\text{H}^+ \text{s})^{-1}$)	$k_{D,P}$ ($10^{-4} (\text{H}^+ \text{s})^{-1}$)	K_4 (kPa^{-1})
413 K	2.1	0.3	6.7
423 K	5.4	1.0	4.1
433 K	14.8	3.7	3.0
443 K	33.0	9.3	2.0

Table 2.3. Estimated 1-propanol monomer to propene rate constant $k_{M,P}$, 1-propanol dimer to propene rate constant $k_{D,P}$ and 1-propanol dimer formation equilibrium constant K_4 for 1-propanol elimination in the presence of water. Parameters are determined by fitting Eq. (4) to experimental data (see **Fig. 2.8**).

T (K)	$k_{M,P}$ ($10^{-4} (\text{H}^+ \text{s})^{-1}$)	$k_{D,P}$ ($10^{-4} (\text{H}^+ \text{s})^{-1}$)	K_4 (kPa^{-1})
413 K	0.8	0.2	19.2
423 K	2.5	0.6	10.9
433 K	8.6	1.9	7.3
443 k	22.6	5.5	4.3

The rate constants $k_{M,P}$, $k_{D,P}$ as well as 1-propanol dimer adsorption constant K_4 evaluated from fitting the measured propene formation rates at four different temperatures (**Fig. 2.4a**) by Eq. (4) are tabulated in **Table 2.2**. The two measured rate constants $k_{M,P}$ and $k_{D,P}$ reflect the stability of a charged TS with respect to adsorbed 1-propanol monomer and the charged dimer species, respectively. As seen from Table 2.2, the rate constant for 1-propanol monomer to propene ($k_{M,P}$) is larger than the corresponding rate constant for 1-propanol dimer to propene ($k_{D,P}$) at each specific temperature, reflecting the relatively lower activity of 1-propanol dimer. Additionally, temperature exert influence on the $k_{M,P}$ and $k_{D,P}$ to different extent. The rate constant $k_{D,P}$ increase by a factor of 31, two times large than that for $k_{M,P}$ upon increasing temperature from 413 to 443 K. This implies the larger activation barrier for 1-propanol dimer to propene compared with 1-propanol monomer to propene.

Prior to interpreting the water impact on the kinetic and equilibrium for propene formation, it is important to illustrate the water influence on the surface species. The full coverage of surface acid sites was achieved under 1-propanol equilibrium pressure above 0.04 kPa at temperature of 433 K, so we can anticipate that the surface acid sites are fully covered by 1-propanol species (monomer and dimer) under our actual dehydration conditions (0.075-4 kPa; 413-443 K). Moreover, the IR results of

the co-adsorption of 1-propanol and water evidently demonstrate that water was not capable of remaining adsorbed on the acid sites of zeolite in the presence of 1-propanol, but water can diffuse into the pores and interact with the adsorbed alcohols (see the detailed discussion in section 2.3.4.1). This finding, taken together with the IR observation of the full coverage of 1-propanol on acid sites under reaction conditions, leads us to postulate that introduced water cannot directly occupy the acid sites to form water monomer or dimer surface species, and the role of water on adsorption is that water laterally interacts with the adsorbed 1-propanol and solvates or stabilizes the adsorption intermediates.

Based on the context above-discussed, the model presented in Eq. 4 is applicable to the case in the presence of water. The kinetic and equilibrium parameters in Eq. 4 were fit to the experimental data (**Fig. 2.4b**), and the estimated values are shown in **Table 2.3**. The rate constants of both 1-propanol monomer to propene $k_{M,P}$ and 1-propanol dimer to propene $k_{D,P}$ were observed to be attenuated by the present water by comparing the rate constants in **Table 2.3** with respect to that in **Table 2.2**. In going from 413 to 443 K, the inhibition effect of water on $k_{M,P}$ significantly decreases and $k_{M,P}$ decreases by 62% and 32% at 413 K and 443 K, respectively. However, $k_{D,P}$ is not so sensitive to temperature change and $k_{D,P}$ decreases by an average constant value of around 40% in the temperature range of 413 to 443 K.

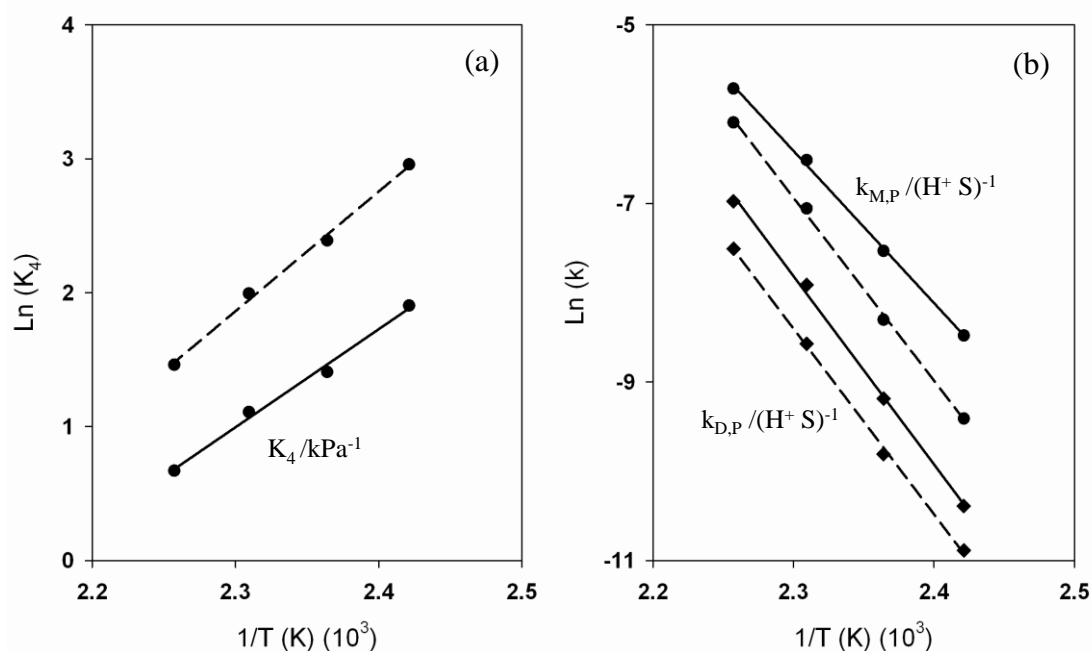


Fig. 2.8. 1-Propanol dimer formation equilibrium constant K_4 as a function of temperature (a); 1-propanol monomer to propene rate constant $k_{M,P}$ (●) and 1-propanol dimer to propene rate constant $k_{D,P}$ (◆) as a function of temperature (b). The solid and dashed lines represent the conditions in the absence and presence of water, respectively.

According to the transition state theory, the intrinsic activation enthalpies and entropies as well as the 1-propanol dimer formation enthalpy were obtained by plotting the natural logarithm of regressed rate constants ($k_{M,P}$ and $k_{D,P}$) or equilibrium constant (K_4) against the inverse temperature in the absence and presence of water (413–443 K, **Fig. 2.8**). These parameters are summarized in **Table 2.4**. Enthalpy barrier for 1-propanol dimer to propene ($\Delta H_{D,P}^\ddagger = 175 \text{ kJ mol}^{-1}$) are higher than for 1-propanol monomer to propene ($\Delta H_{M,P}^\ddagger = 142 \text{ kJ mol}^{-1}$), as expected from the lower value of $k_{D,P}$ relative to $k_{M,P}$ and the rapid increase of $k_{D,P}$ compared with $k_{M,P}$ with increasing the temperature. Concomitantly, activation entropies increase from $25 \text{ J mol}^{-1} \text{ K}^{-1}$ for $\Delta S_{M,P}^\ddagger$ to $90 \text{ J mol}^{-1} \text{ K}^{-1}$ for $\Delta S_{D,P}^\ddagger$ in parallel with the gain of activation enthalpies. The interesting finding is the influence of water on the activation barrier.

As shown in **Table 2.4**, the activation enthalpy of $\Delta H_{M,P}^\ddagger$ increases from 142 to 170 kJ mol⁻¹ in the presence of water, a value comparable with $\Delta H_{D,P}^\ddagger$ of 175 kJ mol⁻¹, indicating that the additional 1-propanol and the introduced water give rise to the similar inhibiting effect on 1-propanol elimination to propene reaction. Similarly, the activation entropy of $\Delta S_{M,P}^\ddagger$ (87 J mol⁻¹ K⁻¹) in the presence of water resembles $\Delta S_{D,P}^\ddagger$ (91 J mol⁻¹ K⁻¹). The variation of activation enthalpy $\Delta H_{D,P}^\ddagger$ (175-173 kJ mol⁻¹) and activation entropy $\Delta S_{D,P}^\ddagger$ (91-80 J mol⁻¹ K⁻¹) for 1-propanol dimer to propene in the presence of water is not pronounced and can be seen as almost invariant, which indicates that the water has weak effect on 1-propanol dimer to propene route.

Table 2.4. Activation enthalpies and entropies for 1-propanol elimination to propene in the absence and presence of water at 433 K. The subscript M,P denotes 1-propanol monomer to propene and D,P denotes 1-propanol dimer to propene.

	Without water	With water
$\Delta H_{M,P}^\ddagger$ (kJ mol ⁻¹)	142	170
$\Delta H_{D,P}^\ddagger$ (kJ mol ⁻¹)	175	173
$\Delta S_{M,P}^\ddagger$ (J mol ⁻¹ K ⁻¹)	25	87
$\Delta S_{D,P}^\ddagger$ (J mol ⁻¹ K ⁻¹)	91	80
ΔH_4 (kPa ⁻¹)	-64	-75

2.3.3 Mechanism and kinetics of 1-propanol dehydration to dipropyl ether

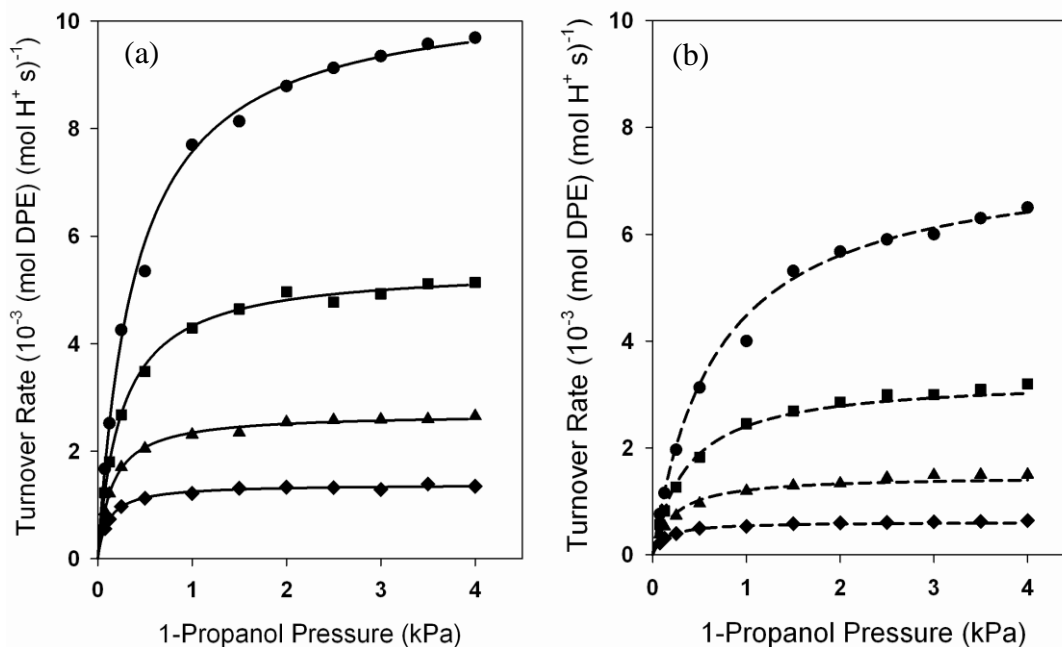
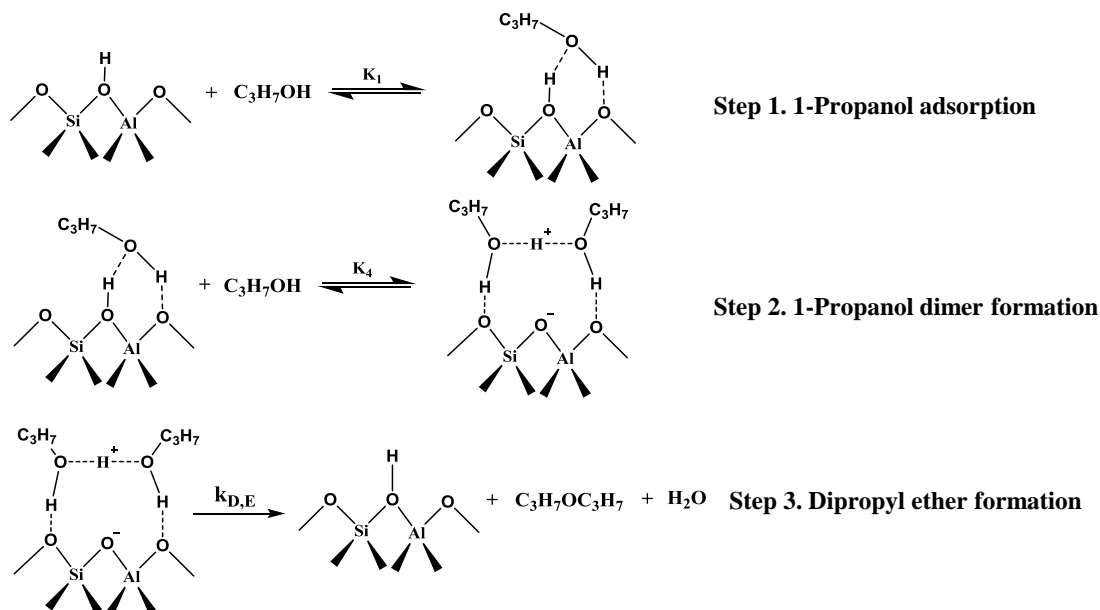


Fig. 2.9 Measured dipropyl ether turnover rates (per H^+) as a function of 1-propanol pressure (0.075 - 4 kPa) over H-MFI (Si/Al = 26) at 413 K (\blacklozenge), 423 K (\blacktriangle), 433 K (\blacksquare), and 443 K (\bullet). The solid and dash curves represent the fitting of experimental data points to Eq. (5) in the absence of water (a) and in the presence of water (b) ($P_{\text{water}} = 0.53$ kPa).

The measured turnover rates (per H^+) for dipropyl ether formation as a function of 1-propanol pressure (0.075-4 kPa) on H-MFI (Si/Al = 26) are shown in **Fig. 2.9**. The turnover rates increase with increasing 1-propanol pressure and then gradually become insensitive to 1-propanol at higher pressure (**Fig. 2.9a**), as also observed for methanol and ethanol on MFI or POM catalysts [50, 67, 68]. As expected, the turnover rates for DPE formation are also inhibited at each specific temperature with water added (**Fig. 2.9b**).

Prior to analyzing the measured rate data, the reaction mechanism should be well interpreted. Two plausible mechanisms, namely dimer-mediated direct route and alkoxide-mediated sequential pathway are usually proposed for bimolecular alcohol dehydration reaction [50, 67-69]. The direct mechanism includes the adsorption of

1-propanol to form 1-propanol monomer (Step1, Scheme 2.2) and then co-adsorption of a second 1-propanol molecule to form protonated 1-propanol dimer (Step2, Scheme 2.2). The dimer then directly decomposes to form DPE and water (Step3, Scheme 2.2). In sequential dehydration route, the adsorbed 1-propanol monomer first eliminates water to form surface-bound propoxide species (see Step 2a in Scheme 2.1), followed by the reaction of propoxide intermediate with a 1-propanol molecule to form DEE.



Scheme 2.2. Proposed sequence of elementary steps for 1-propanol dehydration to form dipropyl ether.

The sequential mechanism shares the same rate-limiting step with the E1 mechanism for 1-propanol monomer to propene, so the derived rate equation for 1-propanol monomer to propene (Eq. 2 in section 2.3.2.2) is also applicable to bimolecular 1-propanol dehydration to DPE via sequential pathway. The rate equation for the direct route of DPE formation (Scheme 2.2), under the assumption of surface covered species of 1-propanol monomer and protonated dimer, can be expressed as (derivation in Appendix):

$$\frac{r_{\text{C}_3\text{H}_7\text{OC}_3\text{H}_7}}{[\text{H}^+]_0} = \frac{k_{\text{D,E}}K_4 \text{C}_3\text{H}_7\text{OH}}{1+K_4 \text{C}_3\text{H}_7\text{OH}} \quad (5)$$

in which $k_{D,E}$ is the rate constant for DPE formation (Step 3, Scheme 2.2) and K_4 is the adsorption equilibrium constant for protonated dimers (Step 2, Scheme 2.2), respectively. Significant dimer coverages reflected in the second term in the denominator of Eq. (2) would cause the negative rate dependence with increasing 1-propanol pressures, as the observations for propene formation at low pressure range (**Fig. 2.4**). However, the measured turnover rates did not decrease with increasing 1-propanol pressure, a consequence that sequential mechanism is not involved in DPE formation route. The Langmuir-type rate expression of **Eq. 5** for the direct route seems reasonable to describe the measured rate data.

$$\frac{[H^+]_0}{r_{C_3H_7OC_3H_7}} = \frac{1}{k_{D,E}} + \frac{1}{k_{D,E}K_4[C_3H_7OH]} \quad (6)$$

Eq. (5) can be written in a linear form as Eq. (6), which accurately describes the kinetic effects of 1-propanol pressure on DPE formation turnover rate as shown by the linear dependence of inverse DPE turnover rate on 1-propanol pressure (**Fig. 2.10**). The regression analysis of the pressure dependence of DPE formation turnover rates give rise to accurate estimates for intrinsic rate constant for dimer activation ($k_{D,E}$, Step 3, Scheme 2.2) and the equilibrium constant for 1-propanol dimer formation (K_4 , Step 2, Scheme 2.2). These two parameters can be obtained from the values of the slope of the intercept in **Fig. 2.11** and are listed in **Table 2.5**. The regressed rate constant for activation of 1-propanol dimer ($k_{D,E}$) increases from $1.4 \cdot 10^{-3} \text{ (H}^+ \text{ s)}^{-1}$ to $10.5 \cdot 10^{-3} \text{ (H}^+ \text{ s)}^{-1}$ with increasing the temperature from 413 to 443 K, in parallel with the decrease of equilibrium constant (K_4) from 8.7 to 2.4 kPa^{-1} , consistent with the expectation.

In the presence of water, the intrinsic rate constant for DPE formation $k_{D,E}$ and the equilibrium constant for 1-propanol dimer formation K_4 are determined by regressing measured 1-propanol intermolecular dehydration rates to the functional form of Eq. (6) and the corresponding parameters are tabulated in **Table 2.6**. The value of $k_{D,E}$ decrease by 57% and 32% and at temperature 413 and 443 K, respectively, implying the significant inhibiting effect at low temperature, consistent with the finding for

1-propanol monomer to propene. The values of K_4 evaluated from the 1-propanol pressure dependence of DPE turnover rates (**Fig. 2.11**) from Eq. (6) are comparable with the values of K_4 that derived from the pressure dependence of propene synthesis rates (**Fig. 2.8**) from Eq. (4). K_4 evaluated from these two independent data sets with and without water is tabulated in **Table 2.7**. The consistency in the value of the equilibrium constant for formation of 1-propanol dimer K_4 supports the mechanism for propene formation and DPE synthesis proposed in Scheme 2.1 and Scheme 2.2.

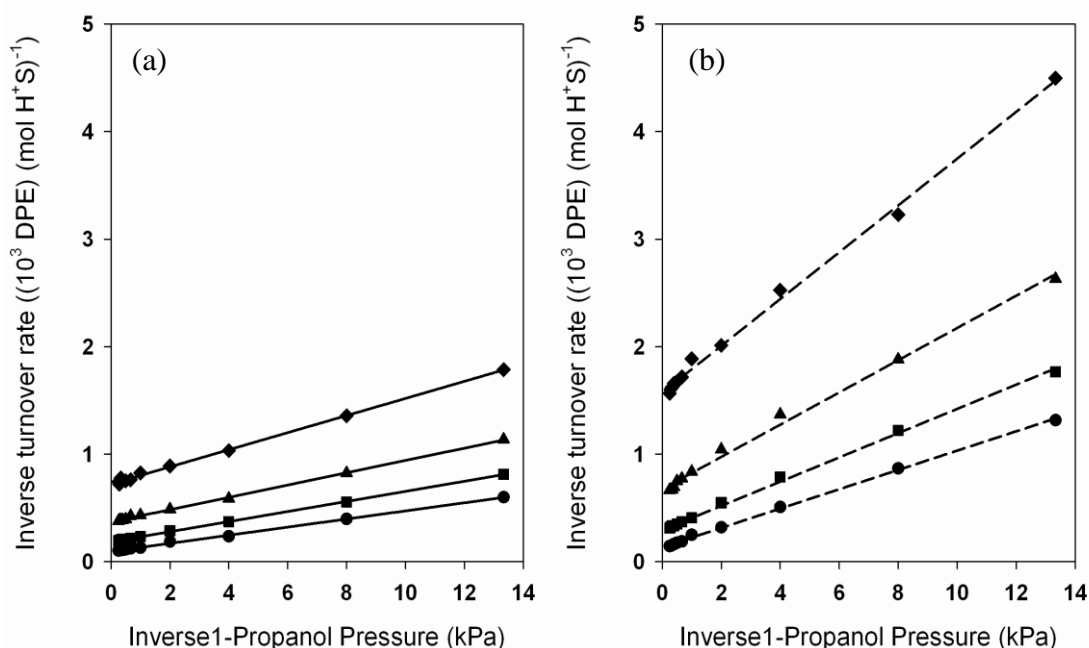


Fig. 2.10 Inverse dipropyl ether turnover rates (per H^+) as a function of inverse 1-propanol pressure (0.075 - 4 kPa) over H-MFI (Si/Al = 26) at 413 K (\blacklozenge), 423 K (\blacktriangle), 433 K (\blacksquare), and 443 K (\bullet). The solid and dash curves represent the fitting of experimental data points to Eq. (6) in the absence of water (a) and in the presence of water (b) ($P_{\text{water}} = 0.53$ kPa).

Table 2.5. DPE formation rate $k_{M,P}$ and 1-propanol dimer formation equilibrium constant K_4 (see Scheme 2.2) for 1-propanol dehydration to DPE in the absence of water. Parameters are determined by linear regression of experimental data to Eq. (6).

	k_5 ($10^{-3} (\text{H}^+ \text{s})^{-1}$)	K_4 (kPa^{-1})
413 K	1.4	8.7
423 K	2.7	6.2
433 K	5.4	3.8
443 K	10.5	2.4

Table 2.6. DPE formation rate $k_{M,P}$ and 1-propanol dimer formation equilibrium constant K_4 (see Scheme 2.2) for 1-propanol dehydration to DPE in the presence of water. Parameters are determined by linear regression of experimental data to Eq. (6).

	k_5 ($10^{-3} (\text{H}^+ \text{s})^{-1}$)	K_4 (kPa^{-1})
413 K	0.6	17.7
423 K	1.5	10.2
433 K	3.3	6.4
443 K	7.1	3.6

Table 2.7. Comparison of the equilibrium constant K_4 derived from propene formation experimental data and DPE synthesis data.

T (K)	K_4 (kPa^{-1}) (from propene)		K_4 (kPa^{-1}) (from DPE)	
	Without water	With water	Without water	With water
413 K	6.7	19.2	8.7	17.7
423 K	4.1	10.9	6.2	10.2
433 K	3.0	7.3	3.8	6.4
443 k	2.0	4.3	2.4	3.6

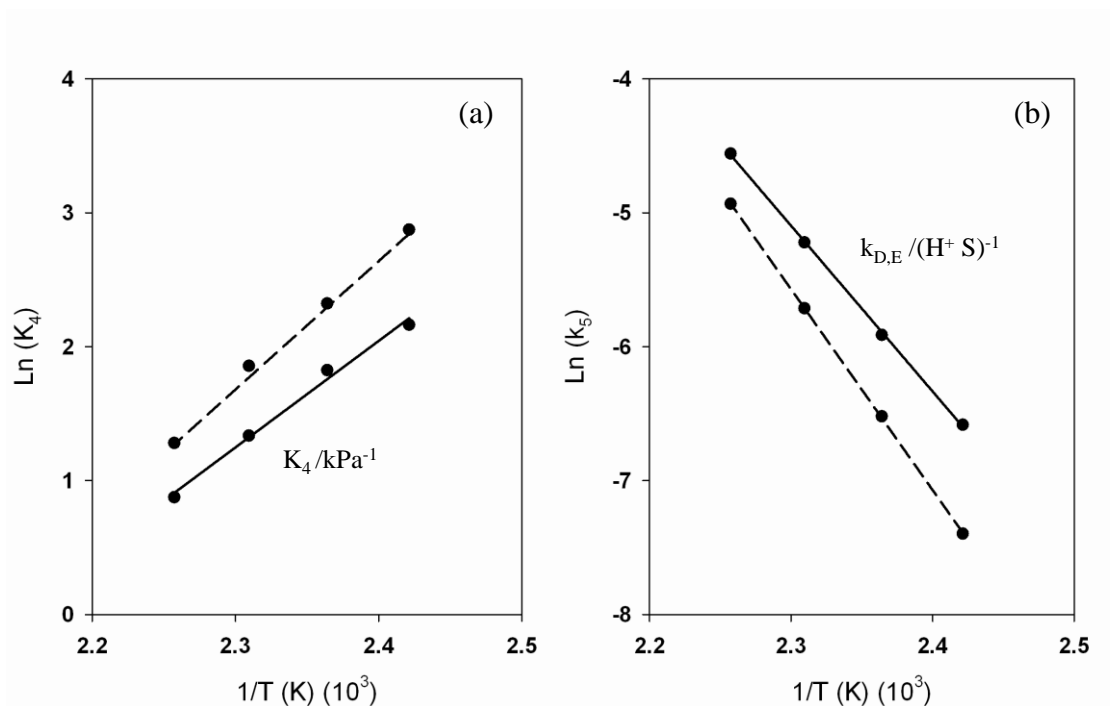


Fig. 2.11 1-propanol dimer formation equilibrium constant K_4 as a function of temperature (a); 1-propanol dimer to DPE rate constant $k_{D,E}$ as a function of temperature (b). The solid and dashed lines represent the conditions in the absence and presence of water, respectively.

The intrinsic activation enthalpies and entropies as well as the 1-propanol dimer formation enthalpy K_4 were determined by plotting the natural logarithm of regressed rate constants ($k_{D,E}$) and equilibrium constant (K_4) against the inverse temperature in the absence and presence of water (**Fig. 2.11**). As shown in **Table 2.8**, the activation enthalpy of $\Delta H_{D,E}^\ddagger$ increases from 103 to 115 kJ mol^{-1} in the presence of water, demonstrating that added water not only inhibits the unimolecular elimination reaction but also the dimolecular dehydration reaction. The activation entropy for DPE is negative value ($\Delta S_{D,E}^\ddagger = -54 \text{ J mol}^{-1} \text{ K}^{-1}$), in agreement with the negative activation entropy reported for methanol dehydration to DME [69], but in contrast to the positive activation entropy for propene formation ($\Delta S_{M,P}^\ddagger = 25 \text{ J mol}^{-1} \text{ K}^{-1}$, $\Delta S_{D,P}^\ddagger = 90 \text{ J mol}^{-1} \text{ K}^{-1}$). With water added, activation entropy for DPE synthesis ($\Delta S_{D,E}^\ddagger$) increases from $-54 \text{ J mol}^{-1} \text{ K}^{-1}$ to $-7.5 \text{ J mol}^{-1} \text{ K}^{-1}$ in parallel with the increasing of activation enthalpy, whereas activation enthalpy is still dominant for the dehydration

reflecting from the inhibiting effect of introduced water.

Table 2.8. Activation enthalpies and entropies for 1-propanol dehydration to DPE in the absence and presence of water at 433 K. The subscript M,P denotes 1-propanol monomer to propene and D,P denotes 1-propanol dimer to propene.

	Without water	With water
$\Delta H_{\text{zero}}^{\ddagger}$ (kJ mol ⁻¹)	103	115
$\Delta S_{\text{zero}}^{\ddagger}$ (J mol ⁻¹ K ⁻¹)	-54	-7.5
ΔH_4 (kJ mol ⁻¹)	-66	-76

2.3.4 Mechanistic understanding of the kinetic attenuation effect of water

When water was co-fed into the gas phase, both of the turnover rates for 1-propanol elimination to form propene (**Fig. 2.4**) and intermolecular dehydration to form DPE (**Fig. 2.9**) decreased apparently under each specific temperature. This result indicates that water exerts a strong inhibition on 1-propanol dehydration process. Such water caused suppression effects on the dehydration reaction of methanol, ethanol, and 2-butanol over zeolites, γ -Al₂O₃ and heteropoly acids were also reported by previous literatures [50, 52, 70, 71].

Water may have dramatic consequences for the structural stability of zeolites at elevated temperature. H-form zeolites may suffer from the steam-catalyzed cleavage of framework Al–O bonds that leads to dealumination at elevated temperatures (above 523 K) [72]. For example, it is reported that acidic H-Y zeolites were unstable upon heating in the presence of water because of the susceptibility of the Al–O bonds to hydrolysis [73]. After contacting with water, Td coordinated framework-associated aluminum atoms (related to Brønsted acid sites) can be transformed into Oh coordination [74, 75], which was unstable and can be reverted back to Td coordination above 400 K, but the Brønsted acid sites cannot be recovered [75]. Whereas, H-form zeolites can remain stable while catalyzing the dehydration of

simple alcohols in the gas phase at moderate temperature range of 343-433 K [72]. The unchanged BAS and LAS acidity of our used catalyst and the long time catalytic stability tested at 433 K in presence of water vapor show that HZSM-5 catalyst are highly stable under our reaction conditions (temperature below 433 K). In contrast to the ethanol dehydration reaction taking place on γ -Al₂O₃ [71], in which water is capable of irreversibly deactivating the active sites of γ -Al₂O₃ in addition to attenuating ethylene and diethyl ether formation rate.

2.3.4.1 Co-adsorption of 1-propanol and water

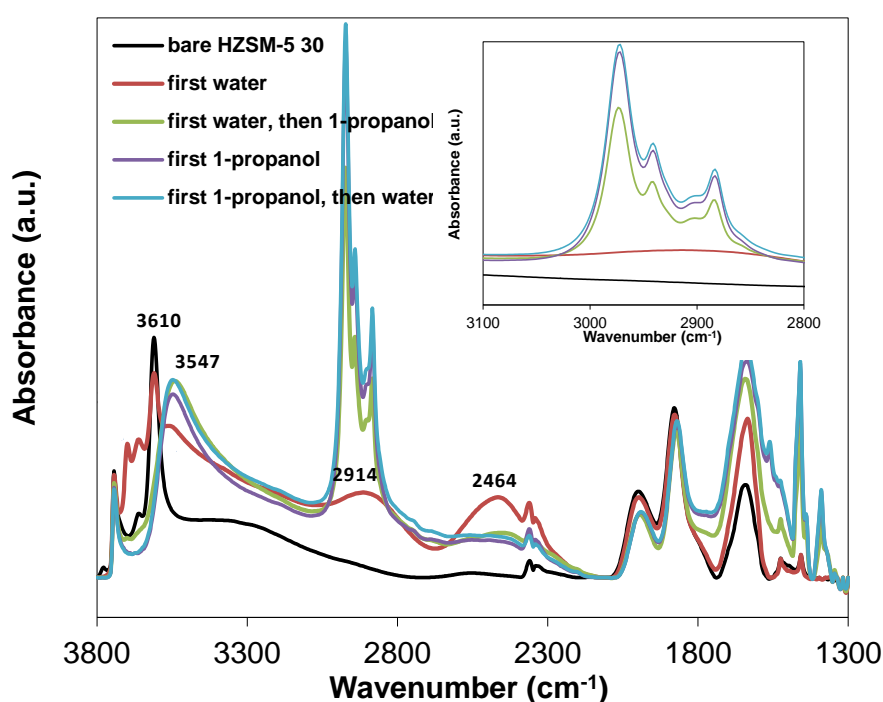


Fig. 2.12 *In situ* IR spectra (after subtracting spectrum of activated zeolite) for 1-propanol ($p = 0.005$ mbar) and water ($p = 0.005$ mbar) adsorption in three different modes with HZSM-5 30 at 323 K in two modes; first water adsorption followed by 1-propanol adsorption, and 1-propanol adsorption followed by water adsorption.

In order to unravel whether or not the inhibited 1-propanol elimination rate is a consequence of the competitive adsorption between 1-propanol and water, the adsorption of 1-propanol and water in sequence was studied at 323 K over H-MFI

catalyst.

The IR spectra of 1-propanol ($p=0.005$ mbar) and water ($p=0.005$ mbar) adsorption on HZSM-5 30 at 323 K in the gas phase are shown in **Fig. 2.12**. The vibrational bands centered at 3740 and 3610 cm^{-1} of the activated HZSM-5 are assigned to the terminal SiOH groups and the Brønsted acid Si-OH-Al groups, respectively, as described in **Fig. 2.2**. In order to understand whether the water adsorption will change the adsorption properties of 1-propanol, two distinct co-adsorption scenarios are designed to compare the water and 1-propanol interaction with zeolite in this *in situ* IR spectroscopy study, that is, Mode A: water adsorption ($p = 0.005$ mbar), followed by 1-propanol adsorption ($p = 0.005$ mbar); Mode B: 1-propanol adsorption ($p = 0.005$ mbar), followed by water adsorption ($p = 0.005$ mbar).

In the first mode, water was first adsorbed, but the coverage remained low as seen from the IR spectra in **Fig. 2.12**. When 1-propanol was subsequently introduced, most of the adsorbed water was expelled from the hydroxyl sites, signifying that 1-propanol has a stronger interaction with acid sites than water (**Fig. 2.12**). In the second adsorption mode, the sequence for adsorbing water ($p = 0.005$ mbar) and 1-propanol ($p = 0.005$ mbar) was reversed. It is shown that the adsorbed 1-propanol remained almost unchanged on the Brønsted acid sites after the water was introduced to the 1-propanol adsorption complex. Thus, the results show that 1-propanol can effectively displace adsorbed water, while water was found hardly to displace adsorbed 1-propanol. Consequently, water is by far weaker in its interactions with acid sites compared with 1-propanol. The conclusion drawn from the co-adsorption IR experiments is supported by the higher heats of adsorption of 1-propanol (-95 kJ mol^{-1} , **Fig. 2.3**) than the value of water (-55 kJ mol^{-1}) determined by the calorimetric measurements. Moreover, similar findings were reported by Gorte [76] et al. when investigating methanol and water adsorption over HZSM-5 catalyst. Even though water molecules are not able to solely interact with the acid sites to form adsorbed water complex in the presence of alcohol, the rapid deuterium exchange of adsorbed methanol with D_2O indicates that water vapor can retain in the zeolite pore and contact with the adsorbed alcohol species [76].

2.3.4.2 Effect of water on the adsorption intermediate and transition state

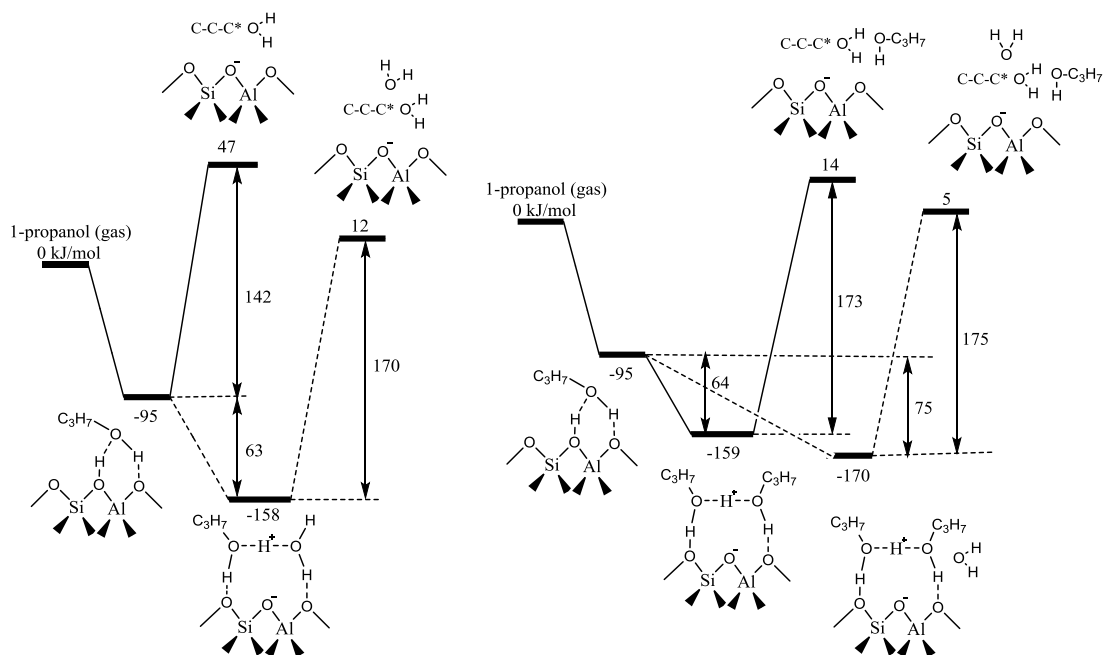


Fig. 2.13 Illustrated energy diagram for 1-propanol monomer (left figure) and dimer (right figure) dehydration to form propene in the absence (solid line) and presence of water (dashed line).

As discussed in section 2.3.2 and 2.3.3, introduced water increases the intrinsic barriers of enthalpy and entropy (energy difference of the transition state relative to the adsorption intermediate) both for 1-propanol elimination to form propene and 1-propanol dimolecular dehydration to form DPE reaction. The experimental estimated energy barrier and adsorption enthalpy, together with DFT calculated adsorption enthalpy (for 1-propanol and water dimer), allow us to deduce the degree to which water stabilizes or solvates the adsorption intermediate and the transition state based on the transition state theory.

Fig. 2.13 illustrates the energy diagram for 1-propanol monomer and dimer dehydration to form propene in the absence and presence of water. The heats of adsorption of -95 kJ mol^{-1} for 1-propanol monomer formation are determined by the calorimetric measurement shown in **Fig. 2.3**. The transition state energy of 47 kJ mol^{-1} is directly derived from the experimentally measured activation enthalpy of 142

kJ mol^{-1} . For the case of water added, water can interact with adsorbed 1-propanol monomer to form protonated 1-propanol and water dimer and the enthalpy for this dimer formation is -63 kJ mol^{-1} calculated from DFT method. On the basis of the measured activation enthalpy of 170 kJ mol^{-1} , the energy of transition state is determined to be 12 kJ mol^{-1} , which indicates that introduced water stabilize transition state by the energy of 35 kJ mol^{-1} relative to the transition state energy of 47 kJ mol^{-1} without additional water introduced. Hence, it is stated that water stabilize the adsorption intermediate (64 kJ mol^{-1} more stable) largely than the transition state (35 kJ mol^{-1} more stable), resulting in the higher activation barrier for propene formation. Even though the concurrent increase in activation entropy from $-54 \text{ J mol}^{-1} \text{ K}^{-1}$ to $-7.5 \text{ J mol}^{-1} \text{ K}^{-1}$, the prevalence of activation enthalpy in Gibbs free energy ends the dehydration reaction inhibited by the introduced water. This finding demonstrates that the strong solvation on the adsorption intermediate is the primary factor in determining the high activation barrier which concomitantly results in the lower rate. And the finding in this contribute is in contrast to the interpretation of water effect on MTO reaction, which argues that water merely stabilizes the transition state for first C-C bond formation step and then water facilitates the reaction with a lower activation barrier [64].

As for the reaction of 1-propanol dimer to propene, after 1-propanol monomer adsorption with the adsorption enthalpy of -95 kJ mol^{-1} , 1-propanol dimer can form and occupy the acid sites with adsorption enthalpy of -64 kJ mol^{-1} estimated from experimental data, a similar value with the adsorption enthalpy of -63 kJ mol^{-1} for 1-propanol and water dimer. Note that the adsorption enthalpy for the second 1-propanol (-64 kJ mol^{-1}) is lower than that for the first 1-propanol (-95 kJ mol^{-1}). The similar results were reported for methanol case [64]. Computations using different methods and cluster size predict the heat of adsorption for one methanol molecule to be -64 to -83 kJ mol^{-1} on HZSM-5 and to adsorb the second methanol gives the heat of adsorption of -55 and -35 kJ mol^{-1} [64]. According to the measured activation enthalpy of 173 kJ mol^{-1} , the transition state energy is determined to be 14 kJ mol^{-1} , which is comparable with the transition state energy of 12 kJ mol^{-1} for 1-propanol

monomer to propene with water introduced. By analysis the adsorption enthalpy and transition state energy of 1-propanol dimer to propene and 1-propanol monomer to propene with water added, we can conclude that introduced water and additional 1-propanol enthalpically solvate the adsorption intermediate and transition state to the same extent and then inhibit the dehydration reaction .

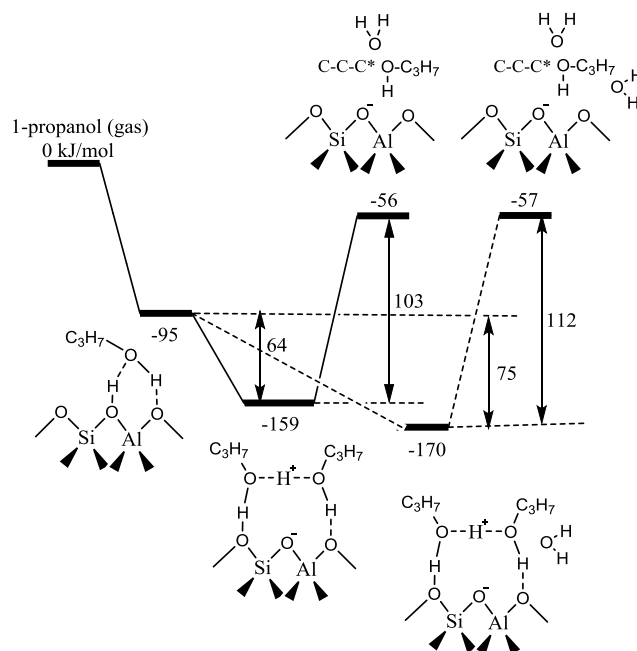


Fig. 2.14 Illustrated energy diagram for 1-propanol dimolecular dehydration to form DPE in the absence (solid line) and presence of water (dashed line).

In the energy diagram of dipropyl ether formation (**Fig. 2.14**), the transition state energy of -56 kJ mol^{-1} is significantly lower than that for propene formation (47 kJ mol^{-1} for 1-propanol monomer to propene), implying the more effective stabilization of 1-propanol with the propyl carbenium ion (DPE formation) than the solvation effect of water on the propyl cation in transition state (propene formation). Similar result was also observed in methanol dehydration reaction POM [67]. The introduced water slightly solvates the adsorption intermediate (64 kJ mol^{-1} more stable), but the transition state energy is not influenced.

2.4 Conclusions

1-propanol dehydration to form propene and DPE was systematically measured at varying 1-propanol pressure (0.075-4 kPa) and temperature (413-443 K). The kinetic and thermodynamic parameters estimated on basis of the mechanism-derived rate equation were used to assess the kinetic attenuation effect of water.

1-propanol dehydration to propene mechanism has been newly developed on basis of the dependence of dehydration rates on pressure. According to the traditional understanding, propene is derived from 1-propanol monomer species. However, in this contribution we find that 1-propanol monomer is not the only starting intermediate to form propene, and adsorbed 1-propanol dimer can also contribute for the propene formation if the reactant pressure is extended to the high enough range. The consistency of the mechanism-derived rate expression with the experimental data supports the proposed mechanism for propene formation. In agreement with the associative mechanism proposed for methanol and ethanol dehydration to the corresponding ethers in literatures, 1-propanol dimolecular dehydration to DPE proceeds via direct/ associative route as well on basis of the accurate analysis of the turnover rate dependence on reactant pressure.

Water has a pronounced attenuating effect on both the propene and DPE synthesis reflecting from the decreased dehydration rate. The inhibited catalytic dehydration activity is not derived from the acidity or structure change of zeolite. The unchanged acidity of used catalyst and no observed deactivation after long time time-on-stream test at 433 K in presence of water vapor show that HZSM-5 catalyst are highly stable and water tolerant under our reaction conditions (temperature below 433 K).

Additionally, our *in situ* IR spectroscopy results clearly demonstrate that the inhibiting effect of water is not a result of competitive adsorption between 1-propanol and water over BAS. The quantitative kinetic assessment of rate constant reveals that the inhibiting impact of introduced water is related to the different extent of solvation of water on adsorption intermediate and transition state. Water appears to better stabilize the adsorbed 1-propanol intermediate than the transition state enthalpically,

leading to the higher activation barrier for elimination step. Moreover, additional 1-propanol involved in 1-propanol dimer to propene route inhibits the dehydration rate in a manner consistent with the introduced water. Additional 1-propanol enthalpically solvate the adsorption intermediate and transition state to the same extent as water and then inhibit the dehydration reaction.

These findings reveal the fundamental and substantial influence of solvation effect of water on the reactivity of alcohol dehydration. Mechanistic understanding of the kinetic attenuation effect of water clears up controversies concerning the water effect and indicates that the large stabilization of water in adsorption intermediate than in transition state, and not the change of acidity or the competitive adsorption between alcohol and water, gives rise to the inhibiting effect.

2.5 Appendix

2.5.1 Derivation of the rate expression for 1-propanol elimination to propene

Here we derive in detail the rate equation for propene formation from the elementary steps outlined in Scheme 2.1 in main text. 1-propanol dehydration via the sequential route (E1 mechanism) proceeds by the adsorptions of 1-propanol onto Brønsted acid sites to form 1-propanol monomer ($[C_3H_7OH]_M$) (Step 1, Scheme 2.1) and then the adsorbed 1-propanol monomer decomposes to form surface-bound propoxide intermediate (Step 2a, Scheme 2.1), which is the rate-limiting step for 1-propanol elimination reaction. The propoxide species further deprotonates and recovers the acid site in parallel with forming propene product (Step 2b, Scheme 2.1).

Based on the above analysis, the rate equation for propene formation from 1-propanol monomer can be expressed in Eq. S-1.

$$r_{C_3H_6} = k_{M,P}[C_3H_7OH]_M \quad (S-1)$$

where $k_{M,P}$ is the intrinsic rate constant of water elimination to form propoxide species (step 2a, Scheme 2.1) and $[C_3H_7OH]_M$ is the concentration of 1-propanol monomers adsorbed on Brønsted acid sites.

Assuming that the quasi-equilibrium is achieved for 1-propanol adsorption (Step 1, Scheme 2.1) and for 1-propanol dimer formation (Step 4, Scheme 2.1) with equilibrium constants K_1 and K_4 , respectively, the number of 1-propanol monomers and dimers can be related to the gas phase 1-propanol pressure as shown in Eq. S-2 and S-3.

$$[C_3H_7OH]_M = K_1 H^+ [C_3H_7OH] \quad (S-2)$$

$$[C_3H_7OH]_D = K_1 K_4 H^+ [C_3H_7OH]^2 \quad (S-3)$$

where $[C_3H_7OH]$ is the 1-propanol pressure, $[H^+]$ represent the concentration of accessible Brønsted acid sites, and $[C_3H_7OH]_M$ and $[C_3H_7OH]_D$ denote the number of surface adsorbed 1-propanol monomers and dimers, respectively. The concentration of

accessible Brønsted acid sites is determined from the balance of surface species, which assumes that 1-propanol monomers and 1-propanol dimers are the most abundant covered surface species. The number of total Brønsted acid sites can be expressed as Eq. S-4.

$$[H^+]_0 = K_1 [H^+] [C_3H_7OH] + K_1 K_4 [H^+] [C_3H_7OH]^2 \quad (S-4)$$

where $[H^+]_0$ is the number of total Brønsted acid sites.

The combination of equations S-1 to S-4 leads to the rate equation for propene formation shown in Eq. S-5.

$$r_{C_3H_6} = \frac{k_{M,P} [H^+]_0}{1 + K_4 [C_3H_7OH]} \quad (S-5)$$

Besides 1-propanol monomer to propene route, propene can also be obtained from 1-propanol dimer and the rate expression for 1-propanol dimer to propene is shown as Eq. S-6.

$$r_{C_3H_6} = k_{D,P} [C_3H_7OH]_D \quad (S-6)$$

The propene rate expression via 1-propanol dimer route can be derived by combination the equations of S-1 to S-4 and S-6 and the obtained equation is shown as Eq. S-7.

$$r_{C_3H_6} = \frac{k_{D,P} K_4 [C_3H_7OH]}{1 + K_4 [C_3H_7OH]} \quad (S-7)$$

Consequently, considering the formation of propene from 1-propanol monomer and dimer route, the overall rate equation for propene formation can be expressed as Eq. S-8 via combination Eq. S-5 and S-7.

$$r_{C_3H_6} = [H^+]_0 \frac{k_{M,P} + k_{D,P} K_4 [C_3H_7OH]}{1 + K_4 [C_3H_7OH]} \quad (S-8)$$

2.5.2 Derivation of the rate expression for 1-propanol dimolecular dehydration to form DPE via direct mechanism

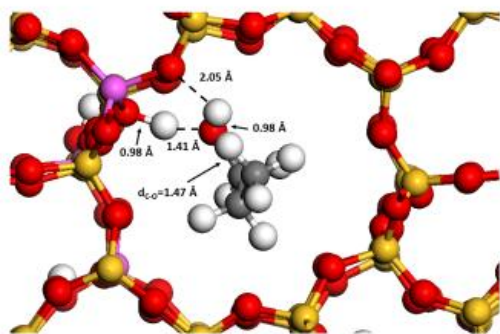
1-propanol dehydration to form DPE via the direct route proceeds starting from the adsorptions of 1-propanol over Brønsted acid sites to form 1-propanol monomers ($[C_3H_7OH]_M$) (Step 1, Scheme 2.2), and subsequently the second C_3H_7OH gas molecule reacts with the adsorbed 1-propanol monomer to form the protonated dimer ($[C_3H_7OH]_D$) (Step 2, Scheme 2.2). Then the protonated 1-propanol dimer decomposes to form DPE and water (Step 3, Scheme 2.2), which is the rate-limiting step. The rate equation for DPE formation can be expressed as Eq. S-9.

$$r_{C_3H_7OC_3H_7} = k_{D,E}[C_3H_7OH]_D \quad (S-9)$$

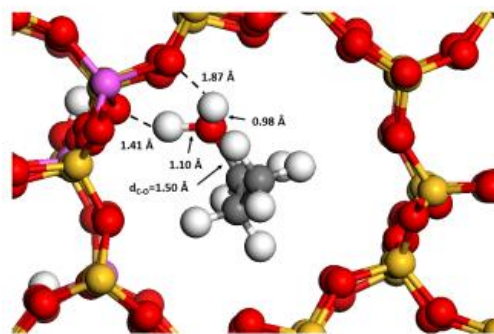
where $k_{D,E}$ is the intrinsic rate constant for DPE formation.

The assumption that the most abundant surface species are 1-propanol monomer and 1-propanol dimer, taken together with the equation S-2 to S-4 and S-9, results in DPE formation expression shown in Eq. S-10.

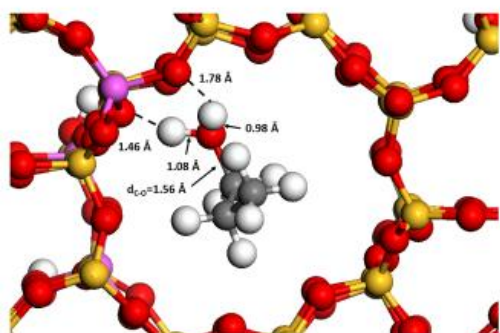
$$\frac{r_{C_3H_7OC_3H_7}}{[H^+]_0} = \frac{k_{D,E}K_4 C_3H_7OH}{1 + K_4 C_3H_7OH} \quad (S-10)$$



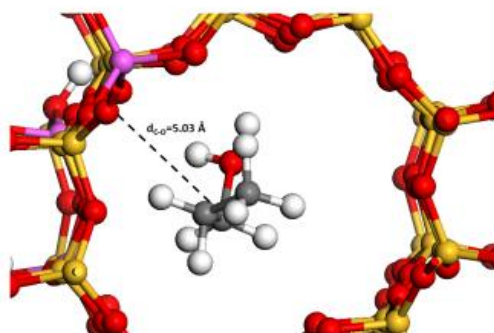
A



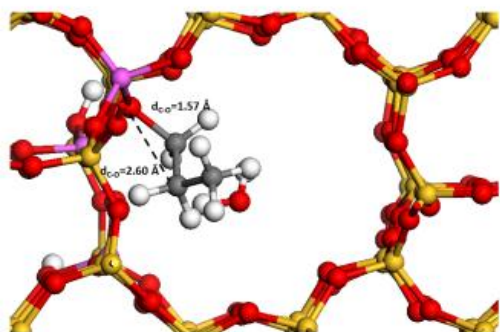
TS1



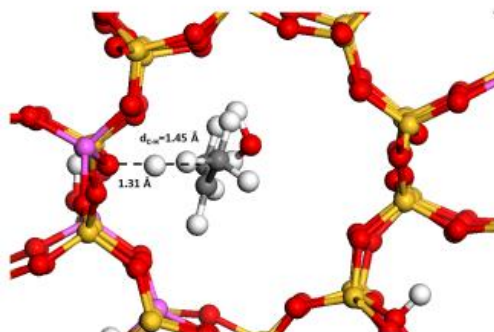
B



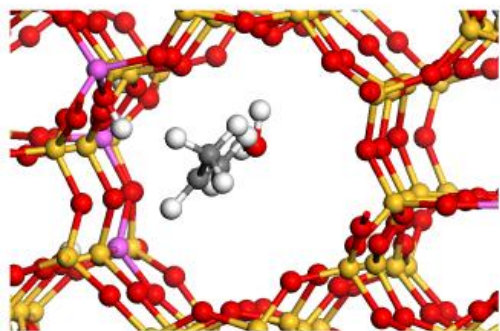
TS2



C



TS3



D

Fig. S1. Configuration structures of reaction intermediates and transition states for reaction of the 1-propanol dehydration to pronene.

2.6 References

- [1] W.R. Moser, R.W. Thompson, C.C. Chiang, H. Tong, *J. Catal.*, 117 (1989) 19-32.
- [2] A.G. Gayubo, A. Alonso, B. Valle, A.T. Aguayo, J. Bilbao, *Appl. Catal. B: Environ.*, 97 (2010) 299-306.
- [3] Y.T. Kim, K.D. Jung, E.D. Park, *Appl. Catal. A: Gen.*, 393 (2011) 275-287.
- [4] Y.T. Kim, K.D. Jung, E.D. Park, *Micro. Meso. Mat.*, 131 (2010) 28-36.
- [5] K. Kongpatpanich, T. Nanok, B. Boekfa, M. Probst, J. Limtrakul, *Phys. Chem. Chem. Phys.*, 13 (2011) 6462-6470.
- [6] C. Zhao, D.M. Camaioni, J.A. Lercher, *J. Catal.*, 288 (2012) 92-103.
- [7] A. Wawrzetz, B. Peng, A. Hrabar, A. Jentys, A.A. Lemonidou, J.A. Lercher, *J. Catal.*, 269 (2010) 411-420.
- [8] B.X. Peng, C. Zhao, I. Mejia-Centeno, G.A. Fuentes, A. Jentys, J.A. Lercher, *Catal. Today*, 183 (2012) 3-9.
- [9] J.A. Dias, S.C.L. Dias, N.E. Kob, *J. Chem. Soc. Dalton*, (2001) 228-231.
- [10] A.G. Gayubo, A.T. Aguayo, A. Atutxa, R. Aguado, J. Bilbao, *Ind. Eng. Chem. Res.*, 43 (2004) 2610-2618.
- [11] T. Okuhara, *Chem. Rev.*, 102 (2002) 3641-3665.
- [12] T.J.G. Kofke, R.J. Gorte, W.E. Farneth, *J. Catal.*, 114 (1988) 34-45.
- [13] M.J. Rice, A.K. Chakraborty, A.T. Bell, *J. Phys. Chem. A*, 102 (1998) 7498-7504.
- [14] S. Jungstittiwong, J. Limtrakul, T.N. Truong, *J. Phys. Chem. B*, 109 (2005) 13342-13351.
- [15] G.W. A. Jentys, M. Derewinski, J. A. Lercher, *J. Phys. Chem.*, 93 (1989) 4837-4843.
- [16] J.N. Kondo, M. Iizuka, K. Domen, F. Wakabayashi, *Langmuir*, 13 (1997) 747-750.

- [17] A.G. Pelmeshnikov, R.A. Vansanten, *J. Phys. Chem.*, 97 (1993) 10678-10680.
- [18] S.A. Zygmunt, L.A. Curtiss, L.E. Iton, M.K. Erhardt, *J Phys. Chem.*, 100 (1996) 6663-6671.
- [19] J. Sauer, P. Ugliengo, E. Garrone, V.R. Saunders, *Chem. Rev.*, 94 (1994) 2095-2160.
- [20] M. Krossner, J. Sauer, *J. Phys. Chem.*, 100 (1996) 6199-6211.
- [21] C.D. Baertsch, K.T. Komala, Y.H. Chua, E. Iglesia, *J. Catal.*, 205 (2002) 44-57.
- [22] J.R. Copeland, X.R. Shi, D.S. Sholl, C. Sievers, *Langmuir*, 29 (2013) 581-593.
- [23] A.G. Gayubo, A.T. Aguayo, M. Castilla, A.L. Moran, J. Bilbao, *Chem. Eng. Commun.*, 191 (2004) 944-967.
- [24] A.G. Gayubo, A. Alonso, B. Valle, A.T. Aguayo, J. Bilbao, *Ind. Eng. Chem. Res.*, 49 (2010) 10836-10844.
- [25] C. Mirodatos, D. Barthomeuf, *J. Chem. Soc .Chem. Comm.*, (1981) 39-40.
- [26] S.H. Li, A.M. Zheng, Y.C. Su, H.L. Zhang, L. Chen, J. Yang, C.H. Ye, F. Deng, *J. Am. Chem. Soc.*, 129 (2007) 11161-11171.
- [27] A. Janda, A.T. Bell, *J. Am. Chem. Soc.*, 135 (2013) 19193-19207.
- [28] S. Schallmoser, T. Ikuno, M.F. Wagenhofer, R. Kolvenbach, G.L. Haller, M. Sanchez-Sanchez, J.A. Lercher, *J. Catal.*, 316 (2014) 93-102.
- [29] S.M. Maier, A. Jentys, J.A. Lercher, *J. Phys. Chem. C*, 115 (2011) 8005-8013.
- [30] J. VandeVondele, M. Krack, F. Mohamed, M. Parrinello, T. Chassaing, J. Hutter, *Comput. Phys. Commun.*, 167 (2005) 103-128.
- [31] S. Goedecker, M. Teter, J. Hutter, *Phys. Rev. B*, 54 (1996) 1703-1710.
- [32] C. Hartwigsen, S. Goedecker, J. Hutter, *Phys. Rev. B*, 58 (1998) 3641-3662.
- [33] M. Krack, M. Parrinello, *Phys. Chem. Chem. Phys.*, 2 (2000) 2105-2112.
- [34] J. VandeVondele, J. Hutter, *J. Chem. Phys.*, 127 (2007) 114105.
- [35] J.P. Perdew, K. Burke, M. Ernzerhof, *Phys. Rev. Lett.*, 77 (1996) 3865.
- [36] C.C. Lee, R.J. Gorte, W.E. Farneth, *J. Phys. Chem. B*, 101 (1997) 3811-3817.
- [37] C.M. Nguyen, M.-F. Reyniers, G.B. Marin, *J. Catal.*, 322 (2015) 91-103.
- [38] S. Grimme, J. Antony, S. Ehrlich, H. Krieg, *J. Chem. Phys.*, 132 (2010) 154104.
- [39] G. Henkelman, B.P. Uberuaga, H. Jonsson, *J. Chem. Phys.*, 113 (2000)

9901-9904.

- [40] G. Mills, H. Jonsson, G.K. Schenter, *Surf. Sci.*, 324 (1995) 305-337.
- [41] A. Bhan, R. Gounder, J. Macht, E. Iglesia, *J. Catal.*, 253 (2008) 221-224.
- [42] R. Gounder, E. Iglesia, *J. Am. Chem. Soc.*, 131 (2009) 1958-1971.
- [43] R. Gounder, E. Iglesia, *Acc. Chem. Res.*, 45 (2012) 229-238.
- [44] A.J. Jones, E. Iglesia, *Angew. Chem. Int. Ed.*, 53 (2014) 12177-12181.
- [45] A.J. Jones, S.I. Zones, E. Iglesia, *J. Phys. Chem. C*, 118 (2014) 17787-17800.
- [46] G. Psfogiannakis, A. St-Amant, M. Ternan, *J. Phys. Chem. B*, 110 (2006) 24593-24605.
- [47] A. Jentys, G. Warecka, J.A. Lercher, *J. Mol. Catal.*, 51 (1989) 309-327.
- [48] H. Thamm, *J. Chem. Soc. Farad. T 1*, 85 (1989) 1-9.
- [49] C.C. Lee, R.J. Gorte, W.E. Farneth, *J. Phys. Chem. B*, 101 (1997) 3811-3817.
- [50] H. Chiang, A. Bhan, *J. Catal.*, 271 (2010) 251-261.
- [51] K.Y. Lee, T. Arai, S. Nakata, S. Asaoka, T. Okuhara, M. Misono, *J. Am. Chem. Soc.*, 114 (1992) 2836-2842.
- [52] J. Macht, M.J. Janik, M. Neurock, E. Iglesia, *Angew. Chem. Int. Edit.*, 46 (2007) 7864-7868.
- [53] J. Macht, M.J. Janik, M. Neurock, E. Iglesia, *J. Am. Chem. Soc.*, 130 (2008) 10369-10379.
- [54] M.J. Janik, J. Macht, E. Iglesia, M. Neurock, *J. Phys. Chem. C*, 113 (2009) 1872-1885.
- [55] W. Alharbi, E. Brown, E.F. Kozhevnikova, I.V. Kozhevnikov, *J. Catal.*, 319 (2014) 174-181.
- [56] S. Delsarte, P. Grange, *Appl. Catal. A: Gen.*, 259 (2004) 269-279.
- [57] H.C. Xin, X.P. Li, Y. Fang, X.F. Yi, W.H. Hu, Y.Y. Chu, F. Zhang, A.M. Zheng, H.P. Zhang, X.B. Li, *J. Catal.*, 312 (2014) 204-215.
- [58] M.J. Antal, M. Carlsson, X. Xu, D.G.M. Anderson, *Ind. Eng. Chem. Res.*, 37 (1998) 3820-3829.
- [59] J. Bedia, R. Ruiz-Rosas, J. Rodriguez-Mirasol, T. Cordero, *J. Catal.*, 271 (2010) 33-42.

- [60] J.H. Kwak, R. Rousseau, D.H. Mei, C.H.F. Peden, J. Szanyi, *Chem. Cat. Chem.*, 3 (2011) 1557-1561.
- [61] S. Roy, G. Mpourmpakis, D.Y. Hong, D.G. Vlachos, A. Bhan, R.J. Gorte, *Acs. Catal.*, 2 (2012) 1846-1853.
- [62] W. Wang, J. Jiao, Y.J. Jiang, S.S. Ray, M. Hunger, *Chem. Phys. Chem.*, 6 (2005) 1467-1469.
- [63] O. Olaofe, P.L. Yue, *Collect. Czech. Chem. C*, 50 (1985) 1834-&.
- [64] S.R. Blaszkowski, R.A. vanSanten, *J. Am. Chem. Soc.*, 119 (1997) 5020-5027.
- [65] C.M. Nguyen, M.F. Reyniers, G.B. Marin, *Phys. Chem. Chem. Phys.*, 12 (2010) 9481-9493.
- [66] C. M. Nguyen, M.F. Reyniers, G.B. Marin, *J. Catal.*, 322 (2015) 91-103.
- [67] R.T. Carr, M. Neurock, E. Iglesia, *J. Catal.*, 278 (2011) 78-93.
- [68] A.J. Jones, R.T. Carr, S.I. Zones, E. Iglesia, *J. Catal.*, 312 (2014) 58-68.
- [69] A.J. Jones, E. Iglesia, *Angew. Chem. Int. Edit.*, 53 (2014) 12177-12181.
- [70] E. Santacesaria, D. Gelosa, E. Giorgi, S. Carra, *J. Catal.*, 90 (1984) 1-9.
- [71] J.F. DeWilde, H. Chiang, D.A. Hickman, C.R. Ho, A. Bhan, *Acs. Catal.*, 3 (2013) 798-807.
- [72] R. Gounder, *Catal. Sci. Technol.*, 4 (2014) 2877-2886.
- [73] J.A. van Bokhoven, B. Xu, *Stud. Surf. Sci. Catal.*, 170 (2007), 1167-1173.
- [74] A. Omegna, J.A. van Bokhoven, R. Prins, *J. Phys. Chem. B*, 107 (2003) 8854-8860.
- [75] B. Xu, F. Rotunno, S. Bordiga, R. Prins, J.A. van Bokhoven, *J. Catal.*, 241 (2006) 66-73.
- [76] A. Ison, R.J. Gorte, *J. Catal.*, 89 (1984) 150-158.

Chapter 3

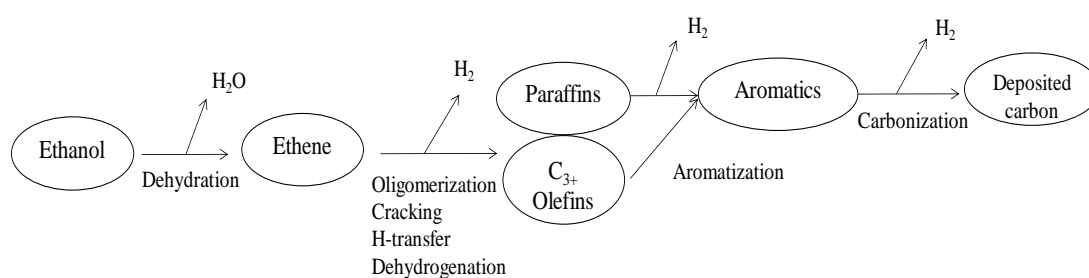
Ethanol conversion to propylene with enhanced stability on P and Zr modified HZSM-5

The successive P- and Zr- co-modified HZSM-5 90 leads to enhanced stability on conversion of ethanol to propylene in the continuous gas phase reaction at 773 K. After a series of condition optimization of temperature, pore confinement, acid concentration, and contact time, the best result is achieved with HZSM-5 90 operating at 773 K and a contact time of $0.03 \text{ g ml}^{-1} \text{ min}^{-1}$, yielding 27% propylene eventually. The P and Zr co-modified HZSM-5 enhances the catalyst life time from 10 to 26 h, maintaining the comparable initial activity. The modified catalysts are systematically characterized to correlate the catalyst activities with catalyst properties. The crystalline properties and pore structures of HZSM-5 are almost unchanged after Zr

and P modification. Determined from IR spectra of adsorbed pyridine and ^{27}Al and ^1H MAS NMR measurements, Brönsted acid sites are reduced after P and Zr co-modification. Moreover, the incorporation of Zr and P efficiently relieves dealumination, evidenced by IR spectroscopy. It also shows that the initial P modification does a significant impact to the electrical field gradient and Brönsted acid strength. The decreased strong Brönsted acid sites suppress dealumination together with coke formation, thus the catalyst life time is extended. The slightly higher acid strength of Zr/P/HZSM-5 also leads to higher concentrations of heavy C_{5+} hydrocarbons formation.

3.1 Introduction

Propylene, one of the most important chemical intermediate for synthesis of chemicals such as propylene oxide and polypropylene, is generally produced by the steam thermal cracking of naphtha from the petroleum, but the propylene yield is low due to existence of the *co*-product ethylene [1,2]. Stimulated by the petroleum crisis and the rapid increasing propylene demand together with environmental protection, it is urgent to seek alternative routes from renewable resources rather than petroleum feedstock [3,4]. Bio-ethanol, produced from the renewable biomass feedstock including corn, sugarcane, and cellulose, is envisioned as a promising energy carrier to produce propylene *via* novel designed catalysts, which can reduce petroleum dependence and carbon dioxide emissions [4-6].



Scheme 3.1 Mechanisms for ethanol conversion over HZSM-5 in the gas phase [10].

The conversion of ethanol to propylene has extensively been investigated with HZSM-5 zeolite including the effect of Si/Al ratio and identification of active sites of HZSM-5, as well as optimization of reaction conditions [6–9]. The polymerization-cracking mechanisms (Scheme 3.1) for ethanol conversion on HZSM-5 in the gas phase proceeds with initial dehydration forming ethylene, which can be oligomerized to C₃₊ olefins and paraffins, and dehydrogenated and aromatized to aromatics over acid sites [10]. Zeolites with a smaller 8-membered-ring pore system such as SAPO-34 [11] and LEV [12] were shown to be able to catalyze propylene production with higher selectivity as a result of the enhanced oligomerization step, but these zeolites suffered from the problems of rapid

deactivation from carbon depositions. Fujitani *et al.* [6] revealed that the fraction of C₃–C₄ hydrocarbons from ethanol conversion was depended on the Si/Al ratio of HZSM-5. Xia *et al.* [7] found that the yield of propene from ethanol was proportional to the number of Brønsted acidic sites. Iwamoto *et al.* [13] reported that Ni ion-loaded mesoporous silica MCM-41 was effective for producing propene from ethanol via the alternative pathway of coupling dehydration, dimerization, isomerization, and metathesis steps.

Modification of parent HZSM-5, for example, via the incorporation of metal into HZSM-5, has been investigated in order to improve the propylene selectivity as well. Although the propylene selectivity can be increased to nearly 30% after modified by Zr [6], Sr [14] or by *co*-modification W and La [15], Fe and P [16], however, the developed metal incorporated-HZSM-5 catalysts still face the problems of poor stability and serious coke formation and lifetime of the modified catalysts could not be sustained more than 10 hours. In this context, we report a strategy by sequential modification of HZSM-5 with Zr and P elements to enhance the catalyst activity and stability for ethanol conversion to propylene in a continuous reactor at 773 K. The pore structure and Si/Al ratios of zeolite, reaction temperatures, and contact times are optimized to enhance the propylene yield. In addition, the surface and pore, configuration structure, acidity of HZSM-5 before and after sequential Zr- and P-modification are comparatively investigated by N₂ sorption, Infrared spectroscopy of adsorbed pyridine, X-ray diffraction, as well as ²⁷Al MAS solid nuclear magnetic resonance measurements, in order to elucidate the relationship of catalyst properties and catalytic activities.

3.2 Experimental section

3.2.1 Chemicals

All chemicals were obtained from commercial suppliers: HZSM-5 zeolite (Clariant company), HBEA (Zeolyst company), HMOR (Zeolyst company), HY (Zeolyst

company), ASA (Sigma-Aldrich), $\text{ZrO}(\text{NO}_3)_2$ (Sigma-Aldrich), $(\text{NH}_4)_2\text{HPO}_4$ (Sigma-Aldrich), ethanol (Aldrich, $\geq 99.8\%$), He (Air Liquide, $>99.999\%$).

3.2.2 Catalyst preparation

The Zr and/or P-modified HZSM-5 catalysts with a Si/Al ratio of 45 were prepared by an impregnation method with $\text{ZrO}(\text{NO}_3)_2$ and $(\text{NH}_4)_2\text{HPO}_4$ as Zr and P precursors, respectively. 5 g HZSM-5 90 powder was suspended in 12 mL of aqueous $\text{ZrO}(\text{NO}_3)_2$ or $(\text{NH}_4)_2\text{HPO}_4$ solution, and water was removed by a vacuum evaporator at 333 K. The residue was dried at 383 K for 12 h and then calcined at 873 K in air for 4 h. Five kinds of Zr and/or P-modified HZSM-5 90 catalysts were prepared under the conditions: (1) Zr-modified HZSM-5 90 with Zr/Al ratios of 0.1, 0.2, and 0.4 mol/mol. (2) P-modified HZSM-5 90 with P/Al ratios of 0.1, 0.2, 0.4, and 0.6 mol/mol. (3) Zr-modified HZSM-5 90 (Zr/Al ratio: 0.4) followed by P modification (P/Al ratio: 0.4), abbreviated as P/Zr/HZSM-5 90. (4) P-modified HZSM-5 90 (P/Al ratio: 0.4) followed by Zr modification (Zr/Al ratio: 0.4), abbreviated as Zr/P/HZSM-5 90.

3.2.3 Catalyst characterization

The specific surface area and pore volume were measured by N_2 adsorption-desorption isotherms performed on a PMI automatic BET-Sorptometer at liquid nitrogen temperature (77 K) after outgassing in vacuum ($p=10^{-3}$ mbar) at 473 K for 2 h.

The X-ray diffraction (XRD) patterns were measured with a Philips X'Pert Pro System (Cu K_α -radiation, 0.154056 nm) at 40 kV/40 mA on a spinner in a 2θ range of 5° to 70° with a step size of $0.019^\circ/\text{s}$.

The IR spectra of adsorbed pyridine was performed a Perkin–Elmer model System 2000 FTIR apparatus at a resolution of 4 cm^{-1} for determining the nature of Brønsted and Lewis acids sites. The samples were pressed into self-supporting wafers and activated in vacuum ($p < 10^{-6}$ mbar) for 1 h at 723 K. After cooling to 423 K, pyridine ($p = 10^{-1}$ mbar) was adsorbed for 1 h and then outgassed for 0.5 h, a spectrum was

recorded at 423 K. The concentrations of Brønsted and Lewis acid sites were calculated from the intensity bands located at 1540 and 1450 cm^{-1} , respectively. For quantification, molar integral extinction coefficients of 0.73 and 0.96 were used for calculation of Brønsted acid sites (BAS) and Lewis acid sites (LAS), respectively.

Temperature-programmed desorption of ammonia was carried out in a 6-fold TPD setup. Approximate 50 mg of the samples was granulated to a particle size between 500 and 710 μm and activated in vacuum ($p = 10^{-3}$ mbar) at 723 K (heating rate = 10 K min^{-1}) for 1 h. After cooling to 373 K, 1 mbar of NH_3 was adsorbed for 1 h followed by outgassing of the samples for 2 h. The temperature was increased to 1043 K at a rate of 7 K min^{-1} , while desorption of NH_3 was monitored by mass spectroscopy using the $m/z^+ = 16$ signal. The acid site concentration was determined by normalization to the sample weight and comparison of the resulting integral area of the desorption peaks with that of a standard zeolite material with known acid site concentration (HZSM-5, $\text{SiO}_2/\text{Al}_2\text{O}_3 = 90$ from Clariant company, 360 $\mu\text{mol g}^{-1}$).

The ^{27}Al MAS NMR spectra were recorded on a Bruker AV500 spectrometer. For ^{27}Al MAS NMR measurements, the samples were hydrated for three nights in a desiccator containing a beaker with water. Spectra measured were the sum of 2400 sweeps with a recycle time of 250 ms. The chemical shifts were referenced using an external standard of solid $\text{Al}(\text{NO}_3)_3$ ($\delta = -0.54$ ppm). For ^1H MAS NMR spectra, the samples were activated in vacuum at 723 K for 1 h to eliminate adsorbed water. Then, they were transferred to a glove box and packed into a 4 mm ZrO_2 rotor in a water- and oxygen-free atmosphere. For recording the spectra, an excitation pulse ($\pi/2$) with a power level of 6.00 dB and a length of 3.80 μs was applied. The recycle time was 40 s. The chemical shifts were referenced to an external standard of adamantane ($\delta = 1.78$ ppm).

3.2.4 Catalytic measurements

Conversion of ethanol in the gas phase was performed in a continuous quartz tubular (diameter: 4 mm) flow reactor at atmospheric pressure. 200 mg catalysts that

was diluted in 500 mg SiC was used as catalysts. After the activation of catalyst in a He flow (flow rate: 20 ml min⁻¹) at 773 K for 1 h, the saturated ethanol vapor in He carrier gas ($P_{\text{ethanol}} = 20$ mbar) was introduced into the reactor. The reaction was carried out at 673-873 K, and the products were analyzed by a gas chromatography (GC) Hewlett Packard 5890 (Series II) equipped with a flame ionization detector (FID) and a Plot-Q column.

3.3 Results and discussion

3.3.1 The influence of pore confinement on products distribution

Table 3.1 Products distribution on ethanol conversion over aluminosilicate materials.^a

Catalyst	Si/Al ₂ ratio	Acidity ^b ($\mu\text{mol g}^{-1}$)	Pore dimensions	Yield (%)				
				C ₂ ⁼	C ₃ ⁼	C ₄ ⁼	C ₁ -C ₄ paraffins	C ₅₊
HMFI	30	852	5.2 x 5.7 Å	11	8.3	6.5	22	52
			5.3 x 5.6 Å					
HBEA	25	556	6.6 x 6.7 Å	89	3.3	1.5	3.1	2.7
			5.6 x 5.6 Å					
			7.0 x 6.5 Å					
HMOR	40	849	Short 8-ring channels 3 Å	98	0.5	0.5	0.6	0.1
HY	30	564	7.4 x 7.4 Å	88	1.6	0.4	9.0	0.2
			11.8 Å supercage					
ASA ^c	16	489	amorphous	87	2.7	0.3	5.7	2.0

^a Conditions: 0.2 g catalyst diluted in 0.5 g SiC, 773 K, $P_{\text{EtOH}} = 0.2$ bar, total flow 20 ml min⁻¹.

^b Acid concentrations are measured by NH₃-TPD.

^c ASA represents amorphous silica-alumina.

The selected aluminosilicate solid acids include HMFI, HBEA, HMOR, HY, and

amorphous silica-alumina (ASA) catalysts (see **Table 3.1**). Measured by the temperature programmed desorption of NH_3 , the acid concentrations of five samples (displayed in the Appendix **Fig. S1**) were in the range from 500 to 850 $\mu\text{mol g}^{-1}$ with Si/ Al_2 ratios from 16 to 40. The acid strength followed the sequence $\text{HMOR} > \text{HMFI} > \text{HY} \approx \text{HBEA} > \text{ASA}$, as determined by the temperatures for maximum desorption rate (**Fig. S1**). **Table 3.1** showed the effect of pore structures on the products distribution of ethanol conversion at 773 K in the continuous reactor. HZSM-5 formed 90% yield of C_{3+} products and 10% yield of ethylene, and in a comparison the large pore zeolites of HBEA, HMOR, and HY produced significant amounts of ethylene (higher than 90%) and trace amounts of heavier C_{3+} products. ASA led to the major product of ethylene with a yield of 87%. Further increasing the temperature to 873 K, the propylene yield concomitantly increases to 15% at the temperature range of 823-873 K (see **Fig. S2**). Yet the propylene yields are still kept at the level lower than 5% with respect to other larger pore catalysts with the identical temperature. The active sites for ethanol dehydration and the subsequent oligomerization and cracking of alkene are considered both as Brønsted acid sites (bridging hydroxyl group) and the surrounding cavities of zeolite pore structures that solvates the confined species. The stability of reaction intermediates and transition states that mediates ethanol transformation in the zeolites is influenced by both electrostatic interaction and van der Waals dispersion force between zeolite cavities and confined hydrocarbon fragments [17,18]. It is suggested that the narrow pore size of HMFI zeolite (see **Table 3.1**) that exerts the most effective stabilizing effect associated with proper acidity concentrations and strengths is beneficial for the ethanol dehydration and the following oligomerization-cracking of ethylene intermediates. Herein HMFI zeolite (HZSM-5) is thus screened as the proper solid acid catalyst for the following study.

3.3.2 Reaction conditions optimizations on ethanol conversion

The reaction conditions are subsequently optimized with temperature, acid concentration, as well as contact time for ethanol conversion over HZSM-5. In the

tested temperature range (from 393 to 673 K) (see **Fig. 3.1**), diethyl ether (DEE) was the major product at the low temperature, and it reached a maximum yield of 72% at 480 K. As temperature was increasing, DEE yield was decreasing and gradually disappeared at 533 K. Ethylene was initially formed at 453 K with a yield of 2%, and was then sharply increased to a maximum yield of 43% at 520 K; After that, the yield of ethylene decreased rapidly due to the oligomerization reaction, which attained a minimum yield of 3% at 593 K. As the temperature further increased, the cracking of heavier hydrocarbons led to the increased ethylene yield. On the other hand, yield of propylene started to appear at around 500 K and slowly increased to 15% at 673 K. Formation of butene maintained a constant yield of 20% from 570 K to 673 K. The heavier hydrocarbons C_{5+} was formed at around 450 K and achieved the maximum yield of 64% at 570 K. With the further increase of temperature to 673 K, the enhanced cracking rates lowered C_{5+} yields. Therefore, it is summarized that in the low temperature of 390 to 520 K, the diethyl ether product is majorly formed, while at an elevated temperature higher than 520 K, ethylene dominates and diethyl ether is decomposing to ethanol. The increased temperature (above 500 K) raises the propylene yield due to integrated ethylene oligomerization and subsequent cracking processes. Furthermore, at temperature above 673 K the fast cracking rates decompose the produced heavier products of C_{5+} hydrocarbons and further increase the propylene yield.

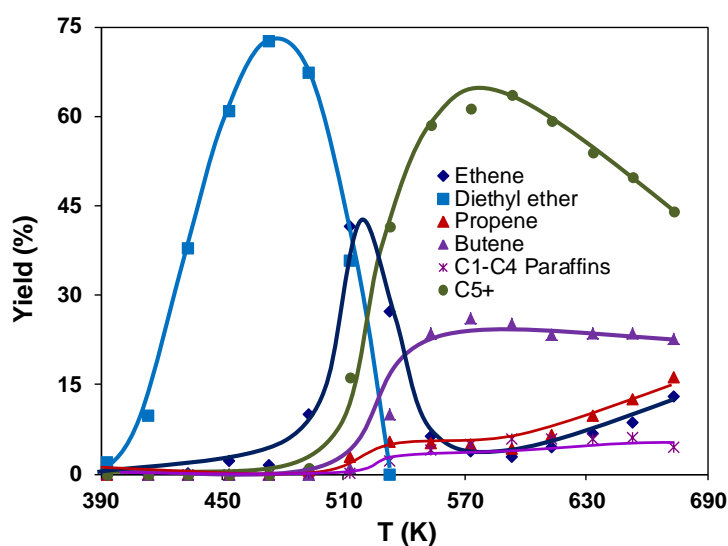


Fig. 3.1 Products distribution on ethanol conversion over HZSM-5 30 as a function of temperature. Reaction conditions: 0.1g HZSM-5 diluted in 0.5 g SiC, 393-673 K, $P_{\text{EtOH}} = 20$ mbar, total flow rate: 10.3 ml min^{-1} .

Apart from the temperature influence, the impact of acidity, i.e., Si/Al₂ ratios (30, 90, and 240) of HZSM-5, is further investigated on product distributions in the temperature range of 673-873 K (see **Fig. S3**). An increase in the Si/Al ratios reduces the surface acidity, which has been verified by IR spectroscopy of pyridine (**Table S1**). Three catalysts all led to 100% ethanol conversion at selected conditions. With HZSM-5 240 having weak acidity, ethylene was predominantly produced with exceeding 87% ethylene from 673 to 773 K, and even at the high temperature of 873 K ca. 82% ethylene was remained. The yields of propylene, butene and paraffins were increased with the temperature, and the highest propylene yield was obtained with 5% at 873 K. In a comparison, C₅₊ hydrocarbons were the main products over the strong acidic HZSM-5 30. At 773 K, 54% C₅₊ hydrocarbons and 22% C₁-C₄ paraffins were produced on HZSM-5 30, while HZSM-5 90 yielded 28% C₅₊ hydrocarbons and 5% C₁-C₄ paraffins. This result implies that the oligomerization step requires high acid concentrations. The yield of propylene was enhanced with an increased temperature, and it reached to a maximum yield of 15% at 823 K. For HZSM-5 90, the yield of ethylene increased sharply from 14% to 57% at temperatures from 673 to 873 K (see **Fig. S3**), whereas the yields of butene, C₁-C₄ paraffins, and C₅₊ hydrocarbons were gradually decreased. The maximum propylene yield attained 26% at 773 K, achieving the best balance of oligomerization and cracking process. It is shown here that acidity has a pronounced impact on the products selectivity, that is lower acidity favours larger amounts of ethylene forming, the higher acidity drives the ethylene oligomerization to form heavier hydrocarbon and the medium acidity is preferred for the propylene selectivity at the reaction conditions. HZSM-5 90 is thus selected to be the best catalyst for ethanol conversion to propylene at 773 K.

Not only the influence of temperature and acidity of zeolites, but also the contact

time of reactants onto acid active sites of HZSM-5 controls the polymerization efficiency of ethylene intermediate (see **Fig. 3.2**). At low W/F of $0.02 \text{ g ml}^{-1} \text{ min}^{-1}$, the direct dehydrated ethylene was predominantly produced at 70% yield with the short contact time at 773 K, whereas at higher W/F of $0.05 \text{ g ml}^{-1} \text{ min}^{-1}$, the subsequent C–C coupling formation of propylene, butene, paraffins, C_{5+} aliphatics, and C_{5+} aromatics was accumulated at attaining a high yield of 80%. This result indicates that the contact time can dramatically alter the product distributions via manipulating the ethylene oligomerization step. A medium W/F of ca. $0.03\text{-}0.04 \text{ g ml}^{-1} \text{ min}^{-1}$ for yielding 26% propylene at 773 K was achieved as the optimal reaction conditions (see **Fig. 3.2**).

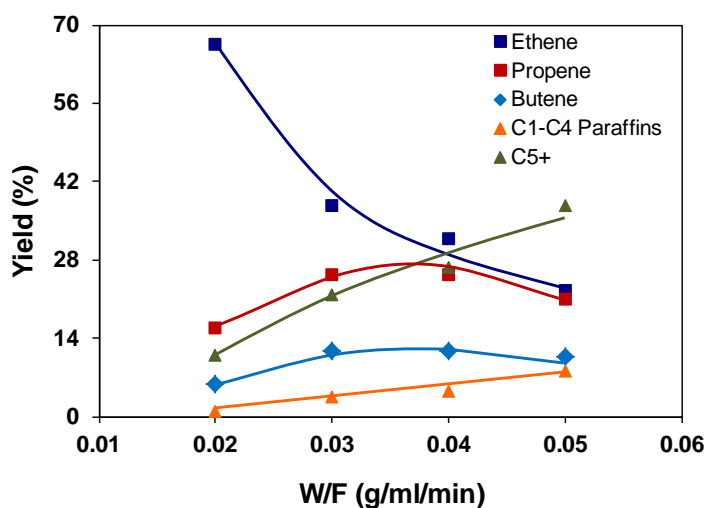


Fig. 3.2 Conversion of ethanol over HZSM-5 90 as a function of contact time. Reaction conditions: 0.1- 0.4 g HZSM-5 90 catalyst diluted in 0.5 g SiC, 773 K, $P_{\text{EtOH}} = 0.2 \text{ bar}$, total flow rate: 20 ml min^{-1} .

Apart from the consideration of selectivity, stability is also evaluated in the time course for the conversion of ethanol over HZSM-5 90 (**Fig. 3.3**). In the initial 10 h, HZSM-5 90 yielded propylene stably at 26%, and afterwards, however, the yield of propylene dropped from 26% to 20%, and the ethylene yield increased rapidly from 35% to 50%. After 66 h, the propylene yield dropped down to 4% accompanied with 85% ethylene yield. Therefore, HZSM-5 catalysts face a severe catalyst deactivation.

The reason for deactivation of HZSM-5 at high temperature is probably attributed to the coke deposition and dealumination of zeolite, which are caused by polymerization of heavy hydrocarbons and the presence of formed water from ethanol dehydration, respectively. In the next step, in order to improve the activity and stability of HZSM-5 for producing propylene from ethanol, modifications of HZSM-5 90 with Zr and P are performed.

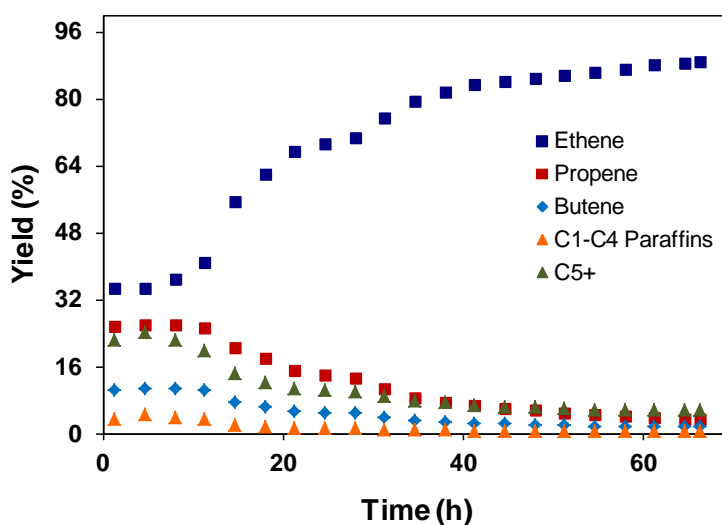


Fig. 3.3 Time-on-stream of products yield for ethanol conversion over parent HZSM-5 90. Reaction conditions: 0.2 g catalyst diluted in 0.5 g SiC, 773 K, $P_{\text{EtOH}} = 0.2$ bar, total flow rate: 20 ml min⁻¹.

3.3.3 Influence of P and Zr modifications on HZSM-5 90

HZSM-5 was modified with P or Zr by impregnating respective $\text{ZrO}(\text{NO}_3)_2$ and $(\text{NH}_4)_2\text{HPO}_4$ solutions. The dependence of the propylene yield versus the P or Zr/Al atomic ratios in modified ZSM-5 90 was plotted in **Fig. 3.4**. Ethanol was converted to olefins (ethylene and propylene), paraffins, as well as heavier aromatics and aliphatics at 100% conversion at 773 K and 0.2 bar ethanol pressure. The yield of propylene was 25.8% over parent unmodified HZSM-5, and P addition yielded an increased propylene to 26.5% at a P/Al ratio of 0.1. Whereas further increasing the P/Al ratio to 0.4 led to a decreased propylene yield to 10%. The same trend was also observed for

Zr-modified HZSM-5 90, which attained the highest propylene yield of 27.2% at a P/Al ratio of 0.4.

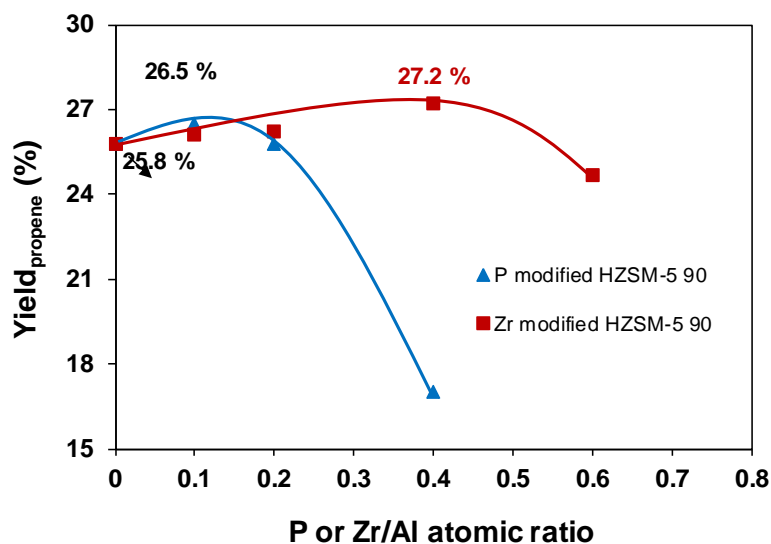


Fig. 3.4 Effect of P and Zr modification on the propylene yield for ethanol conversion over HZSM-5 90. Reaction conditions: 0.2 g catalyst diluted in 0.5 g SiC, 773 K, $P_{\text{EtOH}} = 0.2$ bar, total flow 20 ml min⁻¹.

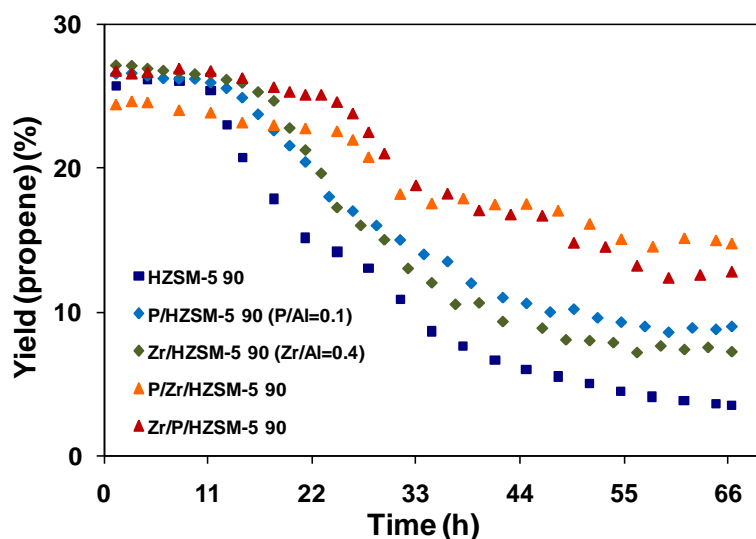


Fig. 3.5 Catalytic performance of modified ZSM-5 90 on conversion of ethanol as a function of time. Reaction conditions: 0.2 g catalyst diluted in 0.5 g SiC, 773 K, $P_{\text{EtOH}} = 0.2$ bar, total flow rate: 20 ml min⁻¹, time on stream: 66 h.

The modified ZSM-5 catalysts with mono- P or Zr slightly enhanced the propene yield (**Fig. 3.5**). The stability test showed that the initial propene yield was slightly enhanced by 2-3% after mono- P or Zr modification, and such catalyst started to deactivate after around 16 h. The modification led to much higher catalyst stability compared to the parent zeolite (life time: 10 h). After a long testing time of 66 h, the propene yield still maintained at 10% and 9% for P/HZSM-90 and Zr/HZSM-90, respectively, while the parent HZSM-90 catalyst only generated 4% propene yield at identical conditions.

In order to further increase the catalytic activity and stability, *co*-modification of P and Zr for HZSM-90 was carried out. The products distribution over parent, mono- P and Zr as well as P/Zr co-modified HZSM-5 90 are compiled in **Table 3.2**. For single P or Zr modification, ethylene yield increased from 35% to 40% and 43%, respectively, however, the C₅₊ hydrocarbons decreased from 22% to 19% and 17%. Ethanol is considered to be firstly converted to ethylene and subsequently ethylene is oligomerized to higher hydrocarbons over acid sites of zeolites. Hence, the increase of ethylene yield and the decrease of C₅₊ hydrocarbons can be ascribed to the variation of acidity by modifying P or Zr elements. It is speculated here that the P or Zr modification of HZSM-5 90 may decrease the number of strong Brönsted acid sites, which will be discussed in detailed in the following characterization section. Shown in **Table 3.2**, it was also found that the P and Zr addition sequence results in quite different product distribution. P/Zr/HZSM-5 90 catalyst led to the similar product distribution compared with single P or Zr modification, with the even higher ethylene yield (50%) and lower C₅₊ hydrocarbons (13%), which implies that sequential Zr-P introduction can further decrease the acidity of the catalyst. In contrast, the ethylene yield was decreased to 29% and the yield of C₅₊ hydrocarbons was enhanced to 25% with Zr/P/HZSM-5 90 catalyst. The much higher heavier hydrocarbons yield indicates that the strong acid sites were increased for the Zr/P/HZSM-5 90 catalyst. The propylene yield was maintained at 27% after two modifications. This observation allows to speculate that the different P and Zr introduction sequence exerts a distinct

impact on the acidity of the catalyst, that is, the acid strength of P/Zr/HZSM-5 90 is decreased compared to the parent HZSM-5 catalyst and strength is enhanced as for the catalyst Zr/P/HZSM-5 90 with reverse addition sequence.

Table 3.2 The effect of P and/or Zr modification on the initial products distributions for ethanol conversion.

Catalysts	Yield (%)				
	Ethylene	Propylene	Butylene	C ₁ -C ₄ Paraffins	C ₅₊
HZSM-5 90	35	26	10	3.4	22
P/HZSM-5 90 (P/Al=0.1)	40	27	11	3.1	19
Zr/HZSM-5 90 (P/Al=0.4)	43	27	10	3.0	17
Zr/P/HZSM-5 90	29	27	14	5.5	25
P/Zr/HZSM-5 90	50	24	10	2.2	13

With respect to the stability issue, deactivation of HZSM-5 catalyst is generally recognized to be caused by the accumulation of carbon deposits and dealumination of the framework aluminium caused by the produced water at high temperature reactions above 673 K [19,20]. Carbon deposition is derived from heavier hydrocarbons via polymerization of attained light olefins over acid sites. The formed fewer C₅₊ compounds after Zr and/or P modifications (see **Table 3.2**) would effectively reduce the amounts of coke formation because of the inhibition of the subsequent polymerization of ethylene and correspondingly extend the catalyst lifetime (see **Figure 3.5**). On the other side, dealumination is led by the produced water from dehydration reactions at high temperature, and such water effect can be efficiently suppressed by addition of Zr or P reported in the former literatures [21,22]. In conclusion, both the reversible coke formation and irreversible dealumination deactivation are partly prevented by P and Zr modifications on HZSM-5 90, which

may eventually enhance the catalyst stability for conversion of ethanol to propylene. To get more insight into the changes of catalyst crystallographic and pore structure, acidity, and Al and H local environment after P and Zr modification, a detailed catalyst characterization is performed.

3.3.4 Characterization of changes of HZSM-5 after P and Zr modifications

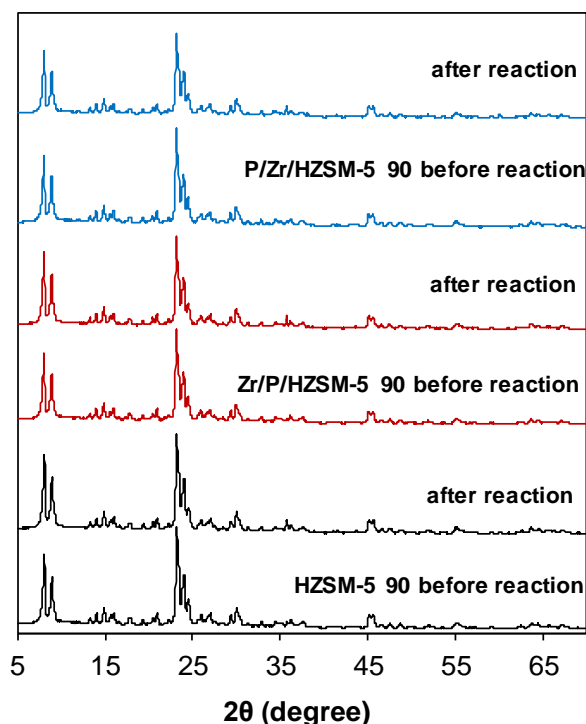


Fig.3. 6 XRD patterns of parent and modified HZSM-5 90 catalysts before and after reaction.

A detailed characterization including measurements of N_2 sorption, X ray pattern, IR spectroscopy of adsorbed pyridine, and 1H and ^{27}Al MAS NMR is subsequently developed. **Fig. 3.6** displays the XRD patterns of unmodified and Zr- and P-*co*-modified HZSM-5 90 before and after reaction. All samples showed a typical MFI structure. Characteristic diffraction peaks of zirconium oxide and crystal phase of phosphate species were not detected in P and Zr modified HZSM-5 90, which means the ZrO_2 amounts are negligible. After *co*-modification by P and Zr, the intensity of XRD patterns at $2\theta = 23.1^\circ$ was slightly decreased to 92% and 96% compared to the parent HZSM-5 90, probably due to slight dealumination during the preparation

procedure. After 66 h reaction time, the crystallinity of HZSM-5 90, Zr/P/HZSM-5 90, and P/Zr/HZSM-5 90 was reduced to 97%, 99%, and 85%, as shown from XRD peak patterns, respectively. This points to the high catalyst stability after P and Zr modifications.

Table 3.3 The physical properties of P and/or Zr modified HZSM-5 90.

Catalysts	BET surface area (m ² g ⁻¹)	Pore volume (cm ³ g ⁻¹)	Micropore volume (cm ³ g ⁻¹)	Mesopore volume (cm ³ g ⁻¹)
HZSM-5 90	424	0.29	0.17	0.12
P/HZSM-5 90	395	0.28	0.15	0.13
Zr/HZSM-5 90	374	0.29	0.13	0.16
Zr/P/HZSM-5 90	387	0.29	0.15	0.14
P/Zr/HZSM-5 90	340	0.24	0.13	0.11

Table 3.3 shows the physical properties of parent as well as P and Zr modified HZSM-5 90 zeolites as analyzed by N₂ sorption measurement. For the parent HZSM5 90, the specific surface area was 424 m² g⁻¹ and the pore volume was 0.29 cm³·g⁻¹. After modification by mono-P, mono- Zr, and co-modified Zr/P, the specific surface area of the catalysts were decreased to around 374-395 m² g⁻¹, but the pore volume was almost comparable with the parent HZSM5 90. The P/Zr/HZSM-5 90 catalyst was, however, different with decreased specific surface area (340 m² g⁻¹) and pore volume (0.24 cm³ g⁻¹). Therefore, P and Zr modified HZSM-5 90 maintains the similar topology structures with the slightly decreased specific surface areas. The shrink of pore volume for P/Zr/HZSM-5 90 is probably because of the formed Zr₃(PO₄)₂ or ZrO₂ deposits during the catalyst preparation process.

Fig. 3.7a shows the IR spectra (in the range of 3000-3800 cm⁻¹) of parent and P and/or Zr-modified HZSM-5 90 catalysts. The bands at 3740 and 3606 cm⁻¹ are ascribed to the respective isolated silanol group (Si-OH) and bridging OH group

(Si-OH-Al). The Brønsted acid sites of bridging OH group (Si-OH-Al) further decreased after P/Zr and Zr/P co-modification, and a new band at 3671 cm^{-1} assigned to P-OH group appeared [23,24]. In contrast, a decrease in the band at 3740 cm^{-1} suggests that the terminal silanol group is occupied upon P or Zr modification.

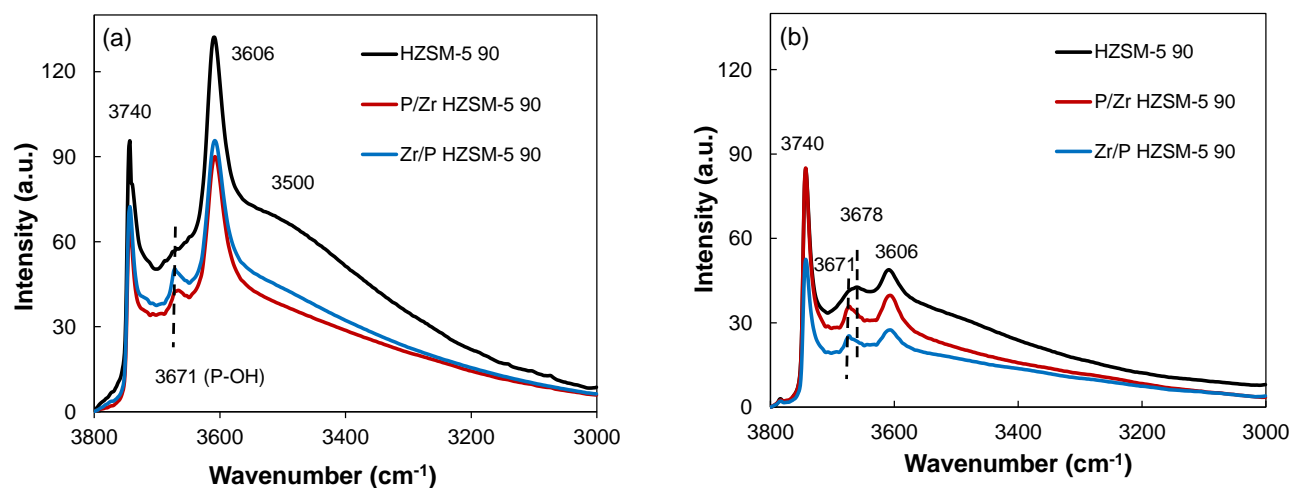


Fig. 3.7 IR spectra for parent and modified HZSM-5 90, (a) before reaction, and (b) after reaction.

The IR spectra of these catalysts after reaction (**Fig. 3.7b**) showed that BAS sites decreased dramatically, probably due to the carbon deposition. For parent HZSM-5 90, a new band at 3668 cm^{-1} (Al-OH) appeared after reaction, which indicates dealumination during the conversion transfers the framework Al to the extra-framework Al [25]. With respect to the P/Zr and Zr/P co-modified HZSM-5 90 after reaction, the P-OH group remained with comparable intensities. In addition, the band of Zr/P/HZSM-5 90 at 3740 cm^{-1} for silanol group decreased obviously, indicating that such catalyst is not quite stable during the reaction. Moreover, the new band at 3668 cm^{-1} (Al-OH) for P/Zr and Zr/P co-modified HZSM-5 90 catalysts, ascribed to the dealumination during the reaction, was much weaker than the parent HZSM-5 catalyst (see **Fig. 3.7b**), suggesting that Zr and P co-modification can reduce dealumination in the high-temperature reaction. This is in good agreement with the enhanced stability of P/Zr and Zr/P co-modified HZSM-5 90 catalysts in the catalytic tests (see **Fig. 3.5**).

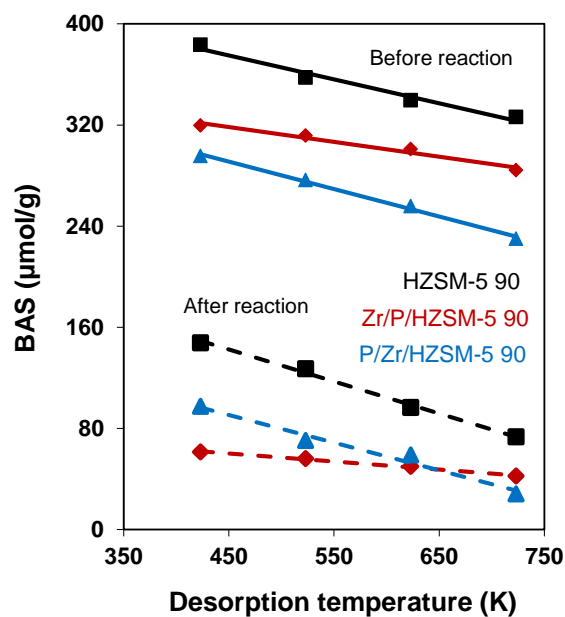


Fig. 3.8 Acidity distributions from IR spectra of adsorbed pyridine in parent and modified HZSM-5 90 catalysts before and after reaction.

Fig. 3.8 shows the results for quantification of the acidity concentrations measured by IR spectroscopy of adsorbed pyridine, and the original IR adsorption data are displayed at Figure S7. The tested catalysts include parent, P and Zr modified HZSM-5 90 before and after reaction (time: 66 h). With fresh Zr/P/HZSM-5 90 and P/Zr/HZSM-5 90, the Brønsted acid site concentrations were decreased by 17% and 30% compared with the parent HZSM-5 90 (see **Fig. 3.8**). It suggests that dealumination may occur during the catalyst preparation process. However, the acidity strength of modified HZSM-5 90 (determined at the higher pyridine desorption temperature of 673 K) was changed in a different way, where Zr/P/HZSM-5 90 had stronger acid strength than the parent HZSM-5 and P/Zr/HZSM-5 (see **Fig. 3.8**). The higher acid strength of Zr/P/HZSM-5 90 would lead to form higher concentrations of C_{5+} hydrocarbons than P/Zr/HZSM-5 90, which is well agreed with the experimental results discussed in the aforementioned part (see **Table 3.2**). After reaction, the Brønsted acid concentration of HZSM-5 90 was decreased by 60%, and in a comparison, such decrease was more pronounced for

P/Zr/HZSM-5 and Zr/P/HZSM-5 catalysts, in which BAS were decreased by 70% and 75%, respectively. The fewer Brønsted acid sites are beneficial for maintaining high catalyst stability via reducing coke formation. In addition, determined by pyridine desorption temperature at 673 K strong acid sites occupied 69% of total Brønsted acid sites in the used Zr/P/HZSM-5 90, while the used P/Zr/HZSM-5 90 only had 29% strong acid sites. This may be attributed to the unequal surface structures after opponent Zr and P addition sequence.

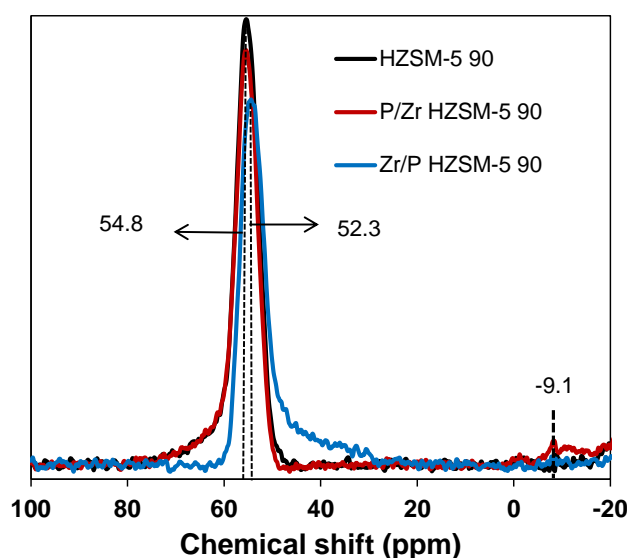


Fig. 3.9 ^{27}Al MAS NMR spectra of parent and P and Zr modified HZSM-5 90.

The ^{27}Al MAS NMR spectra of parent and P and Zr modified HZSM-5 90 are shown at **Fig. 3.9**. The intense peak at 54.8 ppm for HZSM-5 90 is ascribed to tetrahedrally coordinated Al in the zeolite framework. The weak and negligible peak at around 0 ppm indicates that the octahedrally coordinated extra-framework Al almost does not exist in the parent HZSM-5 90. In addition, the weak signal at -9.1 ppm is attributed to octahedrally coordinated Al in the amorphous aluminum phosphate [24,26]. For the initially Zr incorporated P/Zr/HZSM-5 90, the similar and intense peak at 54.8 ppm indicates that the potentially formed ZrO_2 on the surface of the zeolite by Zr incorporation does not induce a strong electrostatic interaction, and

subsequently the further introduced P has minimal influence onto the Al structure. In a comparison, the reverse sequential P and Zr introduction resulted in an asymmetric peak accompanied with a peak shift to 52.3 ppm (from 54.8 ppm). This implies that the sequential P and Zr modification exerts a significant effect on the local environment of framework Al. The main peak showed decreased intensity and peak shift, suggesting a substantial changed electrical field gradient. Very broad resonances in 10-50 ppm range emerged owing to more distorted framework Al.

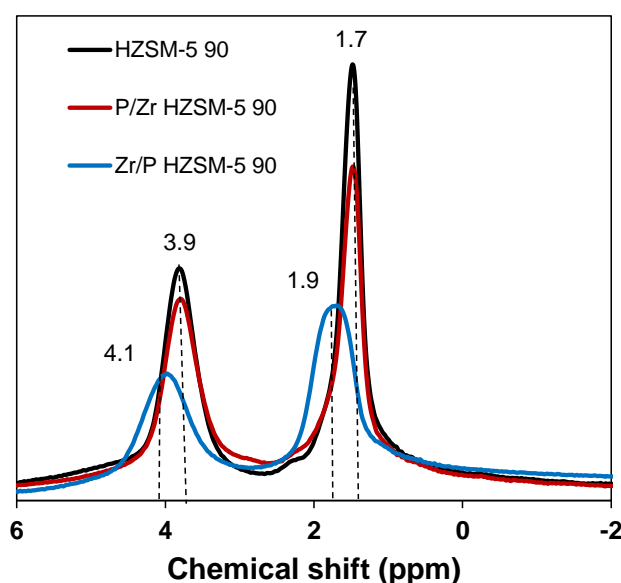


Fig. 3.10 ^1H MAS NMR spectra of parent and P and Zr modified HZSM-5 90.

The structure changes of HZSM-5 90 after Zr and P modifications are also explored by ^1H MAS NMR spectra (see **Fig. 3.10**). The two main resonances at 1.7 and 3.9 ppm for parent HZSM-5 catalyst are ascribed to the terminal Si-OH and bridging OH groups, respectively. The decreased signals at 1.7 and 3.9 ppm for the P/Zr/HZSM-5 90 catalyst are agreed with the IR spectroscopy results that the terminal Si-OH group and Brønsted acid sites of P/Zr/HZSM-5 90 are reduced (see **Fig. 3.7**). In agreement, both signals of terminal Si-OH and bridging OH groups were decreased for Zr/P/HZSM-5 90 catalyst. The chemical shift of Zr/P/HZSM-5 90 catalyst was changed from 3.9 to 4.1 ppm, which is associated with the shifting of tetrahedrally

coordinated Al from 54.8 to 52.3 ppm shown in ^{27}Al MAS NMR spectra. This shift also suggests that the Brønsted acid strength is increased after Zr/P *co*-modification. Besides, the decreased peak area at 4.1 ppm indicates the decreasing acidity density, fitted with acidity results from IR spectra of adsorbed pyridine shown in **Fig. 3.8**.

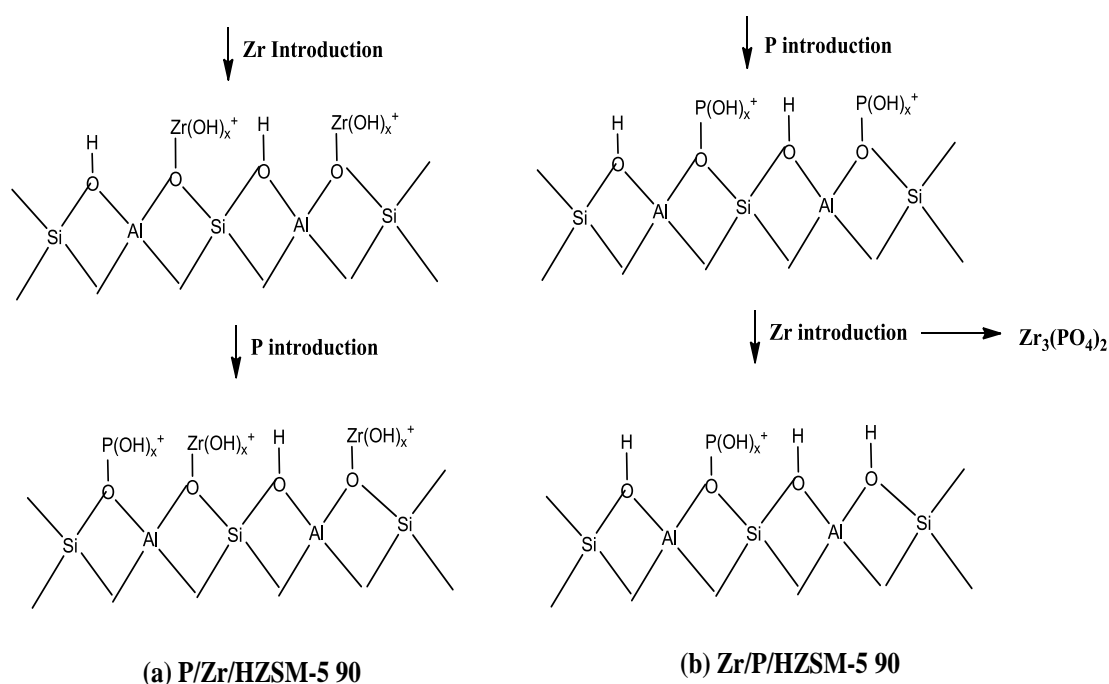


Fig. 3.11 Scheme of the change in the structure of modified acid sites during introducing P and Zr into the HZSM-5 90 catalyst. (a) P/Zr/HZSM-5 90, first Zr introduced and followed by P incorporation; (b) Zr/P/HZSM-5 90, first P introduced and followed by Zr incorporation.

The surface interaction of the introduced P and Zr (different addition sequence) onto the acid sites of HZSM-5 catalyst is proposed in **Fig. 3.11**. After single P or Zr introduction, the new weak acidic sites of P-OH and Zr-OH groups are generated, as illustrated in the literatures [27,28]. For P/Zr/HZSM-5 90 catalyst, upon first introduction of Zr ions into the parent HZSM-5 90, some Brønsted acid sites (hydroxyl group) are substituted by new formed acid site Zr-OH group, and the further addition of P ions can continue to replace the remaining Brønsted acid sites to generate P-OH acidic sites. Because of the weak acidity of P-OH and Zr-OH groups, the acidity of P/Zr/HZSM-5 90 should be decreased apparently compared with the

parent HZSM-5 90, which is highly consistent with our results of IR spectroscopy of adsorbed pyridine and ^{27}Al and ^1H MAS NMR measurements represented in **Fig. 3.8-3.10** and can reasonably explain the higher ethylene yield and lower C_{5+} hydrocarbons yield shown in **Table 3.2**. With respect to Zr/P/HZSM-5 90 with the reverse modification sequence, after introducing Zr ions to P/HZSM-5 90, the Zr ions partially interact with the surface P-OH group to form $\text{Zr}_3(\text{PO}_4)_2$, which is clearly confirmed by the ^{27}Al MAS NMR spectra with a chemical shift of -9.1 ppm (see **Fig. 3.9**). Even though the formed $\text{Zr}_3(\text{PO}_4)_2$ particle would block the acid sites during the reaction, the resulted more isolated Brønsted acid sites would enhance the total acidity strength, proven by the QM-Pot theoretical calculation [29]. The results of IR spectroscopy of adsorbed pyridine (see **Fig. 3.8**) as well as the ^1H MAS NMR measurements (see **Fig. 3.10**) together with the productions distribution from ethanol transformation (see **Table 3.2**) all consistently demonstrated an enhanced acid strength for the Zr/P/HZSM-5 90 catalyst. This is in good accordance with the interpretation of surface chemistry of HZSM-5 90 catalyst modified by P and Zr proposed in **Fig. 3.11**.

3.4 Conclusions

The enhanced stability for ethanol conversion to propylene has been realized with the successive P- and Zr- *co*-modified HZSM-5 90 in the continuous gas phase at 773 K. In a series condition optimization on temperature, pore confinement, acid concentration, and contact time, the best result is achieved with HZSM-5 90 operating at 773 K and a contact time of $0.03 \text{ g}\cdot\text{ml}^{-1} \text{ min}^{-1}$, yielding 27% propylene eventually. The P and Zr *co*-modified HZSM-5 enhanced the catalyst life time from 10 h to 26 h, with maintaining the comparable initial activity. In addition, the modified catalysts are substantially characterized to correlate the relationship of catalyst activities and properties. The crystalline and pore structures are almost unchanged after modification. Determined from IR spectra of adsorbed pyridine, the Brønsted acid sites are reduced after P and Zr *co*-modification. The decreased Brønsted acid sites

suppress coke formation, and thus extend the catalyst life time. The slightly higher acid strength of Zr/P/HZSM-5 also leads to high concentrations of heavier C₅₊ hydrocarbon formation. Moreover, the incorporation of Zr and P efficiently lowers dealumination, evidenced by IR spectroscopy. The changes of Brönsted acid sites are also confirmed by ²⁷Al and ¹H MAS NMR measurements, in which it shows that the initial P modification does a significant impact to the electrical field gradient and Brönsted acid strength. The proposed scheme of interaction of the introduced P and Zr ions with the Brönsted acid sites is highly consistent with the results of ethanol transformation together with IR spectroscopy of adsorbed pyridine IR and ²⁷Al and ¹H MAS NMR measurements.

3.5 Appendix

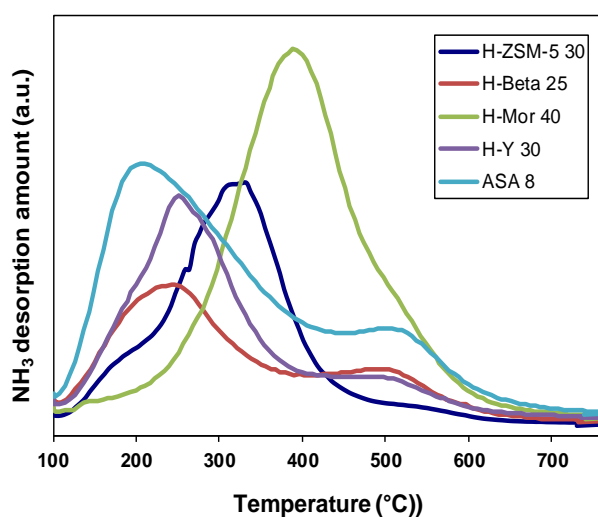


Fig. S1 Temperature programmed desorption of NH₃ on different zeolites.

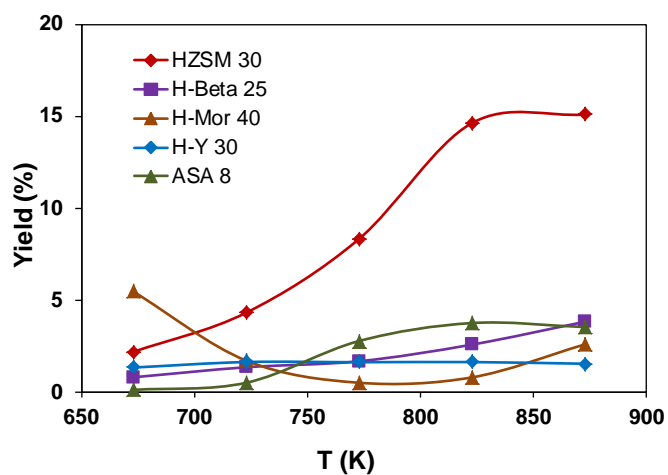


Fig. S2 Products distribution for conversion of ethanol over different kinds of catalysts as a function of temperature. Reaction conditions: 0.2 g catalyst diluted in 0.5 g SiC, 773 K, $P_{\text{EtOH}} = 0.2$ bar, total flow: 20 ml min⁻¹.

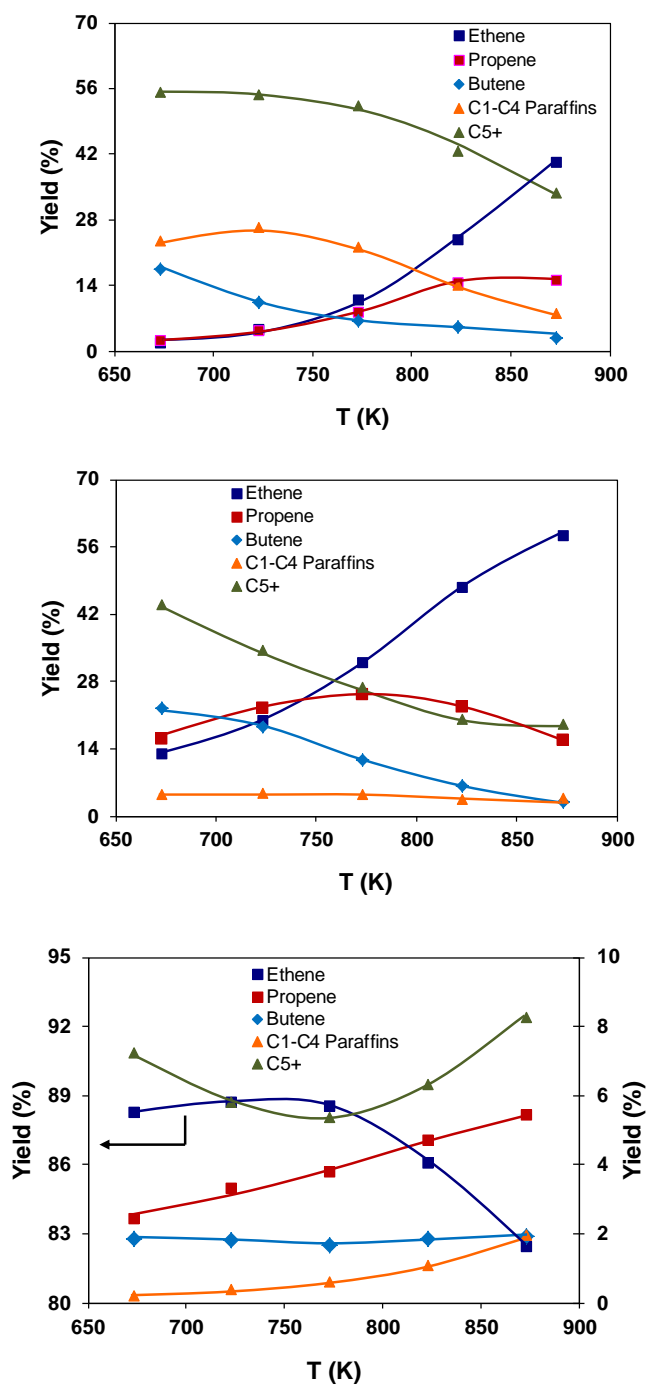
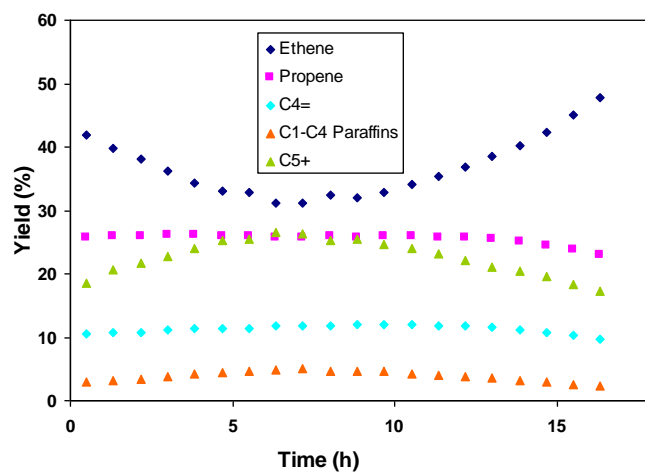


Fig.S3 Products distribution for conversion of ethanol over (a) H-ZSM-5 30, (b) HZSM-5 90, and (c) HZSM-5 240 as a function of temperature. Reaction conditions: 0.2 g catalyst diluted in 0.5 g SiC, 673-873 K, $P_{\text{EtOH}} = 0.2$ bar, total flow: 20 ml min^{-1} .

Table S1. Physicochemical properties of HZSM-5 catalysts.

	HZSM-5 30	HZSM-5 90	HZSM-5 240
Si/Al (mol mol ⁻¹)	15	45	120
BET surface area (m ² g ⁻¹)	423	424	357
Pore volume (cm ³ g ⁻¹)	0.23	0.29	0.22
Brønsted acid sites (BAS) (mmol g ⁻¹)	0.837	0.375	0.141
Lewis acid sites (LAS) (mmol g ⁻¹)	0.211	0.055	0.042

**Fig. S4** Time course of propylene yield for ethanol conversion over HZSM-5 90. Reaction conditions: 0.2 g catalyst diluted in 0.5 g SiC, 773 K, $P_{\text{EtOH}} = 0.2$ bar, total flow: 25 ml min⁻¹.

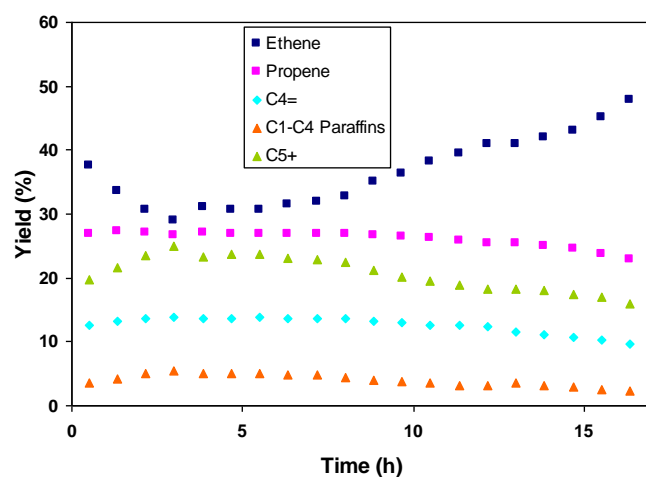


Fig. S5. Time course of propylene yield for ethanol conversion over Zr/HZSM-5 90 (molar Zr/Al = 0.4). Reaction conditions: 0.2 g catalyst diluted in 0.5 g SiC, 773 K, $P_{\text{EtOH}} = 0.2$ bar, total flow: 25 ml min⁻¹.

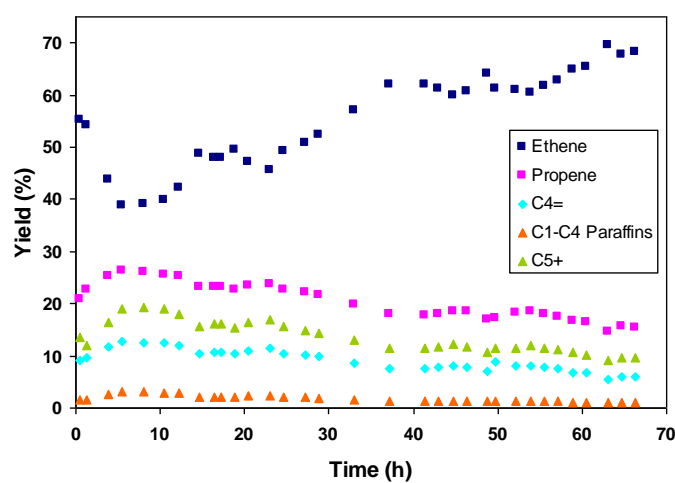
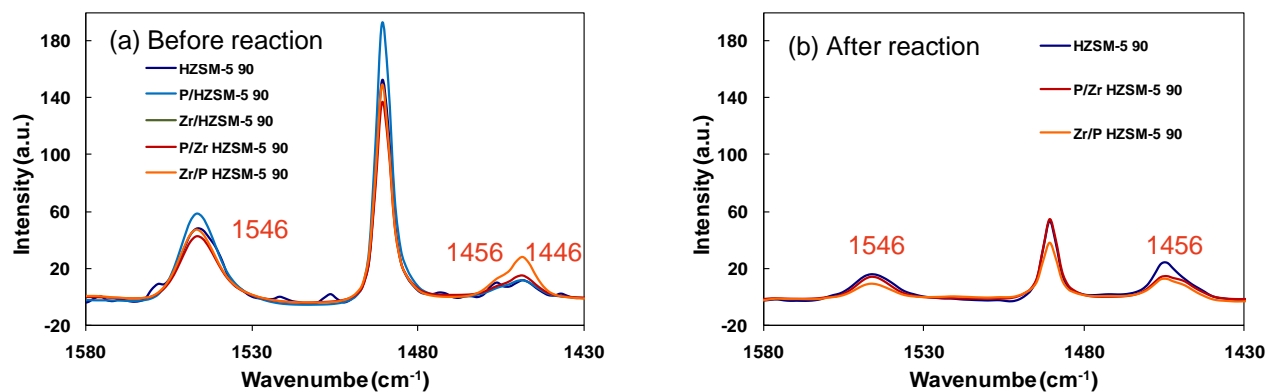


Fig. S6 Time course of propylene yield for ethanol conversion over Zr/P/HZSM-5 90 (molar Zr/Al = 0.4, P/Al = 0.5). Reaction conditions: 0.2 g catalyst diluted in 0.5 g SiC, 773 K, $P_{\text{EtOH}} = 0.2$ bar, total flow 25 ml min⁻¹.

423 K desorption



723 K desorption

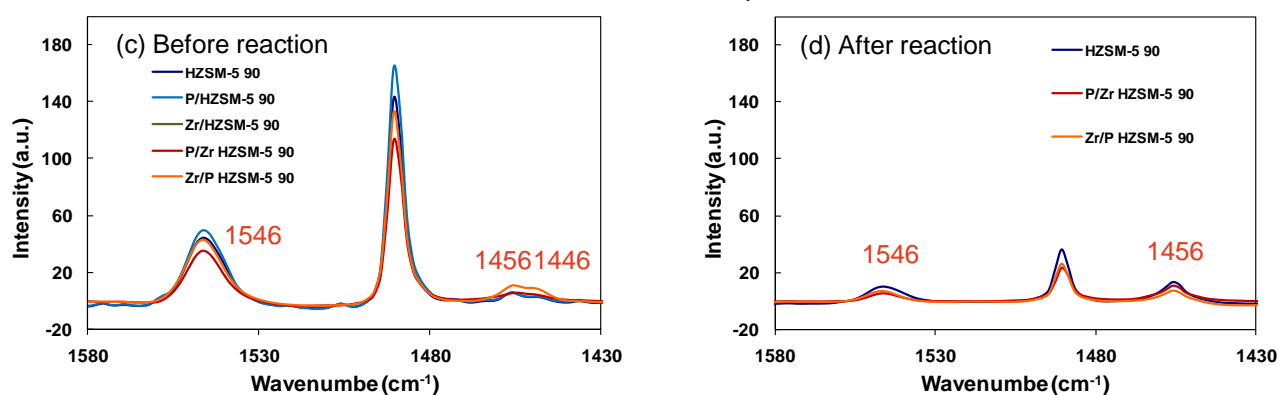


Fig. S7 IR spectra of adsorbed pyridine on parent and P/Zr modified HZSM-5 90 at desorption temperatures of 423 and 723 K.

3.6 References

- [1] J. Liu, C.X. Zhang, Z.H. Shen, W.M. Hua, Y. Tang, W. Shen, Y.H. Yue, H.L. Xu, *Catal. Commun.* 10 (2009) 1506-1509.
- [2] Y. Furumoto, N. Tsunoji, Y. Ide, M. Sadakane, T. Sano, *Appl. Catal. A: Gen.* 417–418 (2012) 137–144.
- [3] Z.X. Song, A. Takahashi, I. Nakamura, T. Fujitani, *Appl. Catal. A: Gen.* 384 (2010) 201–205.
- [4] A.G. Gayubo, A. Alonso, B. Valle, A.T. Aguayo, M. Olazar, J. Bilbao, *Fuel* 89 (2010) 3365-3372.
- [5] A.G. Gayubo, A. Alonso, B. Valle, A.T. Aguayo, J. Bilbao, *Appl. Catal. B: Environ.* 97 (2010) 299–306.
- [6] Z.X. Song, A. Takahashi, N. Mimura, T. Fujitani, *Catal. Lett.* 131 (2009) 364–369.
- [7] W. Xia, A. Takahashi, I. Nakamura, H. Shimada, T. Fujitani, *J. Mol. Catal. A: Chem.* 328 (2010) 114–118.
- [8] T. Meng, D.S. Mao, Q.S. Guo, G.Z. Lu, *Catal. Commun.* 21 (2012) 52–57.
- [9] K. Inoue, M. Inaba, I. Takahara, K. Murata, *Catal. Lett.* 136 (2010) 14–19.
- [10] M. Inaba, K. Murata, M. Saito, I. Takahara, *Green Chem.* 9 (2007) 638–646.
- [11] H. Oikawa, Y. Shibata, K. Inazu, Y. Iwase, K. Murai, S. Hyodo, G. Kobayashi, T. Baba, *Appl. Catal. A: Gen.* 312 (2006) 181–185.
- [12] T. Inoue, M. Itakura, H. Jon, Y. Oumi, A. Takahashi, T. Fujitani, T. Sano, *Micro. Meso. Mater.* 122 (2009) 149–154.
- [13] M. Iwamoto, Y. Kosugi, *J. Phys. Chem. C* 111 (2007) 13–15.
- [14] D. Goto, Y. Harada, Y. Furumoto, A. Takahashi, T. Fujitani, Y. Oumi, M. Sadakane, T. Sano, *Appl. Catal. A: Gen.* 383 (2010) 89–95.
- [15] K. Murata, M. Inaba, I. Takahara, *J. Jpn. Petrol. Inst.* 51 (2008) 234–239.
- [16] M. Inaba, K. Murata, I. Takahara, K.I. Inoue, *J. Chem. Technol. Biotechnol.* 86

- (2011) 95–104.
- [17] Y.Y. Chu, B. Han, A.M. Zheng, F. Deng, *J. Phys. Chem. C* 116 (2012) 12687–12695.
- [18] R. Gounder, E. Iglesia, *Chem. Commun.* 49 (2013) 3491–3509.
- [19] F. F. Madeira, K. B. Tayeb, L. Pinard, H. Vezin, S. Maury, N. Cadran, *Appl. Catal. A: Gen.* 443–444 (2012) 171–180.
- [20] D. Goto, Y. Harad, Y. Furumoto, A. Takahashi, T. Fujitani, Y. Oumi, M. Sadakane, T. Sano, *Appl. Catal. A: Gen.* 383 (2010) 89–95.
- [21] M. Inaba, K. Murata, I. Takahara, K.I. Inoue, *Adv. Mat. Sci. Eng.* (2013) 1–7.
- [22] K. Ramesh, L.M. Hui, Y.F. Han, A. Borgna, *Catal. Commun.* 10 (2009) 567–571.
- [23] A. Jentys, G. Rumpelmayr, J.A. Lercher, *Appl. Catal.* 53 (1989) 299–312.
- [24] N.H. Xue, R. Olindo, J. A. Lercher, *J. Phys. Chem. C* 114 (2010) 15763–15770.
- [25] K. Ramesh, C. Jie, Y.F. Han, A. Borgna, *Ind. Eng. Chem. Res.* 49 (2010) 4080–4090.
- [26] J.Q. Zhuang, D. Ma, G. Yang, Z.M. Yan, X.M. Liu, X.C. Liu, X.W. Han, X.H. Bao, P. Xie, Z.M. Liu, *J. Catal.* 228 (2004) 234–242.
- [27] Y. Furumoto, N. Tsunoji, Y. Ide, M. Sadakane, T. Sano, *Appl. Catal. A: Gen.* 417–418 (2012) 137–144.
- [28] T.S. Zhao, T. Takemoto, N. Tsubaki, *Catal. Commun.* 7 (2006) 647–650.
- [29] M. Sierka, U. Eichler, J. Datka, J. Sauer, *J. Phys. Chem. B* 102 (1998) 6397–6404.

Chapter 4

Summary and conclusions

In this doctoral thesis, 1-propanol dehydration to form propene (intramolecular elimination) and dipropyl ether (intermolecular dehydration) was systematically measured at varying 1-propanol pressure and reaction temperature. New reaction mechanism was proposed for propene formation and was further confirmed by accurate kinetic analysis. The long-standing controversy concerning the essential reason of inhibiting effect of water was revealed on basis of the kinetic assessment of water solvation effect on the adsorption ground state and dehydration transition state.

1-propanol dehydration to propene mechanism has been newly developed on basis of the dependence of dehydration rates on reactant pressure. It is found that 1-propanol monomer is not the only starting intermediate to form propene, and adsorbed 1-propanol dimer can also contribute for the propene formation under higher 1-propanol pressure. As well, the rate expression for propene formation was derived in terms of the proposed reaction elementary steps and dehydration mechanism. The consistency of the mechanism-derived rate expression with the experimental data further confirmed the proposed mechanism for propene formation. Moreover, based on the accurate analysis of the rate dependence on reactant pressure, associative pathway was proven to dominate 1-propanol dimolecular dehydration to form dipropyl ether, in agreement with the associative mechanism proposed for methanol and ethanol dehydration to the corresponding ethers in literatures.

Pyridine IR characterization of used catalysts as well as the time-on-stream test at 433 K in presence of water vapor show that HZSM-5 catalyst are highly stable under reaction conditions (temperature below 433 K) and that the inhibited catalytic dehydration activity does not result from the acidity or structure change of zeolite. Moreover, the preference adsorption of 1-propanol over water based on the calorimetric and IR measurement allows us to conclude that the inhibiting effect of introduced water is not a consequence of competitive adsorption between 1-propanol and water.

The kinetic and thermodynamic parameters estimated on basis of the

mechanism-derived rate equation, together with DFT calculations, reveal that the inhibiting impact of introduced water is related to the different extent of solvation of water on adsorption intermediate and transition state. Water appears to better stabilize the adsorbed 1-propanol intermediate than the transition state enthalpically, which leads to the higher activation barrier for elimination step. Moreover, additional 1-propanol involved in 1-propanol dimer to propene route inhibits the dehydration rate in a manner consistent with the introduced water.

Curriculum vitae

Yuchun Zhi was born on September 7th 1984 in Luoyang, Henan, P. R. China. After finishing the education in high school at his hometown in 2003, he started the study in Department of Materials Science and Engineering at Shandong University, Jinan, China. After receiving his bachelor degree in July 2007, he continued the masters' course study in materials science at State Key Lab. of Crystal Materials at Shandong University under the supervision of Prof. Xutang Tao and received the master degree in July 2010. Then, he joined the research group of Prof. Johannes A. Lercher and commenced on PhD study at the Chair of Technical Chemistry II at Technische Universität München, Germany in January 2011. His research focuses on the elementary reactions of simple alcohols on HZSM-5, especially on the topic of water influence on 1-propanol dehydration reaction, aiming to provide mechanistic and kinetic understanding of the inhibiting effect of water.

List of publications

- [1] **Y. C. Zhi**, C. Zhao, L. Y. Mu, J. A. Lercher. Water impact on 1-propanol dehydration: a mechanistic and kinetic study. (in preparation)
- [2] **Y. C. Zhi**, C. Zhao, J. A. Lercher. Mechanistic and kinetic understanding of 1-propanol dehydration in liquid and aqueous phase. (in preparation)
- [3] **Y. C. Zhi**, C. Zhao, J. A. Lercher. Ethanol conversion to propylene with enhanced stability on P and Zr modified HZSM. (to be submitted)
- [4] G. Piccini, M. Alessio, J. Sauer, **Y. C. Zhi**, Y. S. Liu, R. Kolvenbach, A. Jentys, J. A. Lercher. Accurate adsorption thermodynamics of small alkanes in acidic zeolites. Ab initio theory and experiment. (accepted by JPCC)